12-14-2015

Impact of Formulation and Processing Parameters on Mechanical Properties of Magadiite/Elastomer Composites

Yating Mao
University of South Carolina - Columbia

IMPACT OF FORMULATION AND PROCESSING PARAMETERS ON MECHANICAL PROPERTIES OF MAGADIITE/ELASTOMER COMPOSITES

by

Yating Mao

Bachelor of Science,
Dalian University of Technology, 2011

Submitted in Partial Fulfillment of the Requirements

For the Degree of Doctor of Philosophy in

Chemical Engineering

College of Engineering and Computing

University of South Carolina

2015

Accepted by:

Harry J. Ploehn, Major Professor

James A. Ritter, Committee Member

Xiao-dong Zhou, Committee Member

Hanno zur Loye, Committee Member

John W. Weidner, Committee Member

Lacy Ford, Senior Vice Provost and Dean of Graduate Studies

DEDICATION

I dedicate this dissertation to my parents Yun Mao and Hui Jiang.

ACKNOWLEDGEMENTS

I would like to thank my advisor, Dr. Harry Ploehn, who helped me through my graduate education. Everything that I learned from him will still guide me after my graduation.

I want to thank my committee members to help to better my work.

I appreciate all my lab colleagues. Special appreciation goes to Dr. Shigeng li, who taught me how to use everything in the lab when I was new to graduate school. I really appreciate his help in research and important career advice. Dr. Xiaoming Chen helped me in my project and lab work patiently, even after he left USC.

My appreciation also extends to all the research groups in Horizon building. I had a wonderful time in this building. Dr. Benicewicz gave me very useful guide in the cooperation project. Dr. Frank Chen offered me the permission to use the equipment in his lab. Dr. Hongying Zhao is a great friend and colleague. I am also thankful to Warren for the help and funny conversations.

Many people from other departments in USC helped me in my work. I enjoyed learning in EM center with Dr. Jibin Zhao. Dr. Chao allowed me to run tensile test in his lab.

I want to thank all my friends in department of chemical engineering who helped me to start the new life in the US in 2011. Thanks for Hang Li who offered me exciting cooperative opportunities. I am very thankful to my dear friends Qiuli Liu, Dr. Lujing Zhan, Dr. Lei Zhang, Lei Wang, Chao Wang, I can't forget the time we spent together. Thanks to my great roommates Dr. Xuan Zhao, Yang Cao, Shengnan Meng and Liang Li for spending the beautiful days with me. I miss those days in Pavilion Tower and Granby Oaks.

To my best friends Gloria Sifan Liu and Oclin Lin Wang, the sweetest conversations encouraged me in the past four years, especially when I was recovering from surgery and looking for jobs. Our friendship will be forever. Lai Wei, April Yang, Shixi Qu, Jennifer Zhang, Ying Zhang, Bo Guan, they always gave me strength and made me happy.

Finally, I want to thank my parents Yun Mao and Hui Jiang. Without their love and support, I could never make it. I am very proud of my parents and my family. I miss my grandparents so much. I really wish they were here for me now, but I know they will be watching and helping me every day.

ABSTRACT

This work seeks a better understanding of mechanical reinforcement and energy dissipation in elastomer composites containing the layered silicate magadiite (MGD, $Na_2Si_{14}O_{29}\cdot nH_2O$). We characterized the elastomer's accessibility into MGD interlayer spaces and studied the factors that influence the composite mechanical properties. We also compare the mechanical reinforcement of MGD with montmorillonite (MMT, a layered aluminosilicate clay mineral), which is widely used as filler in other kinds of nanocomposites. The study explores the grafting chemistry, vulcanization, and reinforcement mechanism in MGD/elastomer composites, which may help us to formulate the platelet/elastomer composites with superior mechanical properties and performance in the future.

We continued previous work in our group on the influence of organosilane pre-functionalization on MGD reinforcement.[1] Various organosilane-functionlized MGD (OS-MGD) were reacted with squalene (SQ), a small molecule model for natural rubber. For OS-MGD with larger initial interlayer spacing, more SQ entered the interlayer space. For OS-MGD with smaller initial interlayer spacing, SQ was excluded from intercalation. By calculating the composition based on TGA and EA results, we studied the MGD grafting chemistry and quantified the SQ accessibility into the MGD interlayer space.

[1] Li, S. Reinforcement and Energy Dissipation in Platelet-Filled Elastomers. Ph.D. Dissertation, University of South Carolina, 2012.

Then, we explored various factors that influence the mechanical reinforcement of composites consisting of MGD dispersed in styrene-butadiene rubber (SBR), such as the interlayer spacing, various mixing times, the addition of silane coupling agents, different sulfur sources, the presence of surfactant, and varying elastomer chemistry. Rationalizing the relationship between those factors and composite mechanical properties provides a deeper understanding of the reinforcement mechanism and energy dissipation in MGD/SBR composites.

Finally, we compare the mechanical reinforcement of MGD and MMT in SBR composites directly. Based on XRD results, MMT was speculated to be partially exfoliated after compounding with SBR prepolymer, resulting in greater mechanical reinforcement and higher crosslink density for MMT/SBR composites compared to MGD/SBR composites. This work helps us to understand and formulate elastomer composites containing other members of these two mineral families in the future.

TABLE OF CONTENTS

LIST OF TABLES

LIST OF FIGURES

CHAPTER 1
Introduction

1.1 Project Motivation

In the tire industry, people are familiar with the “magic triangle” for tire performance: rolling resistance, tread wear and traction. A formulation change that leads to improvement of one performance metric usually will lead to decreases in other performance metrics. New additives, like highly dispersible (HD) silica modified with bifunctional silanes, show promise to stretch this triangle by improving one or more performance metrics without hurting others.

In our research, we are trying to stretch the magic triangle through the use of layered silicates with surface chemistry similar to that of HD silica, but with different particle shape, specifically platelets instead of spheres. Because platelets offer a higher surface area per unit weight of filler, formulators may be able to use lower weight loadings to achieve the same mechanical properties as elastomers filled with HD silica. This would reduce tire weight and save energy. The challenge is to understand the relationship between formulation and mechanical properties in platelet-filled elastomers, especially due to the changes and complexities in filler chemistry and microstructure on various length scales.

This study seeks a better understanding of mechanical reinforcement and energy dissipation mechanisms in styrene-butadiene rubber (SBR) composites filled with

magadiite platelets (MGD, unit cell formula unit cell formula $Na_2Si_{14}O_{29}{\cdot}nH_2O$. This research project investigates the silane grafting and vulcanization chemistry of MGD/SBR composites, the influence of grafting chemistry on MGD interlayer spacing and particle dispersion, and how these factors influence composite microstructure and composite mechanical properties.

1.2 Background

1.2.1 Elastomers

Natural rubber (NR) has been obtained from trees for centuries. The elasticity and water proofing ability of NR initially attracted the attention of scientists. In 1839, Charles Goodyear and Thomas Hancock discovered that vulcanization improved the strength and elasticity of rubber and made it less susceptible to temperature changes. NR had low production volume and high market price due to the limited availability of NR from natural sources.[1]

NR was the only available kind of rubber until synthetic rubbers were first produced in the early 1920s. Synthetic rubber was prepared from monomers derived from natural gas and petroleum. Since World War II, due to the growth of synthetic rubber production and the superior properties of synthetic rubber, the market share of NR dropped from 100% in 1940 to 30% in 1978. Since then, the market share rebounded and now remains at 40% due to the large need for NR in radial tire construction. Compared to NR, synthetic rubber has better resistance to light, heat, and organic fluids. It is also possible to modify the chemistry and structure of synthetic rubber so that the properties are tailored to fit the final applications.

Based on properties and structure, synthetic rubbers are divided into several types: diene rubber, saturated rubber, solvent resistant rubber, temperature resistant rubber, specialty rubber, thermoplastic rubber, etc.[1] The applications of some common rubber types will be introduced next.

(1) Diene Rubber

Styrene butadiene rubber (SBR), butadiene rubber (BR) and isoprene rubber (IR) are common diene rubbers. In this group, SBR is produced in the greatest volume. It is used to manufacture tires and tire products due to its excellent abrasion resistance and better cost/performance/processing balance. BR is widely used in the tire treads. IR-based NR polymers are widely used in the treads of heavy duty truck and bus tires because of their good wear resistance and low hysteresis under heavy load conditions.

(2) Saturated Rubber

Saturated rubbers include ethylene-propylene copolymers (EPM), ethylene-propylene-diene terpolymers (EPDM), butyl and halobutyl rubbers (IIR and BIIR/CIIR), and ethylene-acrylic elastomers (EAM). Saturated elastomers possess better environmental aging resistance than diene elastomers. The main applications of EPM and EPDM are in manufacturing of hoses and seals. IIR and BIIR/CIIR are commonly used in inner tubes due to their low air permeability, as well as in some other tire products. EAM is used in automotive applications.

(3) Solvent Resistant Rubber

Nitrile rubber (NBR) is a widely used solvent resistant elastomer. Its principal uses are in seals, O-rings, and gaskets due to its great chemical resistance.[1]

1.2.2 Elastomer Composites

Pure, crosslinked rubber has poor physical properties, so filler materials are added to prepare elastomer composites with improved properties. In fact, elastomer nanocomposites have existed for decades, considering that carbon black and silica particles added to elastomers have an average size ranging from 5 to 100 nm.[2] The concept of the nanofiller was introduced to the rubber industry in 1993.[3] The term "nanocomposite" was first introduced one year later[4]: it represents a kind of material with nanofillers dispersed into a matrix material.[5,6,7] A nanofiller is a particulate material having at least one nanoscale dimension (~100 nm) and thus a large specific surface area (surface area per unit mass of filler). When dispersed uniformly in polymer matrix, the nanofiller may have large interfacial surface in contact with polymer, which could have a decisive effect on nanocomposite properties and performance.[8]

Compared to conventional composites, nanocomposites may be able to achieve comparable (or better) mechanical properties using much lower amounts of filler, reducing weight and improving strength/weight ratio. Also, nanofillers are used to achieve enhanced properties of rubber products, such as tensile strength, hardness, abrasion resistance, flame retardance, electrical conductivity, and permeability. Nanocomposites have attracted considerable academic and industrial attention due to the promise of superior properties.[2]

Carbon black (CB) has been used as a rubber-reinforcing agent since 1904. Most CB is used in the tire industry, because the CB improves the strength and abrasion resistance of automotive tires. Many other rubber products incorporate CB, including conveyer belts and consumer products such as footwear and shock absorbers.[1] However, the application of CB is limited by its dark color, tendency to cause environmental pollution, and shortcomings including poor aging resistance and fatigue.[9]

Going beyond CB, silica is another important reinforcing filler widely used in the rubber industry. After the introduction of silica in passenger tires in the 1990s, the use of silica in the rubber industry developed rapidly. Compared to CB, silica provides higher wet traction and better rolling resistance without much loss of wear resistance. However, the application of silica is restricted by higher process cost and performance issues caused by filler agglomerations in rubber composites.[8,9]

1.2.3 Coupling Agents

The advent of coupling agents improved the performance of silica in rubber composites.[1] Coupling agents are generally bi-functional molecules that establish molecular bridges at the interface between the polymer matrix and the filler surface. Through these interfacial bonds, coupling agents are able to enhance the degree of polymer-filler interaction by reducing surface energy of the fillers.[10]

Among all coupling agents, bis(3-triethoxysilylpropyl)tetrasulfane, known as SI-69 (Scheme 1.1), is often used for tire tread formulation.[11] Utilization of SI-69 in silica-filled rubber compounds improves modulus, compression set, heat build-up, and abrasion resistance. Much research has been done on SI-69 coupling agents, and the steps involved

in the reaction between silica and SI-69.[10] The ethoxy groups of SI-69 react with silanol groups on the silica surface to produce grafted silane. The tetrasulfane group SI-69 opens up under curing conditions. The two sulfur atoms attached to the silanes react with unsaturated (-C=C-) alkene sites in the rubber to produce elastomer-silica crosslinks. The tetrasulfane also releases two sulfur atoms that produce additional crosslinking.[12] The application of SI-69 is the key factor for the success of silica for partial replacement of CB as an active filler in the tread compound of the "green tire".[13]

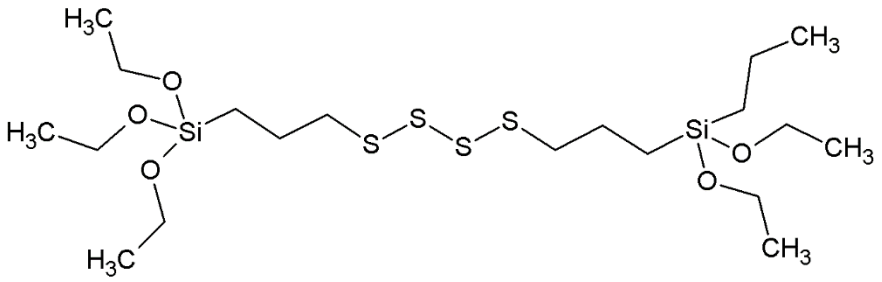

Scheme 1.1 Structure of triethoxysilylpropyltetrasulfide (SI-69).

SI-69 is widely used to promote adhesion between inorganic fillers and polymer matrices. Many articles reported that SI-69 improved dispersion of various fillers, resulting in better mechanical properties. Tian et al.[14] found, using Scanning Electron Microscope (SEM) images, X-ray diffraction (XRD), and Payne effect results, that SI-69 improved the dispersion and enhanced interfacial adhesion of fibrillar silicate clay in SBR composites, which resulted in better hardness, tensile modulus and the tear strength. Alkadasi et al.[15] found after treatment with SI-69, China clay showed better filler dispersion in SBR and improved mechanical properties, such as tensile strength, tensile modulus, Young's modulus, and hardness. In Wang et al.'s work[16], SI-69 modified synthetic mica was better dispersed in ethylene-propylene diene terpolymer (EPDM) and

showed higher modulus and elongation at break values. Ismail et al.[17] studied the influence of SI-69 on mechanical properties of recycled poly(vinyl chloride)/acrylonitrile-butadiene rubber/fly ash (PVCr/NBR/FA) composites. The addition of SI-69 increased the interfacial interaction between fillers and polymer matrix, and also improved the filler dispersion. The resulting tensile strength, tensile modulus, and elongation at break also improved. Sun et al.[18] concluded that SI-69 improved the dispersion of silica in SBR composites and the increased silica-SBR bond strength, leading to enhanced tensile properties of the vulcanized rubber. In conclusion, SI-69 improves filler dispersion as it makes the silicate particles less hydrophilic, which lowers the dispersion energy. Thus the particle dispersion is promoted, resulting in improved mechanical properties.

The effect of SI-69 on mechanical properties is influenced by other compositional and processing parameters during reaction. Ward et al.[19] found that the complex shear modulus and stress-strain results were not changed much by the addition of SI-69 in S-SBR with silica loading lower than 70 phr. They thought that S-SBR interacted with silica by itself, and the addition of SI-69 did not improve the interaction very much. In another study on organically modified MMT (OMMT)/NR composites[20], the addition of SI-69 didn't influence the tensile properties of OMMT/NR composites. They speculated that the mixing temperature of 50ºC was too low, which led to ineffective chemical reaction between SI-69 and OMMT. Other factors are sometimes critical in fully realizing the advantage of SI-69.

Some studies have noted that there is an optimum SI-69 amount in rubber formulations. Excessive SI-69 decreased the crosslink density and led to poor mechanical

reinforcement. Yamsaengsung et al.[21] claimed that in wood sawdust/ NR composites, the crosslink density increased with SI-69 content increasing from 0 to 0.5 wt%, and then decreased with greater amounts of SI-69. Similar results were reported in silica/SBR composites[18], fly ash/NR composites [22]and silica/NR/SBR blends[23]. They attributed this phenomenon to either the steric hindrance effect from tri-ethoxylsilypropyl groups, or the formation of mono- and poly-layers from self-condensation of the SI-69. The addition of an optimum amount of SI-69 improves the crosslink density and mechanical properties effectively. Excessive SI-69 levels may diminish mechanical reinforcement.

The addition of SI-69 in elastomers also influences the scorch time (the time delay before curing begins) and the cure time (the time to achieve 90% of complete crosslinking). Increases in scorch time and cure time with increasing SI-69 amounts were reported in grass fiber/NR composites[24], NR/SBR blends filled with silica from fly-ash[25], and NR composite containing short cellulose fiber/silica hybrid filler[26]. However, the addition of SI-69 decreased the cure time in SBR/NBR blends filled with CB/silica.[27] Thus, the influence of SI-69 on scorch time and curing time depends on the chemistry of the filler/elastomer system.

Some studies compare the performance of SI-69 with other coupling agents. Sun et al.[18] observed that silica/SBR composites with SI-69 had better performance for some properties, such as tensile strength, modulus, shore hardness and resilience rate, when compared with other coupling agents, including: γ-amino propyl- triethoxysilane (KH550), γ –glycidoxypropyltrimethoxysilane (KH560), 3-(trimethoxysilyl)-1-propan-amine (KH540), 3-(methacryloxy) propyl-trimethoxysilane (KH570), and vinyltriethoxysilane (KH151). Ko et al.[13] studied the effectiveness of coupling agents by

preparing silica/SBR composites containing various silanes. They used two bifunctional silanes: SI-69 and 2,5-(triethoxysilylpropylthia)-1,3,4-thiadiazole (S4), and four monofunctional ones: 3-octanoylthio-1-propyltriethoxysilane (NXT), 1-[3-(octanoylthio)propyl]-1,1,3,3,3-pentaethoxy-1,3-disilapropane (S1), bis[3-(octanoylthio)-1-propyl]-diethoxysilane (S2), 5-(triethoxysilylpropylthia)-2-potassium-1,3,4-thiadiazolate (S3). It was concluded that the bifunctional silanes produced more crosslinking than the monofunctional ones. Each bifunctional silane molecule connected two different silica particles with two separate polymer chains. Silanes containing nitrogen atoms (e.g. S3 and S4) led to shorter cure time. SI-69 promoted the tensile properties and abrasion resistance the best, but it was not as good as NXT, S1 and S2 at improving the rolling resistance and wet traction of tire materials. Thus, the choice of silane depends on the final application of the material.

1.2.4 Other Nanofillers

In addition to CB and silica, other novel nanofillers have been extensively studied: nanoclay, carbon nanotubes, graphenes, nanocellulose and ceramics.[2,28,29,30,31,32,33,34,35] The resulting rubber nanocomposites showed excellent mechanical properties, thermal stability and electrical conductivity.[2,36] Rubber composites based on nanoclays, known better as layered silicates, are reviewed in the next section.

1.2.5 Rubber Vulcanization

Rubber vulcanization is the process by which chemical and physical crosslinks are formed between individual polymer chains. It is an irreversible process. Vulcanized rubber shows superior mechanical properties compared to uncured, green rubber. The physical properties of vulcanized rubber are determined by the vulcanization process.[37]

The curing process is commonly characterized using an oscillating disk rheometer. The principle is to monitor the torque required to maintain given amplitude of oscillation at a specific temperature. It is assumed that the measured torque during vulcanization increases in proportion to the degree of crosslinking. The curing curve, a plot of torque versus time, provides information on polymer crosslink formation during vulcanization, and is extensively used to monitor the quality of rubber materials.[37]

Usually, each curing curve consists of three regions: scorch delay, curing, and overcure. Scorch delay is an initial period in which the cure rate is very low. Most of the accelerators react during the scorch delay period. Short scorch delay may cause processing problems. The formation of three dimension network occurs during curing period, indicated by a sudden increase of cure rate. At the end of curing reaction, a plateau in torque is observed in the third region, known as overcure, indicating the maturity of the network. Different polymers show different overcure trends, such as increase, equilibrium or reversion.[2]

Sulfur vulcanization has been utilized primarily in the rubber industry for over 70 years. Sulfur vulcanization reactions could only proceed quickly due to the presence of accelerators and activators. Without these, the reaction is not efficient and takes a long time. The addition of activators and accelerators optimizes the vulcanization process, such as shortening the cure optimum time, lowering reaction temperatures, and improving thermal and oxidative antidegradation.[2,37]

Accelerators speed the crosslinking reaction and reduce the required sulfur amount, thus avoiding “bloom” and improving compound aging. There are many types of accelerators, such as sulfonamides, thiazoles, guanidines, dithiocarbamates. The

2-benzothiazyl sulfonamides are the most common accelerators used in rubber industry. During vulcanization, sulfonamides produce crosslinking and also provide scorch delay time for processing. Usually, accelerators are used in combination.[37]

The accelerators must be activated by activators. The most commonly used activators are zinc oxide and stearic acid. The stearic acid reacts with the zinc oxide and solubilizes the zinc ion to react with accelerators.[38] The mechanism of sulfur vulcanization involves Zn^{+} ions (from reaction between steric acid and zinc oxide) first forming complexes with accelerators. The resulting complex with sulfur and activators produces the active sulphureting agent that creates rubber polysulfides. The rubber polysulfides react and form crosslinks (C-Sx-C). However, the mechanism of rubber vulcanization is still in dispute concerning whether the main reaction occurs via ionic or free-radical mechanism.[2,39,40]

In this work, n-cyclohexylbenz-thiazylsulfenamide (CBS) accelerator is used as the primary accelerator. Diphenylguanidine (DPG) is used as an activator for sulphenamides and as secondary accelerator in tire tread compounds. It is widely used in silica/rubber to achieve low rolling resistance.[38,39] The stearic acid and zinc oxide are also activators.

1.3 Layered Silicates in Rubber Composites

Nanocomposites filled with layered silicates have been well known since the famous work on Nylon 6 by Toyota.[3,41] Clay minerals are obtained from natural sources, can be purified and sold in large quantities of relatively low cost, and are not regarded as being harmful to human health. Small amounts of clay minerals in rubber material have

been found to improve mechanical properties (such as tensile strength, tear strength, abrasion resistance), increase solvent resistance or biodegradability, and decrease permeability and flammability.[2]

1.3.1 Montmorillonite

Montmorillonite (MMT) plays a major role among the nanofillers. It is an abundantly available natural resource with low price and important properties, like high aspect ratio (length/thickness), the unique intercalation/exfoliation characteristics, and a safe toxicological profile.[42]

MMT has a 2:1 layered structure consisting of an octahedral sheet (O) of alumina sandwiched between two silica tetrahedral sheets (T), with the T and O sheets covalently linked by the apical tetrahedral oxygens.[35,43] Three sheets (TOT) form one clay layer. These layers, called platelets, are stacked to form MMT particles. Due to isomorphous substitution of Fe^{2+} for Al^{3+} in the octahedral sheets, each MMT layer has a net negative charge that is balanced by cations in the interlayer space. The interlayer cations are hydrated and loosely bound; they may be exchanged with other cations, so that MMT has a relatively large cation exchange capacity.[43]

In each layer, strong iono-covalent interactions exist to keep the layer in one piece. The layers are held together by relatively weak forces in the direction perpendicular to the layers, so that upon dispersion into water, MMT layers are easily separated, or exfoliated, into individual platelets.

The aspect ratio is defined as the average ratio of platelet length to thickness. The reinforcement and gas barrier performance of MMT platelet fillers may depend on the

aspect ratio and platelet-matrix interaction.[44] Our group's previous work[45] used atomic force microscopy (AFM) to quantify the distribution of MMT platelet aspect ratio, lateral dimensions, and the degree of exfoliation in water. The aspect ratio of MMT platelets closely follows a log-normal distribution. Exfoliated MMT platelets usually have aspect ratios in the range between 50 to 2000.[44]

Due to the presence of hydrated interlayer cations, MMT platelets are hydrophilic and have poor interaction and adhesion with organic polymers. The majority of past studies show that when no compatibilizing ingredients are added, pristine MMT shows little or no change in interlayer distance, indicating that polymer does not enter the interlayer spaces.[2] In order to improve compatibility with rubber, MMT may be modified by organophilic surfactants, such as primary alkyl amines and various alkyl ammonium cations. The resulting organo-modified MMT (OMMT) has better dispersion in rubber matrices, resulting in improved mechanical properties.[8,46]

1.3.2 MMT/rubber composites

As nanofillers in rubber, clay minerals have excellent features: high aspect ratio and nano scale thickness. However, platelets tend to stack and form agglomerates in rubber.[2] Only when fillers are intercalated or exfoliated by polymer, the resulting composites are classified as nanocomposites.[9] Intercalated nanocomposites occur when polymer intercalates into the interlayers. This may be caused by the penetration of polymer chains or the structural reorganization of organic modifier. Exfoliated nanocomposites occur when individual clay layers are isolated and separated randomly. This may be caused by intercalation of polymer chain into interlayers sufficient to fully separate platelets, or by progressive peeling off of platelets.[2,9] The best performance is

thought to be achieved in exfoliated nanocomposites in which platelets have greatest interaction with rubber matrix through large interfacial surface area, resulting in superior reinforcement.[2,9]

MMT has been used as a filler in various rubber composites, including NR, SBR, BR and EPDM. Past studies of each kind of rubber composite will be reviewed below.

(1) Styrene Butadiene Rubber

There have been many reports about OMMT/SBR nanocomposites in which intercalated or partially exfoliated MMT improves mechanical properties.[47,48,49,50,51,52] Mousa et al.[49] reported that the incorporation of up to 10 phr OMMT* improved the tensile stress and modulus at 300% elongation. MMT platelets with high aspect ratio were most effective in reinforcing the material. Zhang et al.[50] found that the tensile properties and hardness of OMMT/SBR were comparable to CB/SBR when OMMT filler loading was less than 40 phr. However, there are not many studies that compare OMMT/rubber with CB/rubber composites using formulations that are realistic for tire rubber mixes.

(2) Natural Rubber

Natural rubber (NR) is also commonly used as the matrix for nanocomposites.[53,54,55,56,57,58,59] OMMT has shown outstanding performance in reinforcing NR composites. Varghese et al.[58] prepared OMMT/NR nanocomposites with 10 phr OMMT. The nanofillers were partially exfoliated in rubber composites based on

* phr denotes "per hundred rubber" by weight. Thus 10 phr OMMT in SBR represents a mixture of 10 g OMMT per 100 SBR.

XRD results and TEM images. Compared to pristine MMT, OMMT/NR showed shorter curing time and enhanced tensile properties. In a work on OMMT/NR composites by Arroyo et al.[60], both tensile strength and elongation at break of NR composites with 10 phr OMMT were superior to the composite with 40 phr CB. Some groups have reported that OMMT pre-intercalated by fatty acid or prepolymer will result in enhanced mechanical properties. Rooj et al.[55] pre-intercalated OMMT with fatty acid with 22 carbon atoms (docosanoic acid). Then, NR nanocomposites were prepared with 4 phr pre-intercalated OMMT. MMT showed an intercalated structure with interlayer spacing of 5.4 nm in NR composites. Compared with unfilled NR, tensile strength and modulus at 300% elongation improved 114% and 203% respectively. Similar results were obtained in Das et al's work.[61] In Boonchoo et al.'s work[54], polyisoprene–montmorillonite (PIP–MMT) nanocomposites were synthesized via microemulsion polymerization. The pre-intercalated PIP increased the interlayer distance of MMT from 3.1 nm to 3.8 nm. NR with PIP-MMT showed improved tensile strength and elongation at break compared to unfilled NR.

(3) Nitrile Rubber

Many studies reported nanocomposites with nitrile rubber (NBR) as the matrix and OMMT as fillers.[62,63,64,65,66] Sousa et al.[64] found that the incorporation of OMMT in NBR nanocomposites improved tensile properties compared to unfilled NBR. XRD showed intercalated structure of MMT in NBR. Alhmadi et al.'s work[66] showed OMMT was exfoliated in NBR nanocomposites. Especially when nanofiller contents were more than 5 phr, both modulus and ultimate strength were much larger in OMMT/NBR than MMT/NBR. In Mohamed's work[63], in OMMT/NBR with 5 phr and 10 phr OMMT,

gamma radiation of nanocomposites improved the thermal stability and filler dispersion more than OMMT/SBR.

(4) Ethylene Propylene Diene Terpolymer

Another extremely durable polymer, ethylene propylene diene terpolymer (EPDM), has also been used to prepare rubber nanocomposites.[67,68,69] Zheng et al.[67] treated MMT with methylbis(2-hydroxyethyl)cocoalkylamine, and then prepared EPDM nanocomposites containing 15 phr pretreated OMMT. Fillers showed exfoliated structure in nanocomposites, which was verified by XRD patterns. The resulting exfoliated nanocomposites show great improvement in modulus and hardness. Ahmadi et al.[68] compared the mechanical reinforcement of OMMT and MMT in EPDM composites. When OMMT loading was from 2 to 10 phr, an exfoliated structure was obtained based on XRD results and TEM images. OMMT/EPDM nanocomposites show superior tensile properties, hardness and solvent resistance compared to MMT/EPDM composites.

1.3.3 Magadiite

Magadiite (MGD) belongs to a group of aluminum-free layered silicate hydrates[43] that has attractive properties, including resistance to acids, good ion exchange properties, and ability to intercalate organic cations. Other minerals belonging to this group include kanemite, octosilicate, kenyaite, and makatite. Hydrothermal synthesis conditions and the ratio between the sodium and siliceous components play decisive roles in the formation of two-dimensional structure in layered silicates.[43]

The general formula for layered silicate hydrates is $(Na\cdot 2H_2O)_aH_a\cdot [a(Si_2O_5)\cdot b(Si_2O_4)]\cdot (cH_2O)$ ($a \geq 1$, $b \geq 0$, $c=2$ in the fully hydrated state). The silicate layers are

composed of $[SiO_4]$ and $[SiO_3OH]$ units. Arrangements of the $[SiO_4]$ tetrahedral of some layered silicates are shown in Scheme 1.2. The interlayer space contains cations to neutralize the layer negative charge.

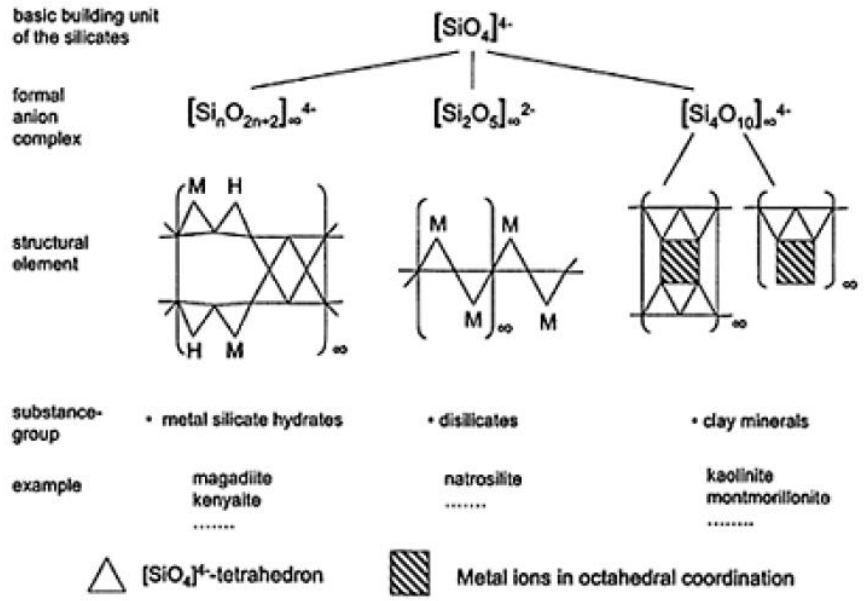

Scheme 1.2 Arrangements of the [SiO4] tetrahedra as structural building units of silicatic layered materials. Reproduced with permission from *Handbook of Layered Materials*.[43]

The SiO_2/Na_2O ratio is used to classify layered silicates into different groups. The basal spacing d and the interlayer distance Δd are characteristic features for the layered silicates.[43] Some research shows with the increase of the SiO_2/Na_2O ratio, the basal spacing d decreases.

Of all the layered silicate hydrates, the crystal structures of kanemite and makatite are the only ones to have been confirmed. Because no single crystal of magadiite has been found, its crystal structure is not determined yet. According to many TGA and NMR results, the unit cell composition is expressed as $Na_2Si_{14}O_{29}{\cdot}nH_2O$ (n=5-11). Although

improvements in analytical technology will help us to better understand the sodium silicate hydrate group, so far the structural relationship among group members has not been figured out.[43]

In MGD, interlayer sodium cations compensate the negative charged layers. The compensating cations are loosely bound and easily exchanged by inorganic and organic cations.[70] Iler published a study of layered silicates cation-exchanged with metal cations, including Li^+, Na^+, Mg^{2+} and hexadecyltrimethylammonium cations in early 1960s.[71] Other metal cations such as Zn^{2+}, Eu^{3+} and Co^{2+} have been exchanged and absorbed into MGD.[72,73,74] Due to its cation exchange ability, MGD has been explored for use as molecular sieve, cation exchanger, adsorbent and catalyst support. The lack of covalent bond formed during cation-exchange reaction makes intercalated cations easily released or exchanged.[75]

Incorporation of organic cations has been studied due to the potential application of organo-modified modified MGD (OMGD) in polymer composites. OMGD has larger interlayer spacing, making it much easier to be intercalated further by other organic molecules. Lagaly et al.[76] explored MGD cation exchange and reported the interlayer sodium cations were exchanged by alkylammonium-, dimethyldialkylammonium-, trimethylalkylammonium, and alkylpyridinium cations. They also reported the surface area of the MGD unit cell ($Si_{14}O_{29}$) to be 0.55 nm^2. Kooli et al.[77] quantified the maximum amount of cetyltrimethylammonium cations (CTA^+) exchanged per unit mass of MGD as 1.16 mmol /g. Wang et al.[78,79] treated MGD with various octadecylammonium $Ch_3(CH_2)_{17}NH_{3-n}(CH3)_n^+$ (n=1,2,3) and quaternary ammonium cations with chain length

ranging from C12 to C18, in order to explore the influence of various ammonium cations on MGD interlayer distance and layered structure.

It is possible to control interlayer distance and grafting density by covalent modification of the MGD interlayer surface. Mostly MGD intercalated by alkylammonium cations have been used as intermediates. Layered silicates can be modified covalently by various silanes, known as silylation. Okutomo et al.[80] used the dodecyltrimethylammonium-exchanged MGD as the intermediate and studied silylation of MGD by trimethylchrolosilane, triethylchlorosilane, triisopropylchlorosilane, butyldimethylchlorosilane, octyldimethylchlorosilane, and octadecyldimethylchlorosilane. Isoda et al.[81] successfully reacted γ-methacryloxypropyltrimethoxysilane with dodecyltrimethylammonium-exchanged MGD. Fujita et al.[82] used various amounts of octyltrichlorosilane to react with dodecyltrimethylammonium-exchanged magadiite. They found for samples reacted with lower amounts of silane, the resulting MGD absorbed more alcohol guest molecules and showed larger final interlayer distance. The covalent modifications make it possible for MGD to immobilize various functional groups. The resulting silane functionlized MGD may have a wide variety of applications, such as selective adsorbents, nanoparticle supports, and active fillers for nanocomposites.[70]

1.3.4 Magadiite/Polymer Composites

Magadiite has not been used as widely as MMT as the inorganic filler in polymer composites. Several reports describe the use of MGD in epoxy, polystyrene, and SBR composites in order to compare the reinforcement performance directly with composites based on MMT. In Hansen et al.'s work,[83] after MGD was treated by

cetyltrimethylammonium cations (CTA^+) the resulting CTA-MGD was intercalated with 3-(2-aminoethylamino) propyltrimethoxysilane (AAPTS) or aminopropylmethyldiethydiethoxysilane (APMDS). The AAPTS-MGD and APMDS-MGD had interlayer distances of 2.419 nm and 1.862 nm, respectively. AAPTS-MGD was mixed with SBR prepolymer in toluene suspension, with the mass ratio of modified MGD to SBR at 1:20. AAPTS-MGD/SBR had exfoliated structure based on XRD results. AAPTS-MGD/SBR and APMDS-MGD/SBR had a 3.4% and 3.1% reduction, respectively, in gas permeability compared to the control SBR. However, mechanical properties of composites were not reported. A considerable amount of toluene was needed to achieve MGD exfoliation via this preparation method, which is not practical in industry.

Wang et al.[84] treated MGD with styryldimethylhexadecylammonium cations, and the resulting organo-MGD (OMGD) was used to prepare polystyrene nanocomposites via bulk polymerization. The mass ratio of OMGD to monomeric styrene was 3:100. They also prepared OMMT/PS composites using the same procedure.[85,86] OMGD/PS composites showed better Young's modulus than OMMT/PS composites. They speculated the larger MGD platelets might provide stronger filler-polymer interaction. Wang et al.[78] modified MGD with a mix of octadecylammonium cations and octadecylamine. By adjusting the ratio of octadecylammonium cations to octadecylamine, three OMGD structures were obtained: monolayer, lipid, and paraffin structure. These three OMGD materials were reacted with epoxide resins to form OMGD/epoxy composites with 15 wt% OMGD content. The paraffin-like OMGD was the only one to form exfoliated structure in epoxy. It also showed superior tensile strength compared to

pristine MGD and lipid-like OMGD composites. Wang and Pinnavaia[79] also prepared epoxy nanocomposites with various octadecylammonium $Ch_3(CH_2)_{17}NH_{3-n}(CH3)_n^+$ (n=1,2,3) exchanged MGD, denoted as C18A1M-, C18A2M-, and C18A3M-MGD. Composite tensile strength was higher in exfoliated epoxy nanocomposites obtained from C18A1M-MGD and C18A2M-MGD compared to the intercalated structure formed by C18A1M-MGD. At the same time, they also prepared composites of C18A-MMT and epoxy using the same procedure in order to compare with the reinforcement of C18A-MGD directly. When filler loading (wt% SiO_2) was below 5 wt%, C18A-MGD and C18A-MMT showed comparable properties. When filler loading (wt% SiO_2) was higher than 5 wt%, C18A-MMT showed better reinforcement as measured by tensile strength and modulus.

Some previous work aimed at preparing MGD/polymer composites for flame retardancy applications.[87] Wang et al.[84] prepared polystyrene (PS) composites with MGD exchanged with styryldimethylhexadecylammonium cations via bulk polymerization. SEM images of MGD/PS composites clearly showed tactoids, indicating poor interaction between filler and matrix. The addition of OMGD did not change the thermal degradation onset and the pathway, which means that organo-MGD was not a fire retardant for PS. Morgan et al.[88] treated MGD with various inorganic and organic cations and prepared MGD/polyethylene-co-vinyl acetate (EVA) composites. Compared to organo-MGD, pristine MGD showed the better flammability performance in EVA. It was speculated that MGD formed silicate glass to reduce the mass transfer during flaming.

Previous research on MGD/SBR was carried on by Dr. Shigeng Li in his dissertation research in the Ploehn group.[75] The objective of his research was to

investigate MGD as an alternative filler material to silica. MGD has similar surface chemistry to silica, but different filler particle shapes and sizes. Comparing MGD and silica as fillers in SBR was carried out to explore reinforcement mechanisms and energy dissipation in platelet-filled elastomers. In Dr. Li's work, he generally made three types of MGD/SBR composite materials: (1) unmodified MGD in SBR, (2) CTAB pretreated MGD in SBR and (3) SI-69 pre-functionalized CTA-MGD in SBR. For samples with unmodified MGD, the MGD did not disperse well during batch mixing with SBR pre-polymer. Consequently the mechanical properties of cured MGD/SBR composites were poor compared to silica/SBR.

The most interesting material was prepared by blending CTA-MGD with SI-69 and SBR pre-polymer in the batch mixer. The incorporation of CTA^+ expanded the interlayer space of MGD interlayers. The interlayer surface area was believed to be more accessible to SBR pre-polymer in batch mixing, resulting more intimate interaction between the SBR matrix and MGD. CTA-MGD/SBR has improved mechanical properties compared to those of silica/SBR composites based on DMA and tensile test results.

In addition to exploring CTA-MGD/SBR, Li also investigated pre-grafting SI-69 onto MGD and preparing composites using those sulfur-modified fillers. In this work, he found that the added SI-69 would graft onto the MGD interlayer surface, replacing bulky CTA^+. When the graft density of SI-69 on MGD surfaces was high, SBR prepolymer would not enter into the MGD interlayer space. The resulting composites did not have improved mechanical properties. However, when lower amounts of SI-69 were grafted onto the MGD interlayer surface, not all of the CTA^+ was displaced, and the interlayer

spacing remained almost the same as that of CTA-MGD. The composites prepared from the MGD with low SI-69 grafted amounts had the best mechanical properties, superior to those of silica/SBR. However, these composites were prepared without added sulfur as the curing agent, so they did not have mechanical properties as good as those of CTA-MGD/SBR prepared with both added SI-69 and sulfur.

1.4 Squalene Research Review

The previous research of Li[75] showed that MGD with pre-grafted sulfur-functional silanes might be useful. The ability of SBR prepolymer to enter the MGD interlayer space depends on the silane grafting density and possibly other factors. Unfortunately, testing the usefulness of silane-functionalized MGD required the preparation of elastomer composites and characterization of composite structure and properties, which is a long, labor-intensive process. In the present work, Li's sulfur-functionalized MGD materials were reacted with squalene, a model compound for NR, to test the accessibility of MGD interlayers. This work is described in Chapter 2.

Squalene (SQ) is a natural 30-carbon organic compound with six double bonds. It was originally obtained from shark liver oil. Today, plant materials are now used as a source of squalene, including amaranth seed, rice bran, wheat germ, and olives.[89] The structures of squalene and NR are shown in Scheme 1.3.

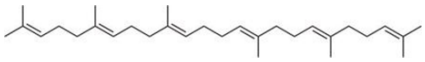

(a) squalene

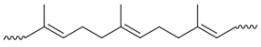

(a) natural rubber

Scheme 1.3 Structures of (a) squalene and (b) natural rubber.

Due to its structural similarity to NR, squalene has been used as a model compound for NR in much research. Bloomfield et al. used SQ in the first published studies of the reactions of sulfur and sulfur compounds with olefinic substances at the end of the 1940s.[90,91] Since then, SQ has been used extensively in the context of the Model Compound Vulcanization (MCV) approach for investigating vulcanization reactions.[92,93] Boretti et al. proved that, compared to simpler model compounds, SQ is a more realistic model compound for polyisoprene in accelerated sulfur vulcanization, because of the adjacent methylenic carbons.[94] Many groups have used SQ/MCV to study various aspects of vulcanization mechanisms, including heating source,[95] filler surface structure,[96] sulfonamide accelerators,[93] zinc oxide, [39,97] and other inorganic activators,[98] and mixed metal oxide nanoparticles.[99]

1.5 Overview of This Work

The overall objective of this work is to study the nanoscale and macro-scale structure of elastomer composites containing layered silicate fillers. It seeks a deeper understanding of the reinforcement mechanisms of layered silicates, mainly MGD, expanded with organic cations and then used in place of silica in realistic tire rubber mixes based on SBR.

As mentioned in section 1.4, Chapter 2 reports on our investigation squalene (SQ), a model compound for NR, which is introduced to explore the ability of elastomer to intercalate into the MGD interlayer space and react with pre-grafted SI-69. This work completes the study of sulfur-functionalized MGD initiated by Li.[75]

Based on Li's dissertation research,[75] CTA-MGD appears to be a promising active filler for SBR. Building upon Li's work, in Chapter 3 we explore various factors that influence the reinforcement mechanism in organo-MGD/elastomer composites. The factors include interlayer expansion by different organic cations, variations in composite formulation (recipe), and variations in processing conditions. MGD structure and the mechanical properties of elastomer composites are characterized, in order to rationalize the relationship between various factors and the reinforcement of elastomer composites by MGD.

In Chapter 4, we compare the SBR mechanical reinforcement by MGD with another widely used layered silicate, montmorillonite (MMT). MGD and MMT are blended into SBR to prepare elastomer composites using the same procedure and recipe. The work aims at comparing the reinforcement of two different layered silicates in rubber composites.

CHAPTER 2

Magadiite Silylated with Sulfur-Functional Organosilanes: Investigation of Structure and Interlayer Accessibility

2.1 Introduction

In Li's previous work[75], organosilane-MGD (OS-MGD) was prepared to explore the influence of silane pre-functionalization on MGD reinforcement. OS-MGD was prepared by reacting CTA-MGD with varying amounts of silane. The OS-MGD showed varying interlayer spacings and silane grafting densities. When a larger amount of silane was used, most of the CTA^+ in CTA-MGD was replaced by silane, resulting in a smaller interlayer spacing and poor mechanical reinforcement in SBR composites. When a lower amount of silane was used, some CTA^+ remained in the interlayers and maintained a large interlayer spacing. The best mechanical properties were observed in SBR filled with OS-MGD with lower silane graft density.

The preparation of rubber composites is complicated, labor- and time-consuming. The cured rubber composites are not soluble in many solvents, which limits the use of characterization methods to study the surface chemistry of the filler. In this chapter, we introduce a small chemical compound, squalene (SQ), to react with OS-MGD in order to study the chemistry of MGD in SBR composites. Much research on rubber vulcanization mechanisms has been carried out using SQ due to its structural similarity (Scheme 1.3) to natural rubber (NR). The reaction of OS-MGD with SQ gives us a way to evaluate the

accessibility of the OS-MGD interlayer to elastomer chains by characterizing the amount of grafting SQ. We also explore the relationship between the initial starting interlayer spacing and the amount of grafting SQ per sulfur site (S-site). To evaluate SQ grafting as a screening test for active fillers in rubber composite formulation, we compare the interlayer spacing of OS-MGD/SBR composites directly with the corresponding layer spacing in OS-MGD/SQ. The preparation and characterization of OS-MGD and OS-MGD/SBR were mostly reported by Li in his dissertation research.[75] In this chapter, we focus on the preparation and characterization of OS-MGD/SQ.

2.2 Materials and Experimental Methods

2.2.1 Material Preparation

2.2.1.1 Modification of Magadiite

Sodium magadiite (Na-MGD) was synthesized using the hydrothermal method[83] and treated with cetyltrimethylammonium bromide (CTAB, Sigma-Aldrich, used as received), resulting in cation exchange of CTA^+ for interlayer protons to produce CTA-MGD.[75]

2.2.1.2 Silylation of CTA-magadiite

Varying amounts of bis-triethoxysilylpropyltetrasulfide (TESPT, also known as SI-69, provided by Michelin Americas Research) were mixed with dried toluene. Then CTA-MGD was added to the SI-69/toluene solution, resulting in various silylated CTA-MGD materials. The samples are denoted as l-SI-69-MGD, m-SI-69-MGD, and h-SI-69-MGD, corresponding to CTA-MGD silylated with low, medium and high initial SI-69

concentration. Another coupling agent, 3-mercaptopropyltriethoxysilane (MPTES, Sigma Aldrich) was also used to prepare silylated CTA-MGD with medium initial concentration. The resulting product was denoted as MPTES-MGD. More details about the reaction may be found in Chapter 3 of Li's dissertation.[75]

2.2.1.3 Squalene Grafting Reaction

Organosilane-grafted MGD (OS-MGD) materials plus appropriate additives (Table 2.1) were dispersed in liquid squalene (SQ, Sigma Aldrich) and subjected to conditions simulating elastomer curing. Liquid SQ was added to a round bottom flask, followed by addition of other chemicals (ZnO, stearic acid, and CBS) with stirring for 20 min. These additives act as activators and accelerators in sulfur-mediated vulcanization. However, no pure sulfur was added in the SQ grafting reaction; the only sulfur in the recipe came from the organosilane grafted on the MGD (OS-MGD). OS-MGD (l-SI-69-MGD, m-SI-69-MGD or MPTES-MGD) was dispersed in the suspension and thoroughly stirred. The flask was then immersed in an oil bath at 150°C and refluxed under N_2 for 24 h. The suspension was cooled and centrifuged, and the solid product was washed with toluene and acetone (twice) to remove excess SQ. The SQ-grafted OS-MGD products (SQ-OS-MGD) were also washed with dilute, aqueous HCl solution (pH 5.0) to dissolve and remove the ZnO. The solid SQ-OS-MGD product was then dried overnight at 80°C.

Table 2.1 List of ingredients and composition used for squalene grafting reactions with organosilane-functional magadiite (OS-MGD).

Ingredients	phr(a)	wt% in mix	weight (g)
squalene	100	93.53	8.999
OS-MGD	2.22	2.08	0.2
ZnO	1.75	1.64	0.1575
stearic acid	1.75	1.64	0.1575
sulfur	0	0	0
CBS (b)	1.2	1.12	0.108
Total	106.92	100	9.622

(a) Parts per hundred rubber by weight.

(b) N-cyclohexyl-2-benzothiazole sulfonamide.

2.2.2 Characterization

Fourier transform infrared spectroscopy (FTIR) measurements utilized a Shimadzu FTIR-8400 spectrometer with a diffuse reflectance solid state attachment (Pike Technologies). FTIR was used to characterize the organic functional groups in organically-modified MGD. Powder samples were placed on the sample stage for measurement.

Thermogravimetric analysis (TGA) data were obtained using a model Q600 TGA (TA Instruments) employing a heating rate of 5ºC/min from room temperature to 800ºC in air. The TGA results were to quantify the amounts of the grafted SQ in MGD.

The structures of various OS-MGD materials were characterized by X-ray diffraction (XRD). XRD patterns were acquired using an X-ray diffractometer (Rigaku Ultima IV, Cu Kα radiation, $\lambda = 1.5418$ Å), typically over the 2θ range of 1-60º with a step size of 0.02º and a scan speed of 1º/min. The XRD measurements were carried out by Dr. Michael Chance and Allison Latshaw from Dr. zur Loye's research group in the Department of Chemistry and Biochemistry.

The weight percentages of C, H, N and S atoms were obtained via elemental analysis (EA, Robertson Microlit Laboratories).

Transmission electron micrographs (TEM) were collected on a Hitachi H8000 transmission electron microscope using an accelerating voltage of 200 kV. TEM was used to observe the morphology of OS-MGD/SQ. The samples were dissolved in CH_2Cl_2 and then ultra-sonicated for 30 min. The resulting solution suspension was dropped onto a lacey carbon grid, dried, and imaged. This work was conducted with the help of Dr. Jibin Zhao from the USC Electron Microscopy Center.

The structures of OS-MGD/SBR composites were characterized by scanning electron microscopy (SEM). SEM images, obtained using a Tescan Vega 3 SBU Variable Pressure SEM, were used to observe the quality of filler dispersion in cured composites. This work was conducted with the help of Dr. Jibin Zhao and Dr. Yingchao Yang from the USC Electron Microscopy Center.

2.3 Results and Discussion

In Li's dissertation research[75], he prepared and characterized all of the OS-MGD materials. His OS-MGD samples were re-characterized in this work (except m- and h-SI-69-MGD) using TGA, EA, and XRD. In all cases, there were no significant differences between our characterization results. In this current work, the composition calculations are based on the TGA (Table 2.2) and EA (Table 2.3) results measured in this study. With regard to TGA results, the weight loss up to 150 ºC is assumed to be due to water loss. There is an extra weight loss above 150 ºC due to MGD dehydroxylation.[75] It is assumed that the ratio of dehydroxylation to residue weight remains constant.[75] The

composition of CTA-MGD and OS-MGD are denoted as $(CTA)_x(OS)_ySi_{14}O_{29}{\cdot}nH_2O$, where x and y indicate the moles of adsorbed CTA^+ and grafting organosilane ("OS") in each unit cell.

For m- and h-SI-69-MGD, grafted silane displaced most of the CTA^+ in the MGD interlayers, resulting in much lower organic weight losses compared to those for CTA-MGD and l-SI-69-MGD (Table 2.2). A considerable amount of CTA^+ was left in the l-SI-69-MGD interlayers, which correlates with the FTIR results from previous work.[75] In the EA results for CTA-MGD and OS-MGD materials (Table 2.3), N% and S% were from CTA^+ and silane SI-69, respectively. The material compositions (Table 2.3) were calculated based on both TGA and EA results. For example, m-SI-69-MGD contains 0.09 mol of CTA^+ and 0.5 mol of SI-69 per mole of MGD unit cells. Both h- and m-SI-69-MGD have similar amount of CTA^+ and SI-69s. l-SI-69-MGD has much more CTA^+ and less SI-69 per MGD unit cell compared to h- and m-SI-69-MGD, due to less intercalation by SI-69 in the l-SI-69-MGD sample. The moles of MPTES per mole of unit cells in MPTES-MGD is two times as much as that for m-SI-69-MGD, which is expected in terms of the silane packing structure in the interlayers. More details about the calculations are shown in Chapter 4 in Li's dissertation.[75]

Table 2.2 Summary of TGA results for CTA-MGD and OS-MGD materials.

Sample	TGA weight (mg)	Residue($Si_{14}O_{29}$) (%)	Dehydroxylation (%)	Water (%)	Organic loss (%)
CTA-MGD	14.81	63.2	1.58	5.24	29.98
h-SI-69-MGD	11.66	80.34	2.01	2.77	14.88
m-SI-69-MGD	14.30	79.27	1.98	2.77	15.98
l-SI-69-MGD	6.28	69.81	1.75	4.19	24.25
MPTES-MGD	12.94	80.67	2.02	3.38	13.93

Table 2.3 Summary of EA results and composition for CTA-MGD and OS-MGD materials; the compositions are denoted as (CTA)x(OS)ySi14O29·nH2O where "OS" stands for organosilane.

Sample	C%	H%	N%	S%	Composition	
					x	y
CTA-MGD	21.43	4.54	1.31	0	1.24	0
h-SI-69-MGD	8.87	1.6	0.12	6.09	0.09	0.5
m-SI-69-MGD	8.94	1.74	0.14	6.47	0.12	0.59
l-SI-69-MGD	18.46	3.97	1.09	1.07	0.95	0.1
MPTES-MGD	10.14	2.3	0.43	3.4	0.35	1.2

After grafting SI-69 or MPTES on the MGD interlayer surfaces, we then treat the OS-MGD materials with SQ in an attempt to simulate the reaction between OS-MGD with SBR. The recipe of the SQ reaction (Table 2.1) is the same as that of MGD/SBR composites prepared previously[75] and in this work (Chapter 3), except that the SQ reaction has no added sulfur.

After reacting with SQ, the interlayer spacing of m-SI-69-MGD increased from 2.26 nm to 2.32 nm (Figure 2.1), a change of 0.06 nm. The layer spacing of MPTES-MGD increased from 2.15 nm to 2.23 nm (Figure 2.2) after reacting with SQ, an expansion of 0.08 nm. m-SI-69-MGD and MPTES-MGD show similar interlayer

expansion. Considering the initial m-SI-69-MGD and MPTES-MGD, most of CTA^+ had been replaced by silane coupling agent due to the moderately high OS concentration (Table 2.3), resulting in MGD interlayer collapse and low OS-MGD interlayer spacing (Figure 2.2). The MGD layers might be physically adhered or chemically crosslinked to each other. Consequently the SQ was unable to enter the interlayer space, resulting in little additional interlayer expansion (no more than 0.1 nm).

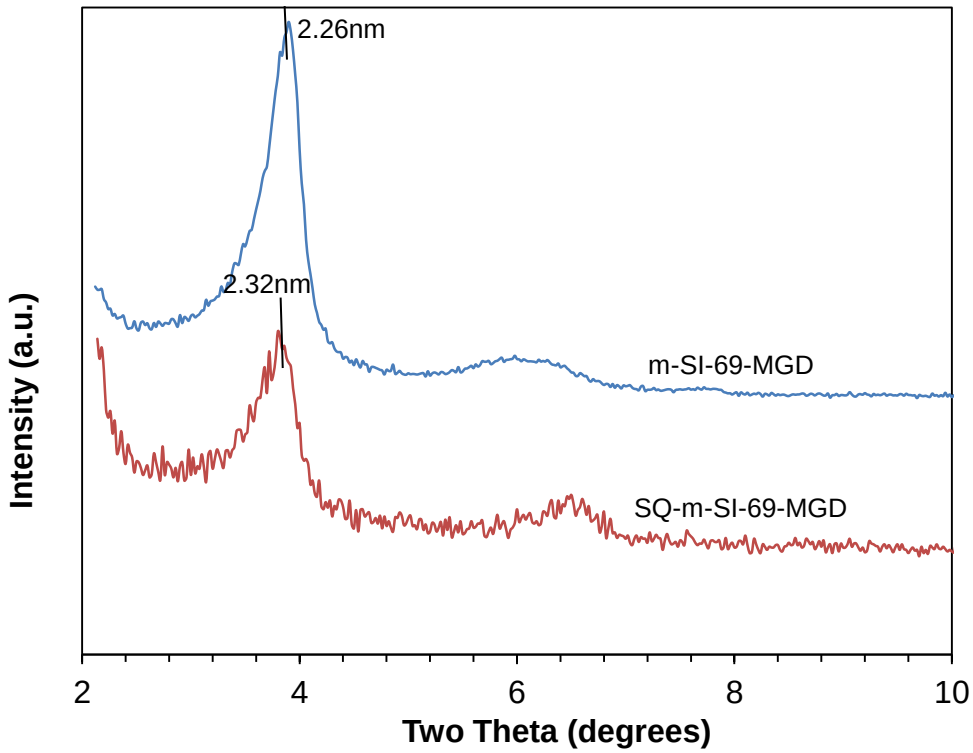

Figure 2.1 XRD patterns for m-SI-69-MGD and m-SI-69-MGD/SQ.

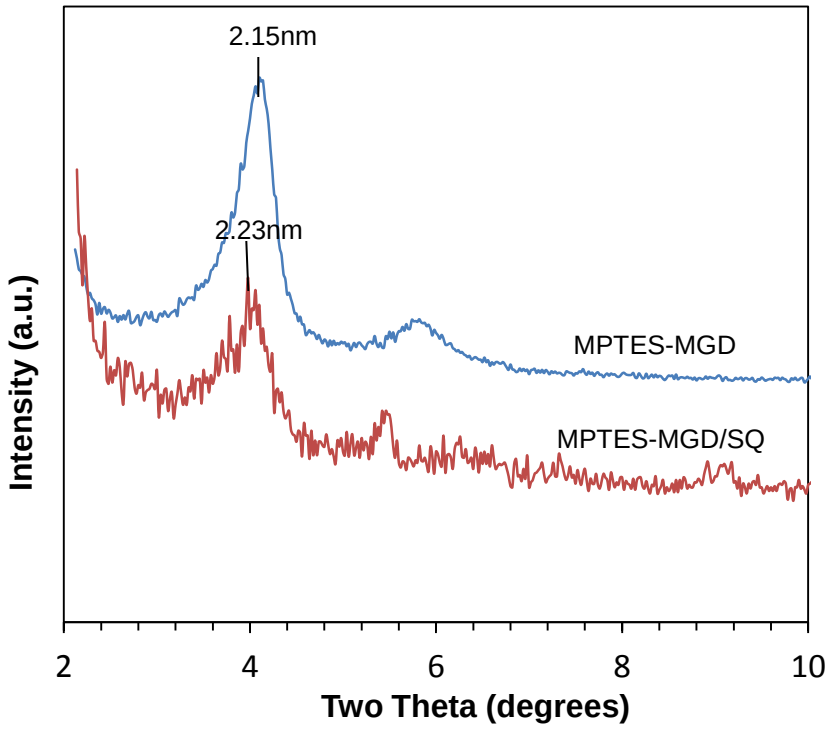

Figure 2.2 XRD patterns for MPTES-MGD and MPTES-MGD/SQ.

Figure 2.3 shows that after reacting with SQ, the interlayer spacing of l-SI-69-MGD increased from 2.88 nm to 3.77 nm. The interlayer space expansion is 0.89 nm, which is much larger than those of the other two OS-MGD with higher degree of silylation. l-SI-69-MGD was prepared with a lower concentration of SI-69, resulting in lower graft density with considerable CTA^+ remaining in the interlayer space (Table 2.3). Thus, the interlayer space of l-SI-69-MGD was still well-expanded by CTA^+ (Figure 2.3). The initial interlayer spacing of l-SI-69-MGD (2.88 nm) was larger than those of m-SI-69-MGD (2.26 nm) and MPTES-MGD (2.15 nm). Thus, l-SI-69-MGD was more readily intercalated by SQ, resulting in a greater interlayer expansion.

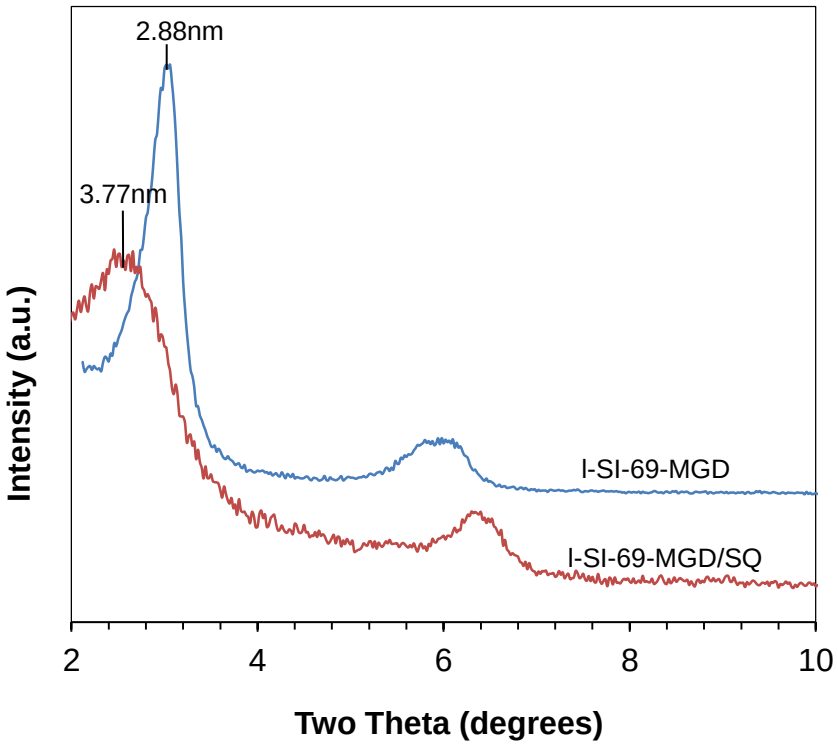

Figure 2.3 XRD patterns for l-SI-69-MGD and l-SI-69-MGD/SQ.

TEM images (Figure 2.4) show the morphology of various OS-MGD/SQ products. The images show a mixture of particles with lower and higher contrast (lighter and darker). The lower contrast particles are OS-MGD, while the higher contrast particles are likely ZnO; this needs to be confirmed based on further characterization using EDS. The dimensions of the OS-MGD particles are up to about 0.5μm, which is consistent with previous studies.[83] However, we do not clearly observe any single platelets in all of the OS-MGD/SQ materials, indicating that exfoliated structures do not exist in these materials. m-SI-69-MGD/SQ and MPTES-MGD/SQ have rosette morphology, which is similar to the morphology of unexpanded MGD.[80] In contrast, the layers of l-SI-69-MGD/SQ appear to be better expanded; several MGD layers are stacked and no rosette

morphology is observed. Observations from TEM images are consistent with the XRD results. l-SI-69-MGD/SQ has larger interlayer expansion, and the corresponding OS-MGD particles are better expanded and dispersed. For m-SI-69-MGD/SQ and MPTES-MGD/SQ, the interlayer spacings barely increased, indicating little SQ intercalation and poorer particle dispersion, which explains the rosette morphology observed in TEM images.

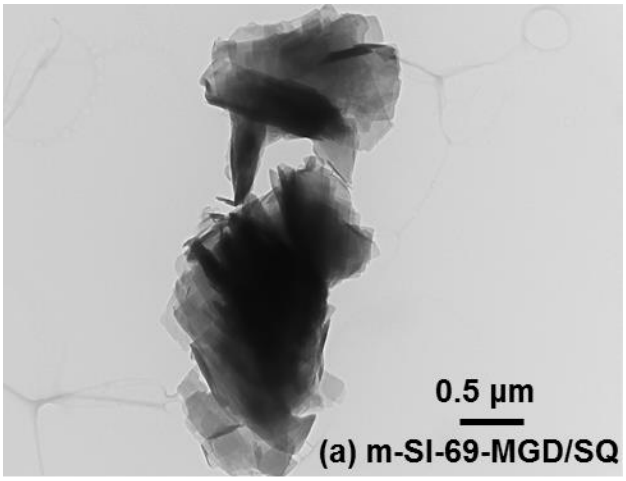

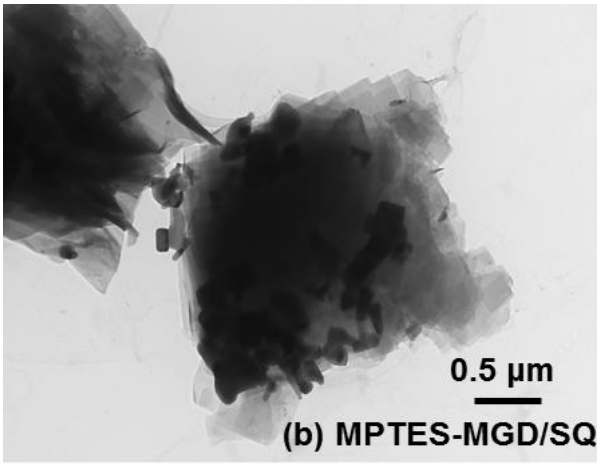

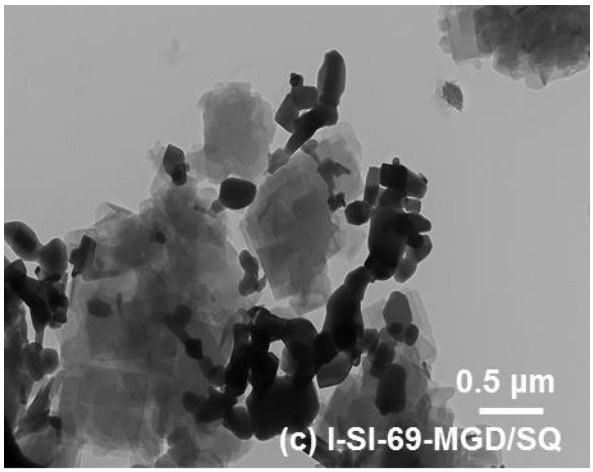

Figure 2.4 TEM images for (a) m-SI-69-MGD/SQ, (b) MPTES-MGD/SQ, and (c) l-SI-69-MGD/SQ.

Figure 2.5 compares the FTIR spectra of SQ and three OS-MGD/SQ samples. In SQ, there are several spectral bands in the C-H stretching region in the range of 2800–3100 cm^{-1}.[100] There are also two characteristic peaks at 1450 cm^{-1} and 1375 cm^{-1} due to C-H deformation in CH_2 and CH_3 groups, respectively.[101] The two peaks appear in pure SQ but not in any OS-MGD and CTA-MGD (Figure 2.6). After reacting SQ with CTA-MGD (product labeled as "CTA-MGD/SQ"), the FTIR spectrum (Figure 2.5) does not have peaks appearing at the two characteristic wavenumber locations of SQ. This indicates that SQ does not graft onto CTA-MGD filler surfaces. In contrast, the SQ characteristic peaks are evident in all of the OS-MGD/SQ samples, indicating that SQ grafts onto the OS-MGD filler surfaces. The only difference between CTA-MGD and OS-MGD is the presence of the grafted silane. Thus, it seems that SQ only grafts onto OS-MGD but not plain CTA-MGD.

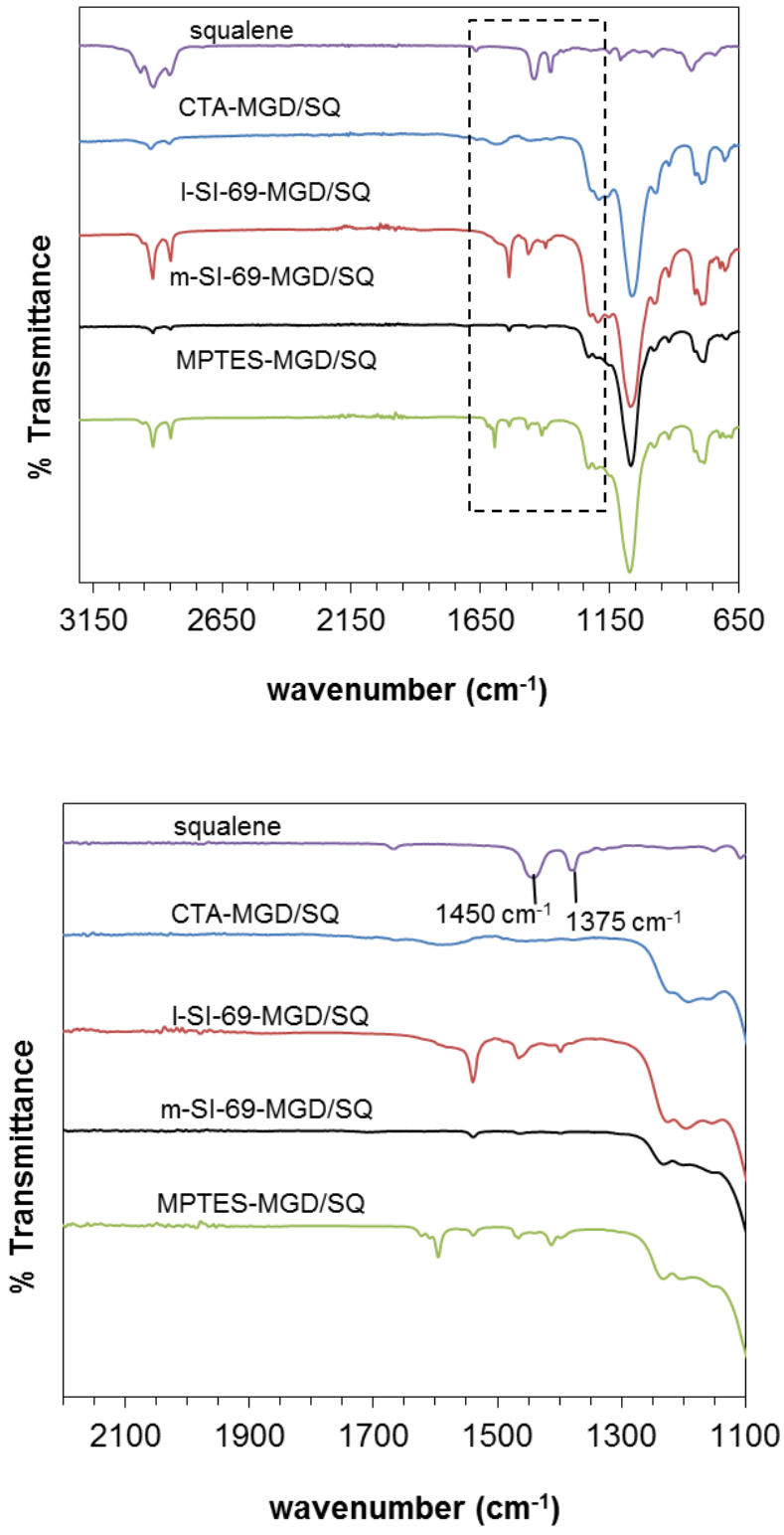

Figure 2.5 IR spectra of SQ, CTA-MGD/SQ, and OS-MGD/SQ. IR spectra with smaller scale are shown for clarity in bottom.

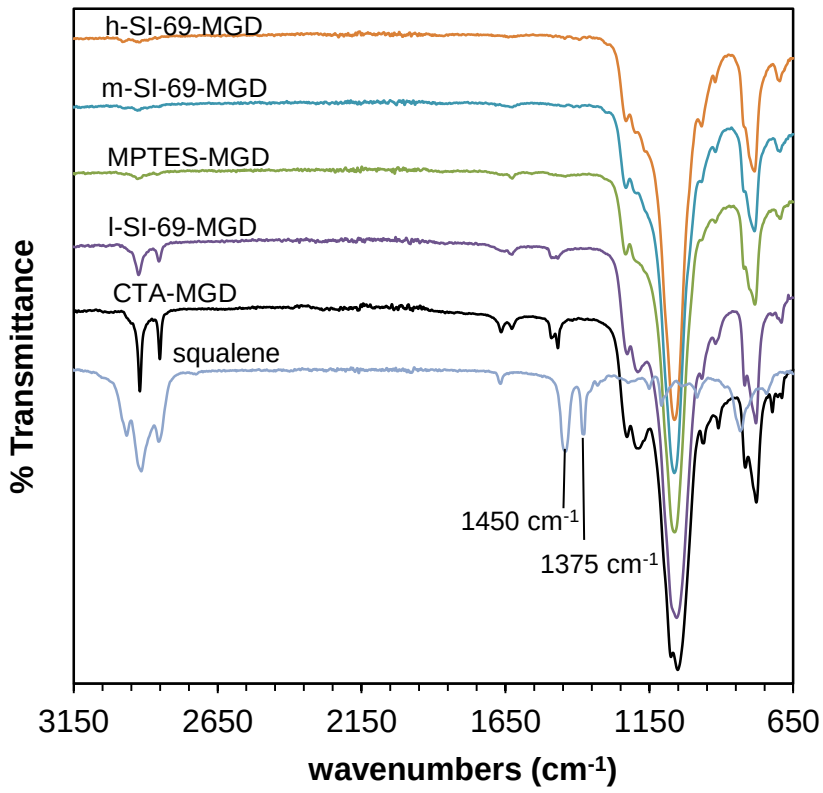

Figure 2.6 IR spectra of SQ, CTA-MGD, and OS-MGD.

Figure 2.7 shows the TGA weight loss for SQ as a function of temperature. The peak of derivative weight loss for SQ decomposition centers around 250 °C. Comparing the TGA weight loss curves of SQ-m-SI-69 (Figure 2.8) and m-SI-69,[75] m-SI-69-MGD/SQ has a broader decomposition temperature range. The peak at 201 °C may be due to decomposition of physically adsorbed SQ because it occurs in the same temperature range as SQ decomposition. Alternately, it may indicate the existence of SQ grafted outside the interlayers. The derivative weight loss peaks at higher temperatures are probably due to the interaction between SQ and OS-MGD. Some SQ may be trapped in the interlayers, resulting extension of the decomposition range to higher temperatures.

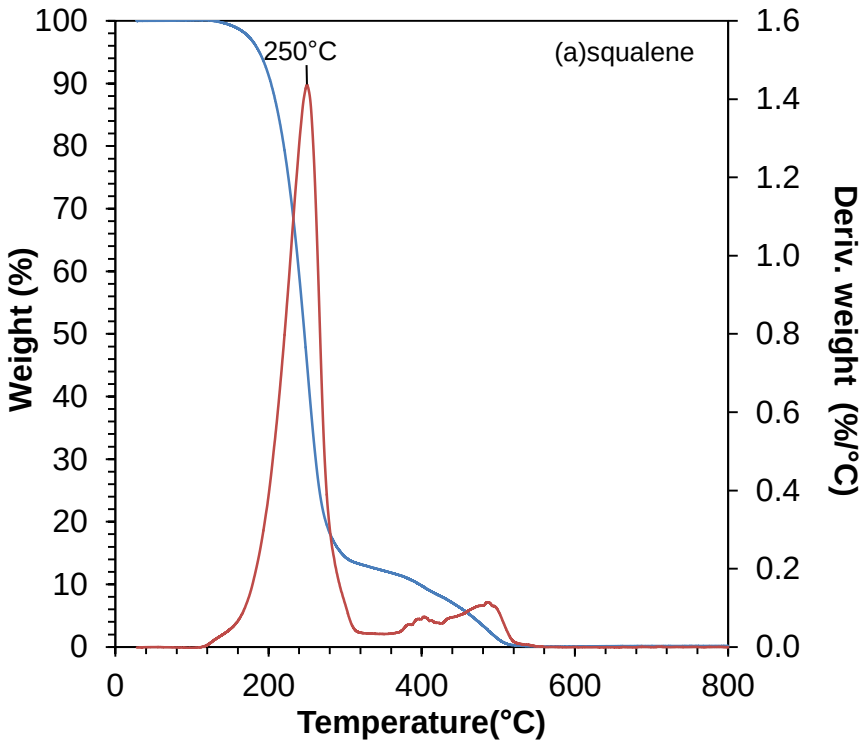

Figure 2.7 TGA weight loss and rate of change (derivative weight) as functions of temperature for pure squalene. The heating rate was 5 °C/min.

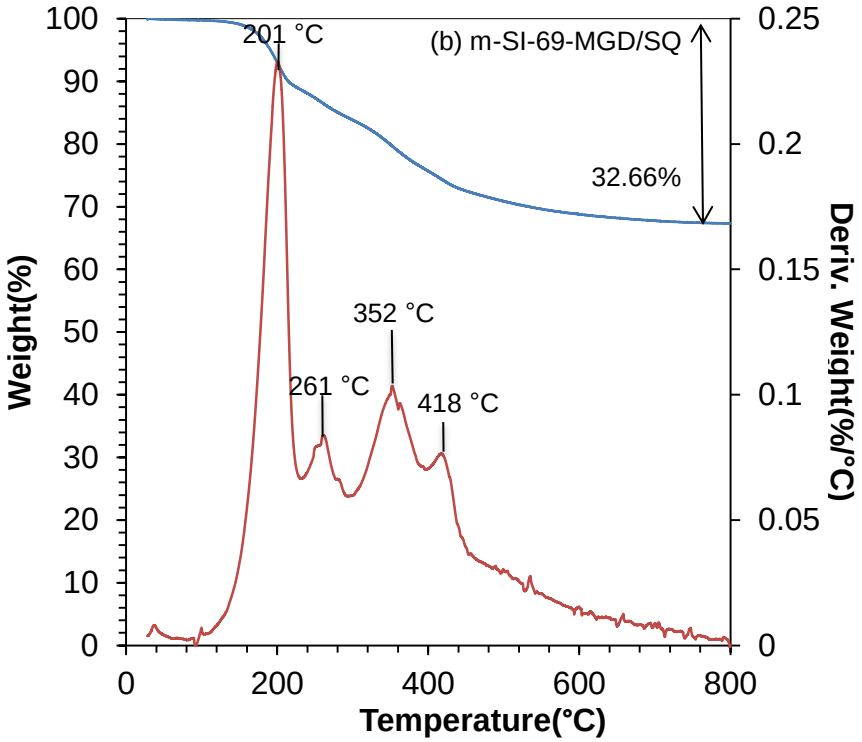

Figure 2.8 TGA weight loss and rate of change (derivative weight) as functions of temperature for m-SI-69-MGD/SQ. The heating rate was 5 °C/min.

We calculate the composition of OS-MGD/SQ (Table 2.5) on the assumption of the composition as $(CTA)_x(OS)_yS_{y'}(SQ)_z\,Si_{14}O_{29}{\cdot}nH_2O$ based on TGA and EA results. In this composition, x, y, y' and z indicate the moles of CTA^+, organo-silane ("OS"), free available sulfur, and SQ per unit cell, respectively. More details about calculating the amount of SQ in m-SI-69-MGD/SQ are shown in Appendix A. The "free available sulfur" represents sulfur measured by EA, beyond that associated with the quantified amount of organosilane. For m-SI-69-MGD/SQ, EA and TGA indicate that the material contains 0.59 mol of grafted SI-69 per mol of MGD unit cells, and thus 1.18 mol/mol of bound S-

sites. In addition, the material contains 0.64 mol/mol of free available sulfur based on 4.26% S from EA.

After m-SI-69-MGD reacts with SQ, both C% and H% increase due to the addition of grafted SQ (Tables 2.3 and 2.5). The organic weight losses for m-SI-69-MGD (Table 2.2) and m-SI-69-MGD/SQ (Table 2.4) are 15.98% and 30.09%, respectively. The extra organic weight loss in m-SI-69-MGD/SQ is due to the presence of grafted SQ. Based on a combination of EA and TGA data (Table 2.5), we estimate that m-SI-69-MGD/SQ contains about 0.58 mol of SQ per MGD unit cell. However, the XRD data (Figure 2.1) clearly shows that the SQ is not located in the MGD interlayer space. Therefore the SQ in m-SI-69-MGD/SQ must be located on the exterior surfaces of the MGD particles.

A simple mechanism may explain all of these results. Upon heating, the m-SI-69-MGD may release its free sulfur (that not linked to carbon atoms), which migrates out of the MGD interlayer and into the liquid SQ. The free S crosslinks SQ molecules, which then either physically adsorb or chemically graft onto the exterior of the MGD particles. This process may promote MGD particle agglomeration (Figure 2.4a) and explain the SQ decomposition at lower temperature seen in Figure 2.8.

Table 2.4 TGA results summary for OS-MGD/SQ products.

Sample	TGA weight (mg)	$Si_{14}O_{29}$ (%)	Dehydroxylation (%)	Water (%)	Organic loss (%)
m-SI-69-MGD/SQ	8.96	67.34	1.68	0.89	30.09
l-SI-69-MGD/SQ	17.79	76.8	1.92	0.48	20.80
MPTES-MGD/SQ	18.33	79.56	1.99	0.53	17.92

Table 2.5 Summary of EA results and composition for OS-MGD/SQ materials. The compositions are denoted as $(CTA)_x(OS)_yS_{y'}(SQ)_z$ $Si_{14}O_{29}\cdot nH_2O$, where x, y, y', and z are the moles of CTA^+, organosilane ("OS"), free sulfur, and squalene, respectively, per MGD unit cell.

Sample	C%	H%	N%	S%	Composition				S-sites	N(SQ):N (S-sites)
					X	Y	Y'	z		
m-SI-69-MGD/SQ	21.21	3.37	0.31	4.26	0.3	0.59	0.64	0.58	1.18	0.49
l-SI-69-MGD/SQ	16.79	2.27	0.42	0.66	0.34	0.1	0.03	0.28	0.2	1.4
MPTES-MGD/SQ	14.68	2.24	0.27	1.66	0.22	1.2	--	0.12	1.2	0.1

The TGA weight loss curve for l-SI-69-MGD/SQ (Figure 2.9) looks similar to that for m-SI-69-MGD/SQ (Figure 2.8), but the final weight losses differ. The derivative weight curves are quite different: l-SI-69-MGD/SQ has a broad peak for derivative weight loss ranging from about 110°C to 520°C. Peaks appear at similar temperatures for both l-SI-69-MGD/SQ and m-SI-69-MGD/SQ. The peak at 198 °C in Figure 2.9 is much smaller than the corresponding peak in Figure 2.8 for m-SI-69-MGD/SQ. Earlier we argued that in m-SI-69-MGD/SQ, all of the SQ is adsorbed or grafted outside the interlayers, resulting in decomposition and weight loss at lower temperature. In contrast, in l-SI-69-MGD/SQ, there may be only a small portion of SQ physically adsorbed or grafted outside the interlayers. Most of the SQ may be intercalated in the interlayer space because of the larger initial interlayer spacing and the ability of the layers to expand further. This provides additional evidence that the MGD sheets in l-SI-69-MGD are not physically or chemically crosslinked by the SI-69. Also, due to the low SI-69 content, there is not as much as free S available to escape and crosslink the SQ outside the MGD particles. Most of the crosslinked SQ may be intercalated in the MGD. The intercalated SQ is "protected" by the MGD layers, resulting in the decomposition shifting to higher

temperature. The lower amount of SQ crosslinked by free S may reduce the incidence of MGD agglomeration, rationalizing the more dispersed morphology observed in Figure 2.4c.

The organic weight losses for l-SI-69-MGD and l-SI-69-MGD/SQ are 24.25% and 20.80%, respectively (Tables 2.2 and 2.4). After reaction with SQ, the organic weight loss becomes less, which differs from what we observe in m-SI-69-MGD/SQ and m-SI-69-MGD. In m-SI-69-MGD, little CTA^+ remains in the MGD interlayers based on TGA, XRD, and IR results. In contrast, a considerable amount of CTA^+ remains in the l-SI-69-MGD interlayers. After reacting with SQ, some CTA^+ is displaced by SQ, as indicated by the decrease in N% from 1.09% (l-SI-69-MGD, Table 2.3) to 0.42% (l-SI-69-MGD/SQ, Table 2.5). In the final l-SI-69-MGD/SQ product, the weight of grafted SQ is less than that of the displaced CTA^+. The l-SI-69-MGD/SBR product therefore shows lower organic weight loss than the starting l-SI-69-MGD.

MPTES-MGD was prepared with a moderate amount of MPTES, similar to m-SI-69-MGD. However, the TGA weight loss and derivative weight curves for MPTES-MGD/SQ (Figure 2.10) look quite different than those of l-SI-69-MGD/SQ and m-SI-69-MGD/SQ. The derivative weight curve has only a main derivative peak at 309°C. There is no apparent peak appearing in the decomposition temperature range of pure SQ. The observation is what we expected. MPTES does not contain "free sulfur" to produce SQ grafted outside the interlayers, resulting in no decomposition peak at lower temperature as seen in the other products of SQ reaction with OS-MGD. Based on EA and TGA results (Table 2.5), MPTES-MGD/SQ contains 0.12 mol SQ per mol of MGD unit cells, all of it grafted to MGD via MPTES. Based on XRD results (Figure 2.2), some of the SQ

may be grafted in the MGD interlayers, but much is probably grafted on the exterior surfaces of MGD particles. This explains the agglomerated morphology of MPTES-MGD/SQ (Figure 2.4b) and the sharpness of the TGA derivative weight peak (Figure 2.10).

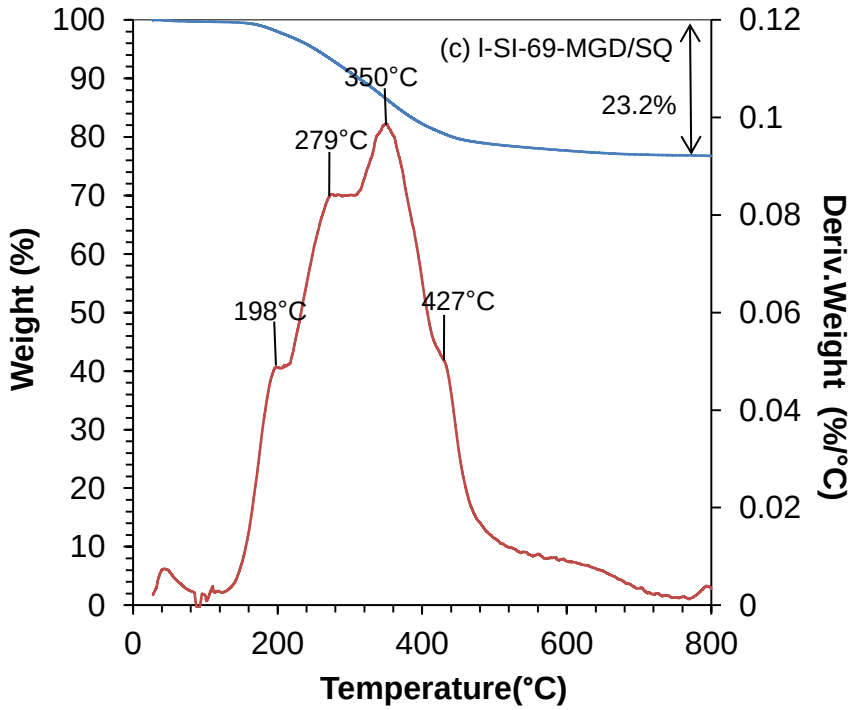

Figure 2.9 TGA weight loss and rate of change (derivative weight) as functions of temperature for l-SI-69-MGD/SQ. The heating rate was 5 °C/min.

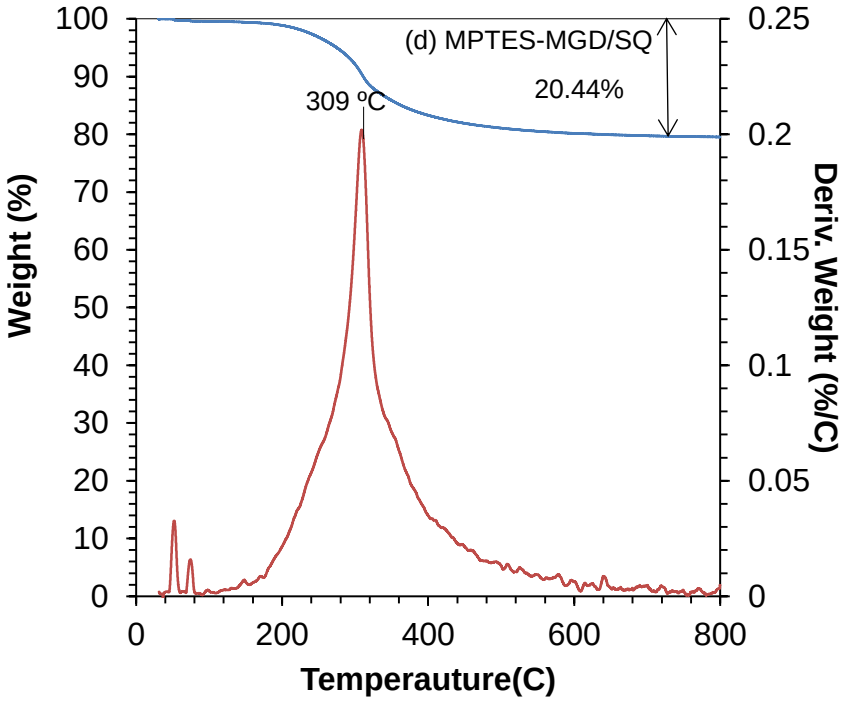

Figure 2.10 TGA weight loss and rate of change (derivative weight) as functions of temperature for MPTES-MGD/SQ. The heating rate was 5 °C/min.

In SI-69-MGD, each grafted SI-69 molecule yields two grafted "S-sites" representing locations for possible crosslinks between the filler and elastomer. The ratio of SQ to S-sites quantifies the efficiency of SQ grafting on the surface of fillers. In Table 2.5, both the amounts of grafted SI-69 and SQ in SQ-l-SI-69 are much less than those for m-SI-69-MGD/SQ, but the ratio of SQ to S-sites for l-SI-69-MGD/SQ is almost three times as much as that for m-SI-69-MGD/SQ.

We speculate that the SQ to S-site ratio is mainly affected by the initial interlayer spacing of OS-MGD. Higher concentrations of l-SI-69-MGD result in displacement of most of the CTA^+, resulting in a smaller initial interlayer spacing in m-SI-69-MGD. The

initial interlayer spacing precludes the intercalation of SQ, limiting the exposure of S-sites to SQ, resulting in less SQ grafted per S-site. It is probable that almost all of the SQ is crosslinked and adsorbed or grafted on the exterior of the MGD particles, away from the S-sites within the MGD interlayer spaces. In contrast, l-SI-69-MGD has larger initial interlayer spacing, allowing more SQ to enter, which enables the full use of the interlayer S-sites to graft SQ. Thus, a larger amount of SQ is attached to each S-site in l-SI-69-MGD compared to that of m-SI-69-MGD.

The tetrasulfane groups of SI-69 break upon heating and release free sulfur. The y' values in Table 2.5 indicate the remaining free available sulfur in OS-MGD/SQ samples. A large amount of free available sulfur remained in m-SI-69-MGD/SQ. This value is almost 30 times as much as that in l-SI-69-MGD/SQ. The free sulfur is either trapped in the interlayers, or escapes to produce SQ-SQ crosslinking outside the interlayers. In m-SI-69-MGD/SQ, the large amount of grafting SQ (Table 2.5) and small interlayer spacing (Figure 2.1) indicate that most free sulfur probably contributed to the SQ-SQ crosslinking outside the interlayers. Little SQ was intercalated, resulting in a small interlayer expansion.

In contrast, for l-SI-69-MGD, due to the low amount of SI-69 present during the SQ reaction, we observe a small amount of SQ grafting to l-SI-69-MGD (Table 2.5). However, the large interlayer expansion of l-SI-69-MGD/SQ (Figure 2.3) indicates that most of the grafted SQ might be located within the MGD interlayer space. Not much SQ was adsorbed or grafted outside the interlayers, which might be explained by the small amount of free sulfur released from the limited SI-69.

Each grafted MPTES molecule yields one S-site and one possible crosslink with elastomer. The ratio of SQ to S-sites is five times lower in MPTES-MGD/SQ than in m-SI-69-MGD/SQ due to the lack of free available sulfur in MPTES. Based on XRD results (Figure 2.2) and the amount of grafted SQ (Table 2.5), MPTES-MGD was barely intercalated by SQ, and little SQ was crosslinked and adsorbed or grafted outside the interlayers.

2.4 Comparison of Organo-silane Modified Magadiite in SQ and SBR.

We propose that SQ grafting may be used as a screening test for OS-MGD/SBR composites. In Li's dissertation research,[75] he studied OS-MGD/SBR prepared with the same recipe as used here to prepare OS-MGD/SQ samples. To date, to our knowledge, there has been no work reporting the use of SQ to study the intercalation chemistry of layered silicates. In this section, we report head-to-head comparisons of the XRD results of OS-MGD/SBR and OS-MGD/SQ in order to study the effectiveness of SQ as a model for predicting the filler behavior in rubber, we also rationalize the relationship between the ratio of SQ to S-sites and OS-MGD reinforcement.

Table 2.6 Interlayer spacings of OS-MGD fillers, OS-MGD/SQ and OS-MGD/SBR composites.

Condition / interlayer spacing (nm) / filler	OS-MGD	OS-MGD/SQ	OS-MGD/SBR
l-SI-69-MGD	2.88	3.77	3.88
m-SI-69-MGD	2.26	2.32	2.32
MPTES-MGD	2.15	2.23	2.31

Table 2.6 shows the interlayer spacings of OS-MGD filler, and the corresponding OS-MGD/SQ and OS-MGD/SBR composites. The interlayer expansions for l-SI-69-MGD are 0.89 nm and 1.00 nm after reacting with SQ and SBR, respectively. The interlayer expansion values for m-SI-69-MGD are both 0.06 nm. The interlayer expansion values for MPTES-MGD are 0.08 nm and 0.16 nm in SQ and SBR composites. Compared to l-SI-69-MGD, both m-SI-69-MGD and MPTES-MGD were barely expanded by SQ and SBR. For all three OS-MGD/SBR composites, the interlayer spacings are either slightly larger or at least equal to those of the corresponding OS-MGD/SQ samples. The slight difference might be due to the strong shear force imparted by the batch mixer during mixing. The similar interlayer spacings between OS-MGD/SBR and OS-MGD/SQ indicate that the SQ reaction successfully simulates the environment during rubber compounding in this work and is able to predict the interlayer spacing of MGD in rubber. The interlayer spacing is one of the most important factors in layered silicate/rubber composite studies. The interlayer spacing predicted by OS-MGD/SQ might be applied to study rubber composites in the future.

In Li's dissertation research[75], he explored the reinforcement of SBR by OS-MGD in OS-MGD/SBR composites. In this current work, the ratio of SQ to S-sites indicates the ability of OS-MGD to graft SQ, which might be relevant to the OS-MGD reinforcement in rubber. L-SI-69-MGD/SQ has a larger SQ to S-site ratio than that for m-SI-69-MGD/SQ (Table 2.5), which correlates with the superior mechanical properties of l-SI-69-MGD/SBR. The SQ to S-site ratio for m-SI-69-MGD/SQ is higher than that for MPTES-MGD/SQ (Table 2.5); however, two corresponding OS-MGD/SBR composites had comparable reinforcement.[75] Compared to MPTES, SI-69 is able to release free

sulfur to produce extra crosslinking, resulting in a higher SQ to S-site ratio. Thus, if using the same kind of silane, the SQ to S-site ratio might be correlated with OS-MGD reinforcement in rubber composites.

2.5 Discussion

Beginning with the sulfur-functional MGD filler prepared in previous work,[75] the accessibility of the sulfur-functional interlayer was evaluated using SQ, a model compound for natural rubber. Various organically-modified MGD materials (CTA-MGD, SI-69-MGD, and MPTES-MGD) were reacted with pure liquid SQ. FTIR results show that SQ can only be grafted onto sulfur-functionalized MGD, but not to plain CTA-MGD. After reacting with SQ, the expansion of OS-MGD interlayers was quantified by XRD. L-SI-69-MGD, with larger initial interlayer spacing, exhibited more SQ intercalation, resulting in even more MGD expansion. In contrast, with smaller initial spacing, m-SI-69-MGD and MPTES-MGD exhibited little additional interlayer expansion after reacting with SQ. The interlayer expansion results were consistent with observations from TEM images. MPTES-MGD/SQ and m-SI-69-MGD/SQ had an aggregated morphology, correlating with less-expanded layers. In contrast, the more-expanded l-SI-69-MGD exhibited less aggregation. TGA and EA results were used to quantify the amount of the grafting SQ and silane. MPTES-MGD and m-SI-69-MGD were barely intercalated by SQ. m-SI-69-MGD/SQ exhibited SQ adsorption or grafting outside the MGD interlayers. This is attributed to the release of excess free sulfur from SI-69, which crosslinks SQ outside of the MGD, followed by physical adsorption or grafting on the exterior surfaces of MGD particles. This promotes MGD particle agglomeration. MPTES-MGD/SQ had little

SQ adsorbed or grafted outside the interlayers due to the absence of free sulfur. In l-SI-69-MGD/SQ, the amount of grafted SQ per unit cell was much lower than m-SI-69-MGD/SQ, but most of the SQ was intercalated into the MGD interlayer. It was calculated that each S-site in l-SI-69-MGD/SQ grafted almost three times more SQ than was grafted in m-SI-69-MGD/SQ.

We reported a head-to-head comparison of XRD results for OS-MGD/SQ and OS-MGD/SBR. For the first time, results from SQ model compound reactions can be used to predict the expansion of the MGD interlayers in MGD/SBR composites. There might be a relationship between the ratio of SQ to S-sites and the magnitude of OS-MGD reinforcement in rubber. As a model molecule for natural rubber, SQ could be used to study the chemistry of layered silicates in natural rubber and other elastomers in order to predict the interlayer spacing and the mechanical reinforcement of layered silicate active fillers.

CHAPTER 3
Organo-MGD/SBR Composites

3.1 Introduction

In previous work on MGD/SBR in our group[75], we began to investigate MGD as a novel filler material in SBR composites. In Dr. Shigeng Li's dissertation research, three types of MGD were studied as fillers in SBR: pristine MGD (Na-MGD), cetyltrimethylammonium (CTA^+) modified MGD (CTA-MGD), and MGD pre-functionalized with sulfur-functional silane (OS-MGD). Na-MGD resulted in poor mechanical reinforcement due to its small interlayer spacing and incompatibility between inorganic Na-MGD and organic polymer. After treatment with CTA^+, the resulting CTA-MGD achieved expanded interlayer spacing and a more "organo-philic" surface. CTA-MGD was intercalated well with SBR based on X-ray diffraction (XRD) results. The final CTA-MGD/SBR composite had superior mechanical properties compared to silica/SBR.

OS-MGD pre-functionlized with varying amounts of sulfur-functional silane were mixed with SBR prepolymer and cured to prepare MGD/SBR composites.[75] The resulting composites show varying MGD interlayer expansion and mechanical reinforcement. In chapter 2, we reported on the use of squalene (SQ) as a model compound for studying the accessibility of OS-MGD interlayer space. The amount of intercalated SQ and the final

MGD interlayer distance were used to quantify the ability of SQ to access the MGD interlayers, which may be determined by the starting interlayer spacing.

As discussed in chapter 2, pre-functionalization of MGD with sulfur-functional silanes was useful for controlling the amount of organosilane grafted onto the MGD. However, the pre-functionalization reaction involves large amounts of toluene and an inert nitrogen atmosphere, which is not practical in industrial processing. In contrast, CTA-MGD showed impressive mechanical reinforcement in CTA-MGD/SBR composites. The CTA^+ cation exchange reaction is a simple process that can be scaled up for industrial production. For this reason, we choose to study mechanical reinforcement of CTA-MGD in more depth to better understand its usefulness for mechanical reinforcement of SBR composites.

In this chapter, we explore various factors that influence reinforcement in organo-MGD/SBR composites (OMGD), such as the relationship between MGD interlayer spacing and mechanical reinforcement in SBR, the reinforcing role of SI-69, the influence of different sulfur sources, and the influence of varying mixing time on filler dispersion and mechanical properties. The impact of CTA^+ on crosslinking is explored in both MGD/SBR and silica/SBR composites. We also prepared MGD/BR and silica/BR composites to explore the MGD reinforcement mechanism in a different elastomer system.

3.1.1 Influence of Varying Interlayer spacing

Extensive research suggests that more intercalated or even exfoliated fillers lead to polymer composites with better mechanical properties.[56,102,103,104] Yehia et al.[56] treated

montmorillonite (MMT) with organic amines of various chain lengths (dodecylamine, hexadecylamine and octadecylamine) and amine-terminated butadiene–acrylonitrile copolymer (ATBN). The various organo-MMT fillers were compared with pristine MMT and carbon black (CB) as reinforcing agents in SBR or NBR. Mechanical reinforcement was characterized by tensile testing. In SBR or NBR, 4 phr ATBN-modified MMT had comparable mechanical reinforcement to 40 phr CB. The reinforcing efficiency increased with the increase of chain length: ATBN > octadecylamine > hexadecylamine > dodecyleamine. Schön et al.[52] used three commercial OMMT (Somasif ME 100, Nanofil, and Nanomer I.42E) to prepare OMMT/SBR composites with 30 phr filler loading. The initial interlayer spacing of OMMT varied from 2.7 nm to 3.6 nm. When the starting interlayer spacing was at 2.7 nm, the SBR polymer was unable to intercalate into the OMMT interlayers during batch mixing. With increasing initial interlayer spacing, the polymer seemed to more easily diffuse into the interlayer space during mixing. Exfoliation/intercalation was observed by TEM after compounding vigorously on a roll mill. With the increasing interlayer spacing of OMMT, OMMT/SBR composite storage modulus increased and loss tangent decreased. Bhowmick and Sadhu et al.[105] reacted MMT with several alkylammonium cations of varying chain length (C_{10}, C_{12}, C_{16} and C_{18}) and compounded the resulting OMMT (4 wt%) into SBR composites. With the increase of alkylammonium chain length, tensile strength and modulus were both improved.

MGD platelets do not exfoliate as readily as MMT, which might be due to stronger van der Waals attraction or hydrogen bonding forces. However, past work clearly shows that intercalation of organic cations leads to MGD interlayer expansion.[43] In this work, we used CTA^+, hexadecylammonium (HDA), and dodecylpyridinium (DP)

cations to treat the MGD, which resulted in OMGD with varying interlayer spacing. Then these fillers were compounded with SBR prepolymer and cured to produce composites. The mechanical properties of these composites were measured. In this way, we hope to rationalize the effect of MGD interlayer expansion on mechanical properties.

Previous work by Li[75] reported XRD characterization of only the starting CTA-MGD filler and the final CTA-MGD/SBR composites. It would help us understand how MGD reinforces the elastomer if we know when the intercalation of SBR occurred during the blending/curing process. Others have explored the interlayer expansion process in other silicate/rubber composites.[106] In this work, we have used XRD to characterize the MGD interlayer spacing at each stage during composite synthesis, including mixing, milling and curing.

3.1.2 Influence of SI-69

Coupling agent bis(3-triethoxysilylpropyl)tetrasulfane, also known as SI-69, is widely used in the tire industry. During vulcanization, the tetrasulfur structure of SI-69 molecules (Scheme 1.1) will break and release two sulfur atoms that are free to participate in elastomer crosslinking. The other two sulfur atoms are still bound to SI-69. The two bound sulfur atoms produce crosslinks between the filler and the elastomers, thus immobilizing the elastomers onto silica surface. In this way, SI-69 improves the mechanical reinforcement of rubber composites.[10]

Due to the chemical similarity of the silica and MGD surfaces, SI-69 may also be used to improve the mechanical properties of MGD/SBR composites. In previous work, Li[75] treated MGD with cetyltrimethylammonium cations (CTA^+), and the resulting CTA-

MGD was compounded with SBR prepolymer with SI-69 added during mixing. XRD results showed that SBR and SI-69 expanded the CTA-MGD interlayer spacing in final cured MGD/SBR composites. Li also pre-functionalized CTA-MGD with varying amounts of SI-69 before batch mixing. This led to different final interlayer spacing in organo silane pre-functionalized MGD (OS-MGD). OS-MGD with the lowest degree of silylation had the largest initial interlayer spacing, and resulted in the highest level of mechanical reinforcement. However, the XRD patterns were only recorded for the final composites. After compounding with SBR prepolymer and SI-69, all of the OS-MGD materials had expanded interlayer spacing. The distinct role of SBR and SI-69 are still unknown. Direct comparison between CTA-MGD/SBR with and without SI-69 has not been made.

In this work, we prepare CTA-MGD/SBR with and without SI-69 and compare the filler dispersion and mechanical properties directly. In order to clarify the role of SI-69 during rubber processing, XRD was used to characterize the interlayer spacing after mixing, milling and curing steps.

3.1.3 Influence of Mixing Time

With the increase of mixing time, the filler dispersion in rubber composites generally improves. Meng et al.[107] explored the effect of mixing time in organo-MMT(OMMT)/polyamide 12 nanocomposites. They observed that with increase of mixing time, OMMT interlayer spacing increased and finally reached exfoliation. This was rationalized in terms of a slippage process of OMMT layers along the lateral direction. In other work on OMMT/polyurethane[108], longer mixing time resulted in increased storage modulus but decreased tensile properties due to the degradation of

polyurethane. Lertwimolnun et al.[109] prepared OMMT/polypropylene nanocomposites with varying mixing time. With increasing mixing time, interlayer spacing remained constant, indicating complete intercalation upon mixing. At the same time, the melt yield stress increased with mixing time, suggesting improvement of filler dispersion. Tunç and Duman[110] found that longer mixing time led to increases in both interlayer spacing and filler dispersion in MMT/methyl cellulose nanocomposites.

These prior results show that longer mixing time results in better filler dispersion. For MGD, what is the ideal batch mixing time? In this work, we prepared MGD/SBR composites using various mixing times and evaluated crosslink density and mechanical performance.

3.1.4 Influence of Surfactant

Organic amines and ammonium cations are well known as efficient accelerators during rubber crosslinking.[2] Song et al.[111] found that the amine groups of OMMT reduced the scorch delay time of SBR and BR composites.[2] Lopez-Manchado et al.[112,113] found that the vulcanization rate increased dramatically in organoclay/natural rubber nanocomposites, which they attributed to amine-treated filler. Mousa[114] found that the crosslink density increased in quaternary amine intercalated MMT/EPDM composites, and they attributed this improvement to both small nanoclay particle size and its amine functionality. Some researchers[115,116] suggested that the presence of amine led to the formation of Zn-sulfur-amine complexes during vulcanization. Ghasemi et al.[117] speculated that surfactant in nanoclay acted as a lubricant, which caused the slippage of rubber chains, thus explaining the increased elongation at break in nanoclay/rubber composites.

In summary, organic amines and ammonium cations found in organo-layered silicates may have a deep influence on rubber crosslinking. Many organic modifiers effectively expand the silicate interlayer space and permit greater elastomer intercalation and increased mechanical reinforcement. The accelerating effect of organic modifiers influences the vulcanization rate and crosslinking density. Intercalated amine and ammonium groups may promote the formation of Zn-sulfur-amine complexes. By enhancing the solubility and reactivity of Zn cations, these complexes amplify the effect of accelerators during vulcanization.[39] Organic modifiers may also act like lubricants to permit more elastomers to penetrate the interlayer, helping to form a well crosslinked structure.[2]

On the other hand, excess organic modifier may weaken the composite network and lead to poor mechanical performance. Wang et al.[78,79] found that in organo-MMT/epoxy composite, at high filler loading, excess ammonium cations and amines decreased the tensile modulus dramatically. Formulating rubber composites without optimizing the amount of organic modifier in nanoclay might lead to decrease of tensile modulus.

In previous research[75], we speculated that CTA^+ may decrease the crosslink density and shorten the scorch delay time. Further experiments in this work are carried out to explore the influence of CTA^+ on crosslink density and scorch delay in CTA-MGD/SBR and CTA-silica/SBR composites.

3.1.5 Influence of Varying Elastomer

Some research papers[111,118,119] report that clay behavior in elastomer composites depends on the chemistry of the elastomers. Sadhu at al.[119] prepared both BR and SBR composites with MMT and OMMT. They found that polymer bulkiness determined the degree of polymer intercalation or filler exfoliation. In BR, MMT showed an exfoliated structure in MMT/BR composites due to the lack of bulky groups in BR. The bulky benzene groups of SBR limited the ability of polymer to enter into the MMT interlayer. After MMT was cation exchanged with octadecyl ammonium, the resulting OMMT was exfoliated in SBR. It was interesting that OMMT interlayer spacing increased from 1.801 nm to 2.104 nm after compounding into BR, rather than being exfoliated like MMT in BR. It was speculated that the lack of bulky side group in BR made it unable to penetrate the interlayers. Song et al.[111] found that the tensile strength and elongation of OMMT/SBR were significantly improved compared to MMT/SBR. However, the mechanical properties of OMMT/BR were only slightly improved than MMT/BR. OMMT and MMT shows different filler dispersion and mechanical reinforcement in various rubber composites.

In Li's previous work[75], the reinforcement mechanism of CTA-MGD was studied only in SBR composites. Will CTA-MGD show the same filler dispersion and mechanical reinforcement mechanism in BR? In this study, we prepared silica/BR and CTA-MGD/BR composites, and compared their structure and properties with CTA-MGD/SBR and silica/SBR composites. This study helps us have a better understanding of MGD mechanical reinforcement and energy dissipation mechanisms in different rubber composites.

3.2 Materials and Experimental Methods

3.2.1 Material Preparation

3.2.1.1 Modification of MGD

Sodium magadiite (Na-MGD) was synthesized using the hydrothermal method[83] and treated with cetyltrimethylammonium bromide (CTAB, Sigma-Aldrich, used as received), resulting in cation exchange of CTA^+ for interlayer protons to produce CTA-MGD.[75]

Na-MGD was also treated with hexadecylamine (HDA, Sigma-Aldrich, used as received) or dodecylpyridinium chloride (DP, Sigma-Aldrich, used as received) to produce MGD intercalated with these organic cations. For the case of HDA, 12.04 g was added to 2000 mL of deionized (DI) water in a 2500 mL beaker, heated to 60°C, and stirred. With stirring, the solution pH was adjusted to the 8.0-9.0 range by adding 1.0 M aqueous HCl solution. According to Lagaly,[76] pH lower than 7.0 will result in cation exchange of protons for Na^+ and prevent cation exchange with alkylammonium cations. High pH does not protonate HDA to give hexadecylammonium cations (HDA^+) suitable for cation exchange into MGD, leaving behind hexadecylamine that has low water solubility. Na-MGD (24.50g) was added to the HDA solution and stirred for 5 days. The ratio of HDA to MGD was 2.16 mmol/g. The suspension was centrifuged at 4000 rpm for 30 min and then washed and centrifuged twice in 50 vol% acetone to remove the excess HDA. The product was dried in an oven at 50°C overnight, resulting in the final HDA-MGD product.

To prepare DP-MGD, 40 g of DP was added to 1500 mL of DI water in a 2000 mL beaker, heated to 60°C, and stirred. With stirring, the solution pH was adjusted to the 8.0-9.0 range by adding 1.0 M aqueous HCl solution. Na-MGD (30.0 g) was added to the DP solution and stirred for 5 days. The molar ratio of DP to MGD was 4.99 mmol/g. The suspension was centrifuged at 4000 rpm for 30 min and then was washed and centrifuged twice in DI water to remove the excess DP. The product was dried in an oven at 50°C overnight, resulting in the final DP-MGD product.

3.2.1.2 Formulation and Preparation of MGD/SBR Composites

Table 3.1 shows the generic recipe for our MGD/SBR composites. The recipe for CTA-MGD/SBR is the same as that used in previous work.[75] In all cases in this study, the filler weight loading was fixed at 26.34 phr based on the inorganic MGD weight. Linking agent SI-69, ZnO, stearic acid, and an accelerator/activator (diphenyl guanidine, DPG) were added during the mixing process outlined in Table 3.2. The curative (sulfur) and an accelerator (N-cyclohexyl-2-benzothiazole sulfonamide, CBS) were added to the green rubber mixture via processing on a four-roll Brabender mill. Finally, the green rubber mixture was cured in a mold under 20,000 lb compression at 150°C for 1 hour to crosslink the SBR chains.

Table 3.1 Generic recipe for MGD/SBR composites.

	Phr basis	weight (g)
S-SBR	100.00	36.04
Wax	10.00	3.56
Filler	26.34 (a, b)	(b)
SI-69	7.25	2.61
ZnO	1.75	0.63
Steric Acid	1.75	0.63
Sulfur	1.35	0.49
CBS	1.20	0.43
DPG	1.30	0.47

(a) Filler loading based on inorganic content, not including surface modifier.
(b) See other tables for filler loadings (phr and weight basis) for all composites.

Table 3.2 Mixing procedure for preparation of silica/rubber, MGD/rubber and MMT/rubber composites.

Initial Temp: 105°C; Mixing Speed: 70 rpm	
	Mixing Step
1	After preheated to 105 °C, add elastomer, DPG and ½ filler. After piston was down, mix for 1 min.
2	Add ZnO, Stearic acid, and the other ½ filler. After piston was down, mix for 1min.
3	Raise and lower piston. Mix for 2 min.
4	Stop mixer

(1) Filler: silica, CTA-MGD, CTA-silica
(2) Curatives (CBS and sulfur) were added on the mill.

Table 3.2 shows the procedure used to blend SBR prepolymer, filler, ZnO and stearic acid. The fillers were blended with SBR using a ThermoHaake batch mixer. After the batch mixer was pre-heated to 105°C, SBR prepolymer, DPG and one-half of the filler was added into the batch mixer set at 70 rpm. Time was counted after the mixer piston was lowered down. After 1 min of mixing, the piston was raised up, and ZnO, stearic acid and the remaining filler was added. After mixing for another minute, the piston was raised and then lowered down immediately. The mixer was stopped after another 2 min of mixing. Green rubber was peeled off from the two screws and quenched

between iron plates. The mixing temperature and blade torque during the process were recorded by computer.

The curatives, including sulfur and N-cyclohexyl-2-benzothiazylsulfenamide (CBS), were mixed into the green rubber on a Brabender two-roll mill loaned to us by Michelin Americas Research. The temperature of roll surface was 30ºC. The distance between two rolls was adjusted to form a "rolling bank" in order to uniformly blend the curatives into the green rubber. The milled rubber sheet was peeled off from the roll and stored in a refrigerator prior to vulcanization.

After mixing and milling, the milled rubber sheet was cut to fit a curing mold provided by Michelin. The filled curing mold was placed in a Carver press with plates preheated to 150 °C. The press was closed and compressed with a force of 20,000 lb for 60 min. After removing the mold from the press, the mold was quenched by cold water.

Table 3.3 List of samples prepared to explore influence of varying interlayer spacing

Sample	ID	filler Phr (a)	filler Phr (b)	SI-69 Phr	sulfur Phr
CTA-MGD/SBR	YM2003	26.34	40.11	7.25	1.35
DP-MGD/SBR	YM1263	26.34	43.79	7.25	1.35
HDA-MGD/SBR	YM1264	26.34	42.58	7.25	1.35

(a) Filler loading based on inorganic content, not including surface modifier.
(b) Filler loading including organic cationic modifier (CTA^+, HDA^+, DP^+).

Table 3.3 lists all of the samples made with varying organic modifier type (CTA, HDA, or DP). These filler materials were characterized by TGA to determine their organic content. The amount of filler in each sample was adjusted so that the inorganic MGD content in each composite was the same (26.34 phr).

CTA-silica was prepared in the same as CTA-MGD. The untreated silica and CTA^+ treated silica fillers were blended with SBR using a ThermoHaake batch mixer at 105°C and 70 rpm. The filler weight loading was fixed at 26.34 phr based on the inorganic silica weight. Table 3.4 lists the sample recipes, highlighting variations in filler loading.

Table 3.4 List of samples prepared to explore the influence of CTA^+ addition.

Sample	ID	filler Phr (a)	filler Phr (b)	SI-69 Phr	sulfur Phr
Silica/SBR	YM2022	26.34	**29.11**	7.25	1.35
CTA-Silica/SBR	YM2074	26.34	**33.13**	7.25	1.35

(a) Filler loading based on inorganic content, not including surface modifier.
(b) Filler loading including organic cationic modifier CTA^+.

Samples were prepared with and without added SI-69 in order to evaluate the role of coupling agent on MGD/SBR composite properties. During vulcanization, sulfur in SI-69 produces two kinds of crosslinking in the matrix. SI-69 contains approximately four atoms (See Chapter 1, Scheme 1.1): two bound to carbon atoms, and two in the polysulfide chains. The "bound S" reacts with the elastomer prepolymer, resulting in coupling between the filler and the elastomer network. The other sulfur atoms are released and act like "free sulfur" that helps crosslink the prepolymer.

Table 3.5 shows recipes for CTA-MGD/SBR composites prepared with different sulfur sources. CTA-MGD/SBR-1 is the standard recipe. CTA-MGD/SBR-2 has no SI-69 added during mixing. CTA-MGD/SBR-3 has sulfur to make up for all sulfur that would have been added by 7.25 phr SI-69. CTA-MGD/SBR-4 has sulfur to make up for "free

sulfur" from that would have been introduced by 7.25 phr SI-69. Both CTA-MGD/SBR-3 and CTA-MGD/SBR-4 have no SI-69 added.

Table 3.5 List of samples prepared to explore influence of sulfur source. The amounts of sulfur and SI-69 are highlighted.

Sample	ID	filler Phr (a)	filler Phr (b)	SI-69 Phr	sulfur Phr
CTA-MGD/SBR-1	YM2003	26.34	40.11	**7.25**	**1.35**
CTA-MGD/SBR-2	YM2007	26.34	40.11	**0**	**1.35**
CTA-MGD/SBR-5	YM2059	26.34	40.11	**0**	**3.08**
CTA-MGD/SBR-6	YM2061	26.34	40.11	**0**	**2.22**

(a) Filler loading based on inorganic content, not including surface modifier.

(b) Filler loading including organic cationic modifier CTA^+.

Table 3.6 shows recipes for CTA-MGD/SBR composites prepared with different mixing times. The mixing time here specifically means Step 3 in Table 3.2. CTA-MGD/SBR-1 is the standard recipe. CTA-MGD/SBR-2 is mixed for 2 min with no SI-69 added during mixing. CTA-MGD/SBR-3 is mixed for 6 min with added SI-69. CTA-MGD/SBR-4 is mixed for 6 min with no SI-69 added during mixing.

Table 3.6 List of samples prepared to explore the influence of mixing time.

Sample	ID	filler Phr (a)	filler Phr (b)	SI-69 Phr	sulfur Phr	mixing time (min)
CTA-MGD/SBR-1	YM2003	26.34	40.11	**7.25**	1.35	**2**
CTA-MGD/SBR-2	YM2007	26.34	40.11	**0**	1.35	**2**
CTA-MGD/SBR-3	YM2010	26.34	40.11	**7.25**	1.35	**6**
CTA-MGD/SBR-4	YM2012	26.34	40.11	**0**	1.35	**6**

(a) Filler loading based on inorganic content, not including surface modifier.

(b) Filler loading including organic cationic modifier CTA^+.

Table 3.7 shows recipes for CTA-MGD and silica compounded into different elastomers. CTA-MGD/SBR-1 and silica/SBR are standard recipes. CTA-MGD/BR and silica/BR are prepared by the same procedure as the standard recipes, except the rubber prepolymer is different.

Table 3.7 List of samples prepared to explore the influence of varying elastomer chemistry.

Sample	ID	filler Phr (a)	filler Phr (b)	SI-69 Phr	sulfur Phr
Silica/BR	YM2072	26.34	**29.11**	7.25	1.35
CTA-MGD/BR	YM2065	26.34	**40.11**	7.25	1.35
Silica/SBR	YM2022	26.34	**29.11**	7.25	1.35
CTA-MGD/SBR	YM2003	26.34	**40.11**	7.25	1.35

(a) Filler loading based on inorganic content, not including surface modifier.

(b) Filler loading including organic cationic modifier CTA^+.

3.2.2 Characterization Methods

Due to the bulky structure of SBR, the filler surface area might not be entirely accessible. The CTAB molecule has a relatively bulky head group structure. In composite research, CTAB is used to measure the filler surface area, denoted as "CTAB surface area". In this work, CTAB surface area of MGD and silica were measured according to ASTM D6845-02.

Fourier transform infrared spectroscopy (FTIR) measurements utilized a Shimadzu FTIR-8400 spectrometer with a diffuse reflectance solid state attachment (Pike Technologies). FTIR was used to characterize the organic functional groups in organically-modified MGD and silica. Powder samples were placed on the sample stage for measurement.

Thermogravimetric analysis (TGA) data were obtained using a model Q600 TGA (TA Instruments) employing a heating rate of 5ºC/min from room temperature to 800ºC in air. The TGA results were to quantify the amounts of CTA^+, HDA^+, or DP^+ exchanged into MGD or adsorbed onto silica.

The structures of MGD fillers and MGD/SBR composites were characterized by X-ray diffraction (XRD). Uncured rubber XRD samples were prepared using a heated Carver press with the help of Dr. Hongying Zhao. XRD patterns were acquired using an X-ray diffractometer (Rigaku Ultima IV, Cu Kα radiation, $\lambda = 1.5418$ Å), typically over the 2θ range of 1-60º with a step size of 0.02º and a scan speed of 1º/min. The XRD measurements were carried out by Dr. Michael Chance and Allison Latshaw from Dr. zur Loye's research group in the Department of Chemistry and Biochemistry.

The structures of MGD fillers and MGD/SBR composites were also characterized by scanning electron microscopy (SEM). SEM images, obtained using a Tescan Vega 3 SBU Variable Pressure SEM, were used to observe the quality of filler dispersion in cured composites.

nSpec® 3D is an automated, rapid optical microscope that provides surface topographies and quantitative roughness measurements. In this work, three dimensional topography images were generated using an nSpec® 3D system using a 50x objective. Samples were cross-sectioned using a cutter loaded with a fresh razor blade prior to measurement. The scans were measured on the cross-section surface. The dispersion rating takes into account the volume of the agglomerates while ignoring basic surface roughness. The dispersion rating also depends on the applied thresholds for peaks and

valleys. A lower dispersion rating value corresponds to higher dispersion. All filler dispersion ratings were measured by collaborators at Nanotronics Imaging, the manufacturer of nSpec® 3D.

Mechanical properties of elastomer composites were evaluated using dynamic mechanical analysis (DMA) and tensile testing. DMA measurements (model RSA III, TA Instruments Inc.) were carried out at constant frequency (1.0 Hz) and strain amplitude (0.05 %) with temperature ranging from -80 ºC to 60 ºC ramped at 3 ºC/min.

Tensile properties were measured at room temperature with dumbbell specimens (4.80 mm wide and 2.20 mm thick in the cross-section) on a tensile tester (Instron model 5566) with a crosshead speed of 25 mm/min. The strain was measured by crosshead separation distance. Reported tensile test values represent the average of three to four specimens.

The crosslink density in our elastomer composites was measured using a method reported previously.[75] Cured rubber samples were cut into 1.0 g pieces and immersed into 100 mL toluene and stored in darkness for 72 h. The solvent was replaced every day. Just after immersion, the rubber sample weight was W_{sw}. After 72 h immersion, the sample was moved to a vacuum oven to dry for 48 h. After drying, the sample weight was $W_{dry.}$ The volume fraction of rubber $\phi_r$was calculated using

$$\frac{1}{\phi_r} = 1 + \frac{W_{sw}\rho_r}{W_{dry}\rho_t} \tag{3.1}$$

In this equation, ρ_r and ρ_t are densities of rubber and toluene, 1.17 g/cm^3 and 0.87 g/cm^3 respectively.

The crosslink density n is calculated according to Flory-Rehner equation,[120,121,122]

$$\ln(1-\phi_r)+\phi_r+\chi\phi_r^2=V_t n\left(\frac{\phi_r}{2}-\phi_r^{1/3}\right) \tag{3.2}$$

where V_t denotes the molar volume of toluene 106.29 mL/mol. χ denotes the Flory-Huggins interaction coefficient for rubber-toluene. In this work we use χ=0.39.[123,124]

M_c is the average molecular weight between two crosslinks per primary rubber chain. It is calculated using

$$M_c=\frac{\rho_r}{n} \tag{3.3}$$

where ρ_r denotes density of rubber, 1.17 g/cm^3, and n is the measured crosslink density.

A rubber process analyzer (RPA) was used to provide viscoelastic data on materials during the curing process, such as scorch delay, cure rate index and optimum cure time. Samples were measured at a constant temperature of 150°C for 60 min. The scorch delay is defined as the elapsed time from the start of the measurement until the onset of rubber vulcanization or crosslinking.

The Cure Rate Index (*CRI*) is a measure of the rate of the cure reaction, calculated as

$$CRI=100/(T_{c90}-T_{s2}) \tag{3.4}$$

where T_{c90} is the time at which 90% of the final torque is obtained and T_{s2} is the scorch time. *CRI* indicates the degree of activation of the reaction in rubber. All cure curves reported here were measured by collaborators at TA Instruments.

3.3 Results and Discussion

3.3.1 Influence of Interlayer spacing on MGD/SBR Composites

3.3.1.1 Organically-Modified Magadiite Fillers

The CTAB surface area of silica was found to be 150±4 m^2/g. The CTAB surface area of ball-milled MGD was measured as 393±8 m^2/g. Compared to silica, MGD has 162 % more surface area per gram that are available to molecules like CTAB or SBR prepolymer.

TGA results are used to calculate the amounts of organic cations present in organically-modified MGD fillers (Table 3.8). Figure 3.1 shows the weight loss and rate of weight change as functions of temperature for MGD. The weight loss of 12.54% up to 150ºC is attributed to water loss. The total weight loss of 14.46% up to 800°C includes losses due to both water and dehydroxylation loss.[75] Thus the weight loss due to dehydroxylation is 1.92%. The residue weight is 85.54%. As in previous work[75], the ratio of dehydroxylation loss to residue weight is assumed to be constant. This ratio, 1.92%/85.54% = 0.022, is consistent with that found in our previous work.[75]

Table 3.8 TGA results for MGD and organically-modified MGD samples.

Sample	ID	Total Weight Loss (%)			Residue (%)	moles of cations per mole $Si_{14}O_{29}$
		Water (%)	Dehydroxylation (%)	Cations (%)		
MGD	YM1001	14.46			85.54	NA
		12.54	1.92	NA		
CTA-MGD	YM1003	34.33			65.67	1.33
		3.90	1.44	28.99		
DP-MGD	YM1232	39.85			60.15	2.07
		2.50	1.32	36.03		
HDA-MGD	YM1240	39.14			60.86	1.67
		9.36	1.34	28.44		

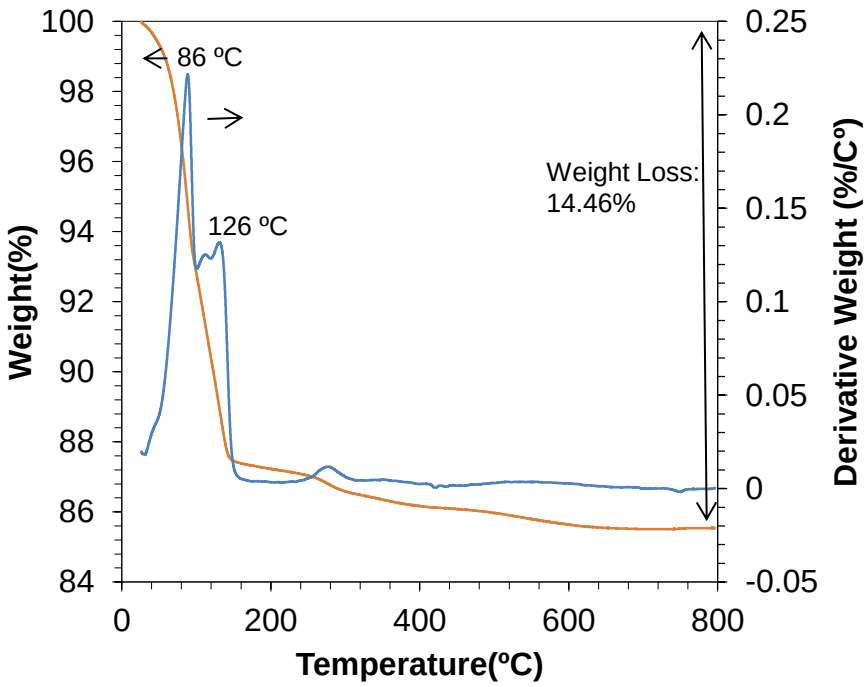

Figure 3.1 TGA weight loss and rate of change (derivative weight) as functions of temperature for MGD. The heating rate was 5°C/min.

Figure 3.2 shows the TGA weight loss of CTA-MGD. The peak at 231°C is due to the decomposition of absorbed CTA^+. The total weight loss, 34.33%, is the combined

loss due to CTA^+ decomposition, water loss, and dehydroxylation loss. The water loss up to 150ºC is 3.90%. The residue weight is 65.67%. Assuming a constant ratio of dehydroxylation loss to residue weight (0.022), the dehydroxylation loss is 1.44%. Subtracting the water and dehydroxylation losses from the total weight loss, the CTA^+ loss is 28.99%. This indicates that CTA-MGD contains 1.33 moles of CTA^+ per mole of $Si_{14}O_{29}$ unit cells (Table 3.8). This calculation agrees with our previous result,[75] which was 1.25 moles CTA^+ per unit cell.

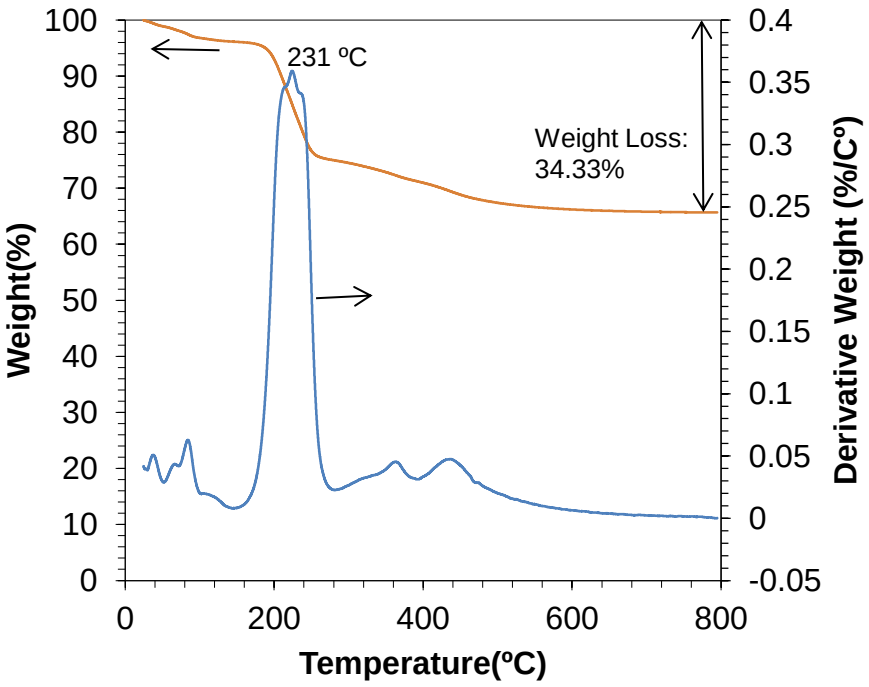

Figure 3.2 TGA weight loss and rate of change (derivative weight) as functions of temperature for CTA-MGD. The heating rate was 5°C/min.

Figure 3.3 shows the TGA weight loss for DP-MGD. The water loss is 2.50% up to 150 ºC. Above this, there are two peaks at 245 ºC and 394 ºC due to the decomposition of absorbed DP^+. Total weight loss is 39.85%, so the residue weight is

60.15%. Considering the 0.022 ratio of dehydroxylation loss to residue weight, the dihydroxylation loss is 0.88%. After deducting dehydrxylation and water loss from the total weight loss, the DP^+ weight loss is 36.03%. This corresponds to 2.07 moles of DP^+ per mole of $Si_{14}O_{29}$ unit cells in DP-MGD (Table 3.8).

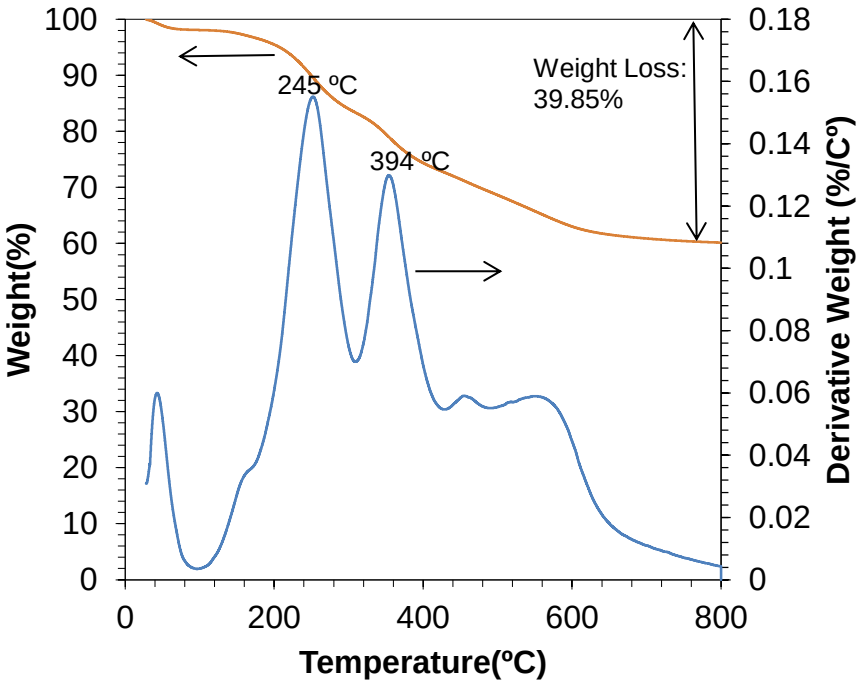

Figure 3.3 TGA weight loss and rate of change (derivative weight) as functions of temperature for DP-MGD. The heating rate was 5°C/min.

Figure 3.4 shows the TGA results for HDA-MGD. Weight loss up to 150 °C (9.36%) is considered to be due to water. Above 150 °C, two peaks at 167°C and 327°C are due to the decomposition of HDA^+. The total weight loss is 39.14%, and the residue weight is 60.86%. The loss due to dehydroxylation is about 1.34 % using the same calculation as for DP-MGD and CTA-MGD. Thus, the weight loss due to HDA^+

decomposition is 28.44%. In HDA-MGD, each mole of $Si_{14}O_{29}$ unit cells contain 1.67 moles of HDA^+ (Table 3.8).

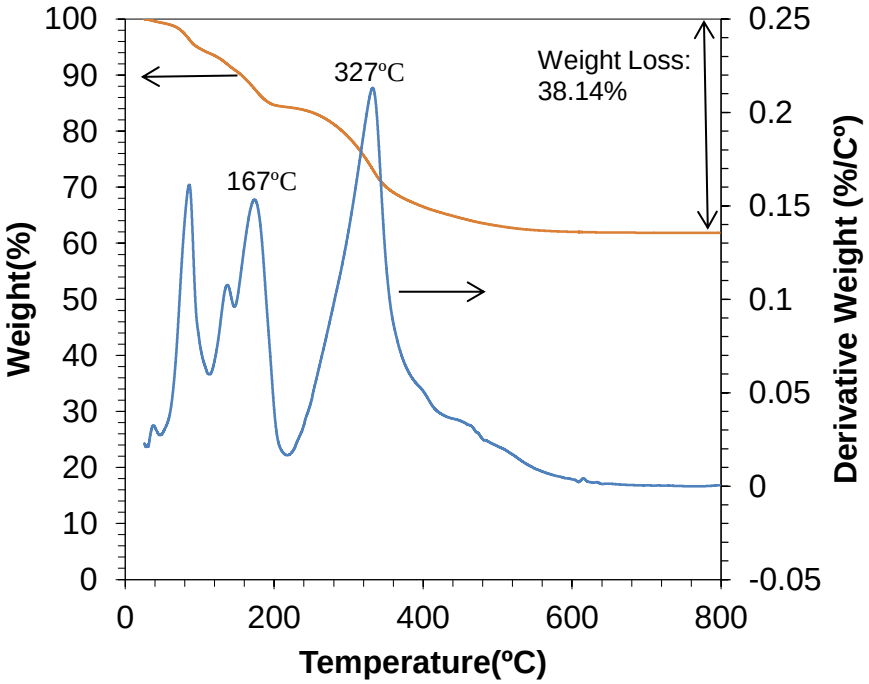

Figure 3.4 TGA loss and rate of change (derivative weight) as functions of temperature for HDA-MGD. The heating rate was 5°C/min.

Figure 3.5 shows FTIR spectra for MGD and organically-modified MGD. After treatment with various organic cations, characteristic CH stretching bands appear at 2916 cm^{-1} and 2849 cm^{-1} and CH_2 scissoring bans at 1467 cm^{-1}. These observations are completely consistent with our previous results.[75] The FTIR characterization results clearly show that various cations have been absorbed onto the MGD surface.

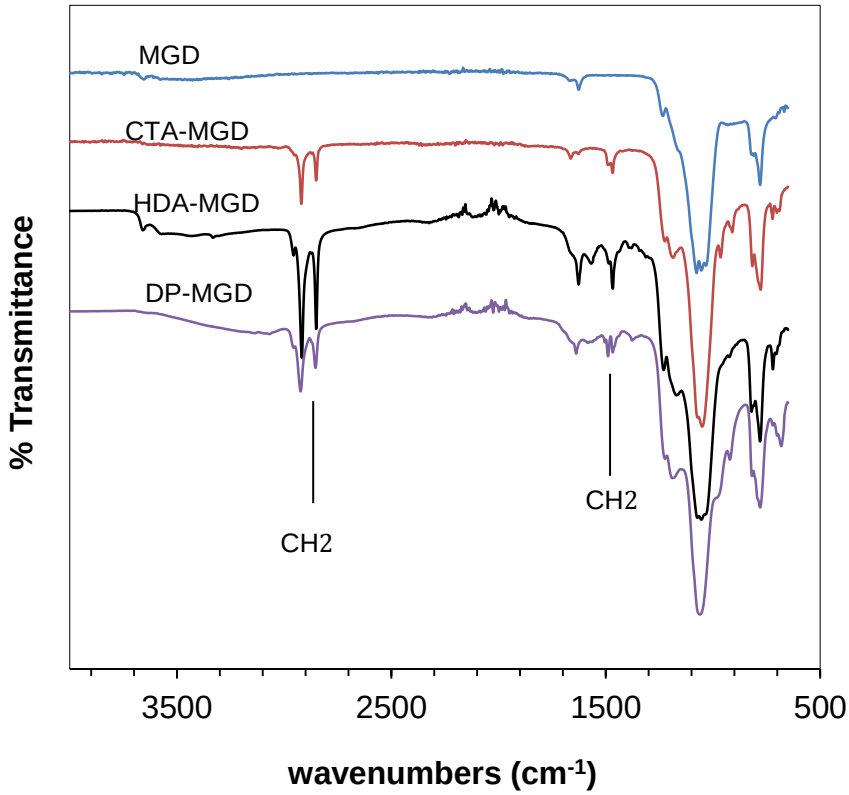

Figure 3.5 FTIR spectra of Na-MGD and organically-modified MGD samples.

XRD patterns (Figure 3.6) provide information on the interlayer spacing in as-prepared Na-MGD and the various OMGD materials used as active fillers in this work. The (001) peak for Na-MGD at 5.7° corresponds to a interlayer spacing of 1.54 nm, in accord with previous results.[83] Cation exchange with CTA^+ leads to uniform expansion of the interlayers, resulting in a measured interlayer spacing of 3.10 nm for CTA-MGD. [75,83] The pattern for CTA-MGD has a second peak at about 5.7°, which we have previously shown to be the CTA-MGD (002) peak, rather than unexpanded Na-MGD.[75] Treatment of Na-MGD with HDA^+ results in considerable expansion of the MGD interlayers: the (001) peak gives an interlayer spacing of 5.81 nm. We are also able to index the (002) and (003) peaks for HDA-MGD. Consequently, the observed peak at about 5.7°

probably represents non-expanded Na-MGD. Treatment of Na-MGD with DP^+ also produces considerable interlayer expansion; peak fitting gives a maximum at 1.78°, corresponding to 4.96 nm interlayer spacing. The breadth of the peak suggests some polydispersity in the interlayer spacing for DP-MGD; however, the absence of any peak at 5.7° suggests uniform expansion and the absence of non-expanded Na-MGD in the DP-MGD material.

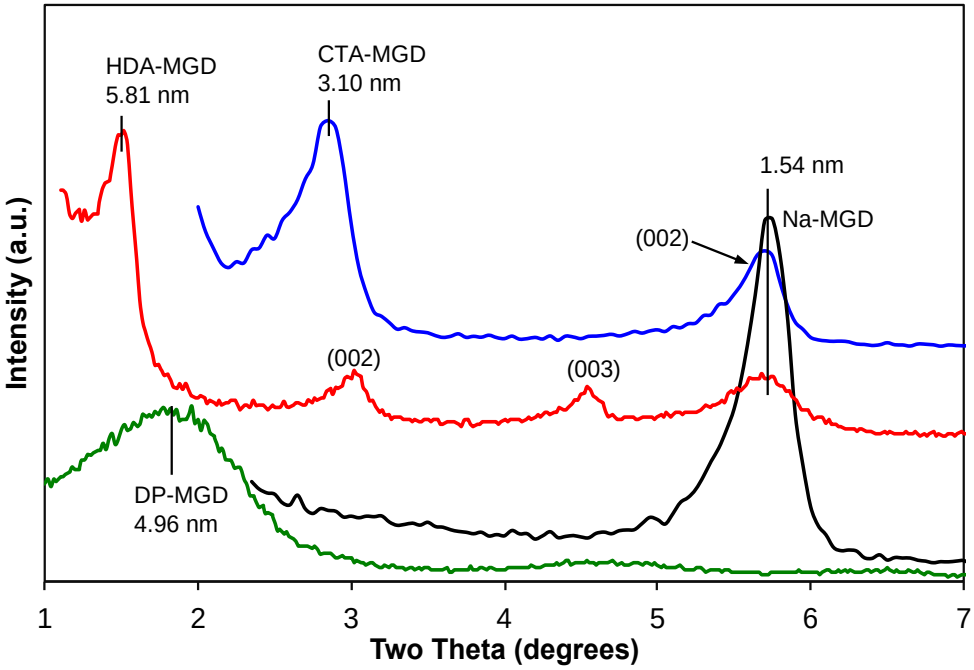

Figure 3.6 XRD patterns for as-prepared Na-MGD and various OMGD materials. All peaks are (001) except as indicated on the plot. Patterns for CTA-MGD and HDA-MGD are shifted upwards for clarity.

3.3.1.2 MGD/SBR Composites

In previous work[75], XRD characterization of MGD/SBR composites showed that SI-69 and SBR expanded the interlayer spacing of CTA-MGD in the final cured composites. However, XRD measurements were not performed to investigate how the

interlayer spacing changed during the various synthesis steps. This question is addressed by the XRD results in Figure 3.7, which compares XRD patterns for the initial CTA-MGD filler and CTA-MGD/SBR composite recorded after each processing step (mixing, milling and curing). The starting CTA-MGD filler has an initial interlayer spacing of 3.10 nm. After batch mixing with SBR and SI-69 for 2 min, the interlayer spacing increased to 4.01 nm. This indicates that some combination of SI-69 and SBR prepolymer intercalated into the CTA-MGD interlayers during the mixing step. After milling with curative addition, the observed interlayer spacing remained unchanged at 4.01 nm. Finally, after curing, the MGD interlayer spacing decreased slightly to 3.91 nm. These results clearly demonstrate that during the preparation of CTA-MGD/SBR composites, intercalation takes place primarily during batch mixing.

Figure 3.8 shows XRD patterns for the initial HDA-MGD filler and HDA-MGD/SBR composite recorded after each processing step (mixing, milling and curing). The starting HDA-MGD filler has a well-ordered layer structure with (001), (002), and (003) peaks at 1.52°, 3.04°, and 4.50°, respectively, all consistent with an initial interlayer spacing of 5.81 nm. In addition, the pattern for HDA-MGD has a significant peak centered at 5.7°, which is consistent with the presence of some Na-MGD that did not undergo cation exchange. After batch mixing with SBR and SI-69 for 2 min, the HDA-MGD interlayer spacing decreases to 4.31 nm, with little change occurring during the subsequent milling step (4.33 nm). The HDA-MGD interlayer spacing increases to 4.66 nm after curing. One cannot say how much of these changes are due to SBR intercalation versus HDA extraction, as suggested below.

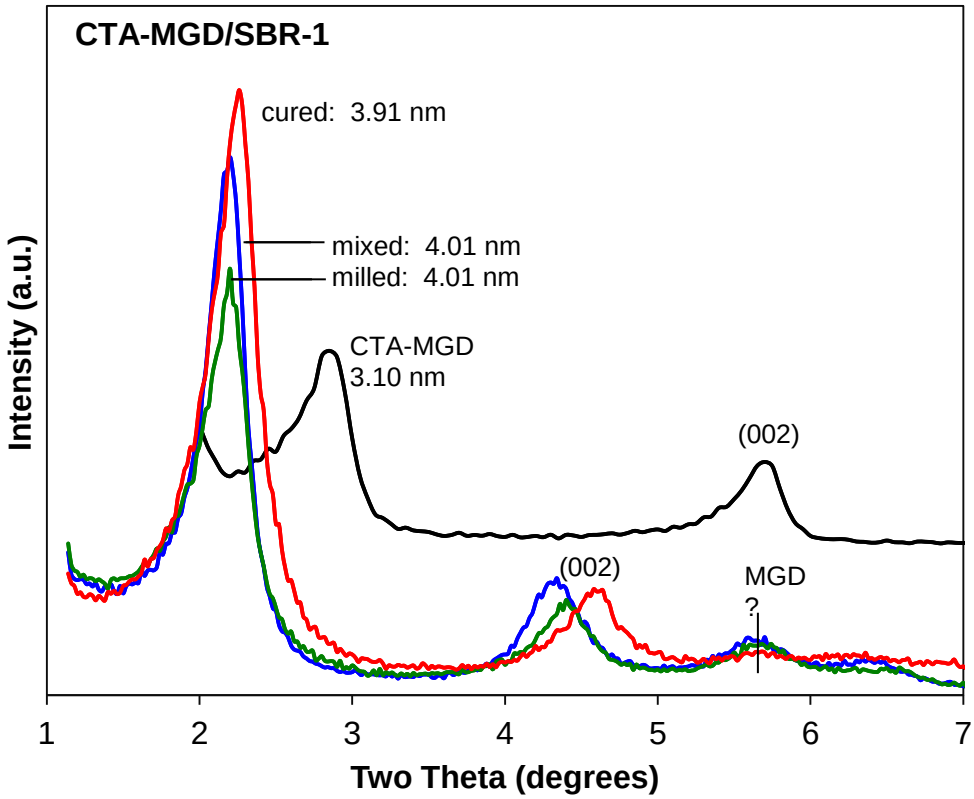

Figure 3.7 XRD patterns for CTA-MGD/SBR-1 composite after batch mixing, milling, and thermal curing (curves labeled “mixed”, “milled”, and “cured”). Composites prepared with SI-69 added in the batch mixing stage.

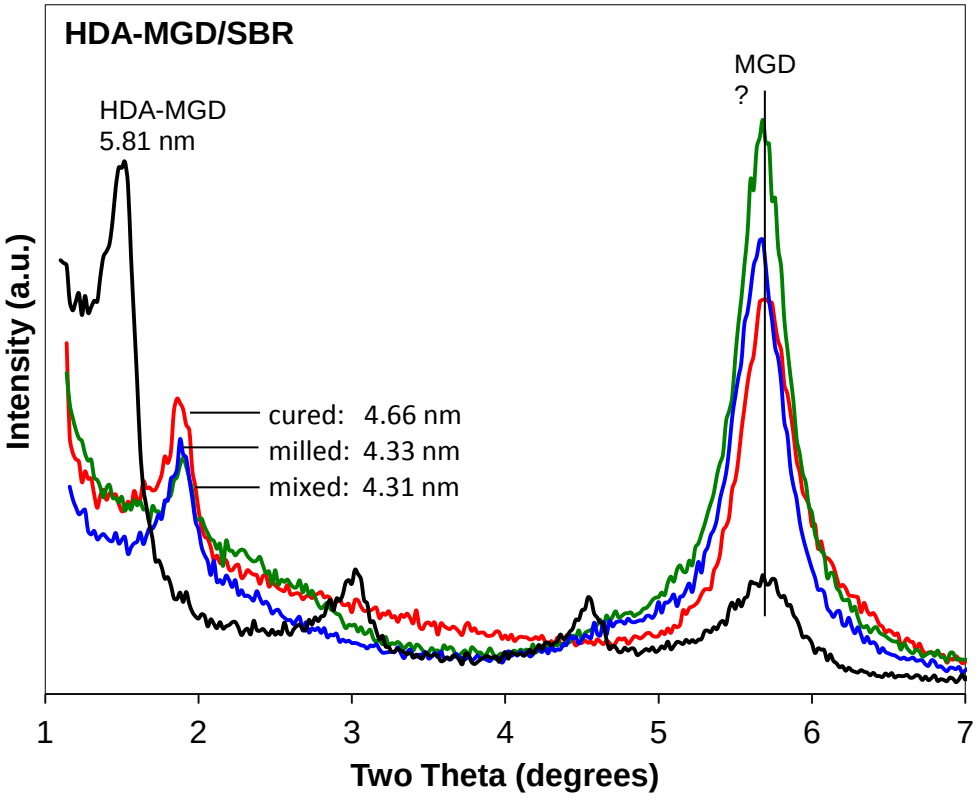

Figure 3.8 XRD patterns for HDA-MGD/SBR composites after batch mixing, milling, and thermal curing (curves labeled "mixed", "milled", and "cured").

The most prominent feature is the dominant peak centered at 5.7° in all of the XRD patterns for the HDA-MGD/SBR composite. This peak appears in the starting HDA-MGD but becomes dominant after batch mixing with SBR, SI-69, ZnO, and stearic acid; the location of the peak does not shift significantly during subsequent milling and curing stages. This evidence suggests that the HDA bilayers can support the considerable expansion seen in HDA-MGD, but the structure does not have sufficient stability to survive the mixing process, resulting in interlayer collapse.[76] As suggested by previous research[75], we speculate that Zn (from ZnO) and/or stearic acid may be forming complexes with HDA, resulting in its extraction from the MGD interlayer spaces. This

would account for the collapse of the MGD layers, leading to a distribution of interlayer spacing values centered near that of Na-MGD, approximately 1.54 nm.

In contrast, the XRD patterns for DP-MGD and its SBR composites (Figure 3.9) do not show any evidence of either non-expanded Na-MGD in the starting DP-MGD, nor collapsed "bare" MGD in the mixed, milled, or cured composites. The starting DP-MGD has a relatively broad but distinct (001) peak centered near 2.0°, indicating a interlayer spacing of 4.96 nm. During the mixing stage, the DP-MGD interlayer spacing decreases to about 4.44 nm, with little change observed after the subsequent milling and curing stages (4.42 and 4.37 nm, respectively). All of the XRD patterns for DP-MGD/SBR composites manifest (002) and (003) peaks consistent with the indicated (001) peaks, indicating a layered structure that does not change much after mixing. Based on these results, we cannot say how much SBR or SI-69 has intercalated into the interlayer space, or if any DP has been extracted. However, the XRD patterns show that DP-MGD does not undergo layer collapse during the synthesis of DP-MGD/SBR composites.

Despite the fact that DP has a shorter alkyl chain length than CTA (12 versus 16 carbons), the DP-MGD filler material has a much larger interlayer spacing (4.96 nm) than CTA-MGD (3.10 nm). This may be due to the bulkiness of DP's pyridinium head group, its orientation on the MGD surface, and the influence of these factors on alkyl chain ordering, tilt angle, and bilayer interpenetration in the MGD interlayer space.[75] Upon incorporation in SBR, the evolution of layer structure in DP-MGD/SBR is similar to that observed for CTA-MGD/SBR-1 (Figure 3.7): in both cases, the MGD interlayer spacing does not change much during the milling and curing stages. The final interlayer spacing

values in DP-MGD/SBR and CTA-MGD/SBR are similar; the main difference is the decrease or increase in interlayer spacing between starting filler and final composite.

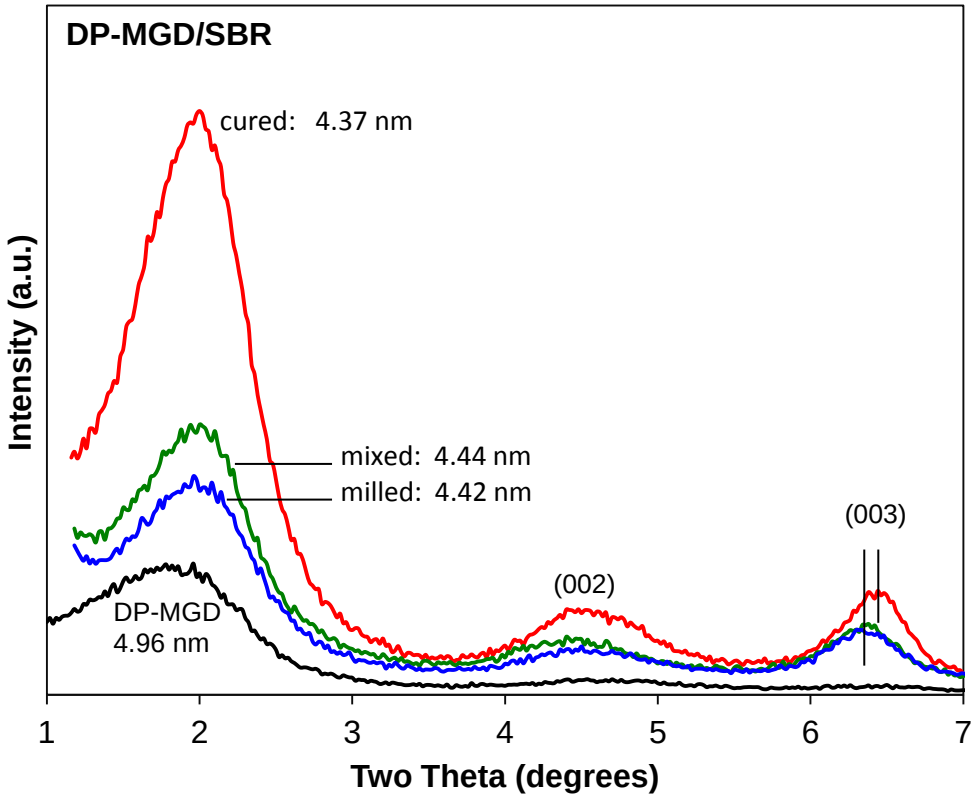

Figure 3.9 XRD patterns for DP-MGD/SBR composites after batch mixing, milling, and thermal curing (curves labeled "mixed", "milled", and "cured").

In our previous work on MGD pre-treatment with SI-69, we demonstrated that SI-69 grafts onto the MGD interlayer surface and displaces some of the adsorbed CTA^+.[75] In the case of CTA-MGD composites, some combination of SI-69 grafting and SBR prepolymer intercalation leads to CTA-MGD interlayer expansion in SBR composites with added SI-69 (Figure 3.7).

We speculate that similar phenomenology occurs in the case of composites incorporating DP-MGD with added SI-69. During mixing of DP-MGD and SI-69 with

SBR prepolymer, some SI-69 likely penetrates the DP-MGD interlayer, displaces DP, and grafts onto the MGD surface. By itself, this process should result in a decrease in interlayer spacing, but not interlayer collapse. At the same time, some SBR prepolymer probably also intercalates into the MGD interlayer, although not enough to produce layer expansion relative to DP-MGD, or even MGD exfoliation. The result for DP-MGD/SBR is a net decrease in interlayer spacing relative to the starting DP-MGD, unlike the increase seen upon blending CTA-MGD with SBR.

Figure 3.10 shows SEM images for silica/SBR and the various OMGD/SBR composites. In all four composites, the filler particles are uniformly well-dispersed in the SBR matrix. The silica/SBR and DP-MGD/SBR composites seem to have a lower level of particle-matrix contrast than the CTA-MGD/SBR and HDA-MGD/SBR composites, possibly implying better particle-matrix adhesion in the former two materials. However, based on these images, we cannot make any definitive statements about quality of interfacial adhesion or the particle aggregation state in these composites.

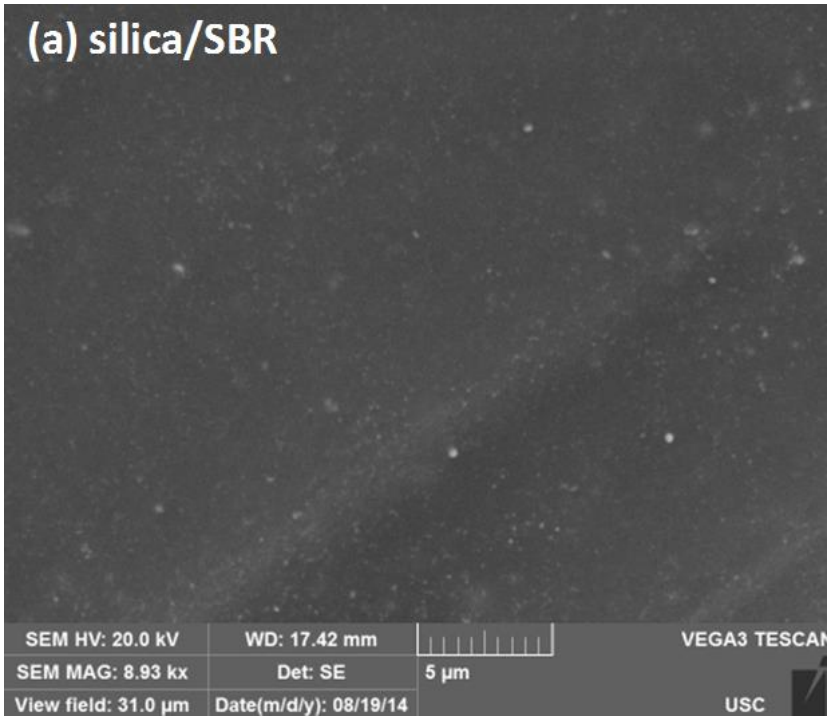
(a) silica/SBR
SEM HV: 20.0 kV
WD: 17.42 mm
VEGA3 TESCAN
SEM MAG: 8.93 kx
Det: SE
5 µm
View field: 31.0 µm
Date(m/d/y): 08/19/14
USC

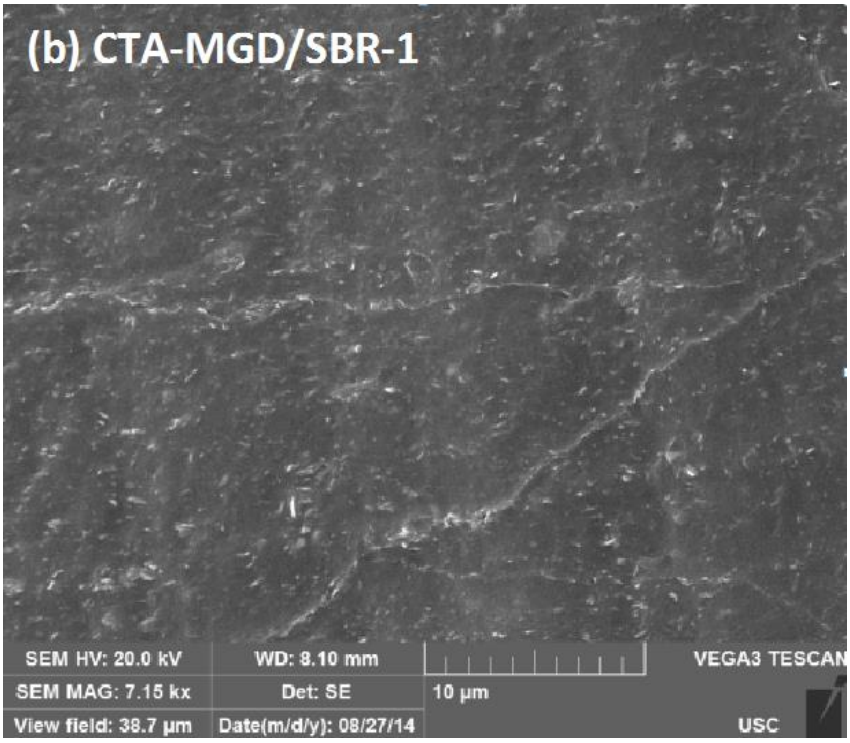
(b) CTA-MGD/SBR-1
SEM HV: 20.0 kV
WD: 8.10 mm
VEGA3 TESCAN
SEM MAG: 7.15 kx
Det: SE
10 µm
View field: 38.7 µm
Date(m/d/y): 08/27/14
USC

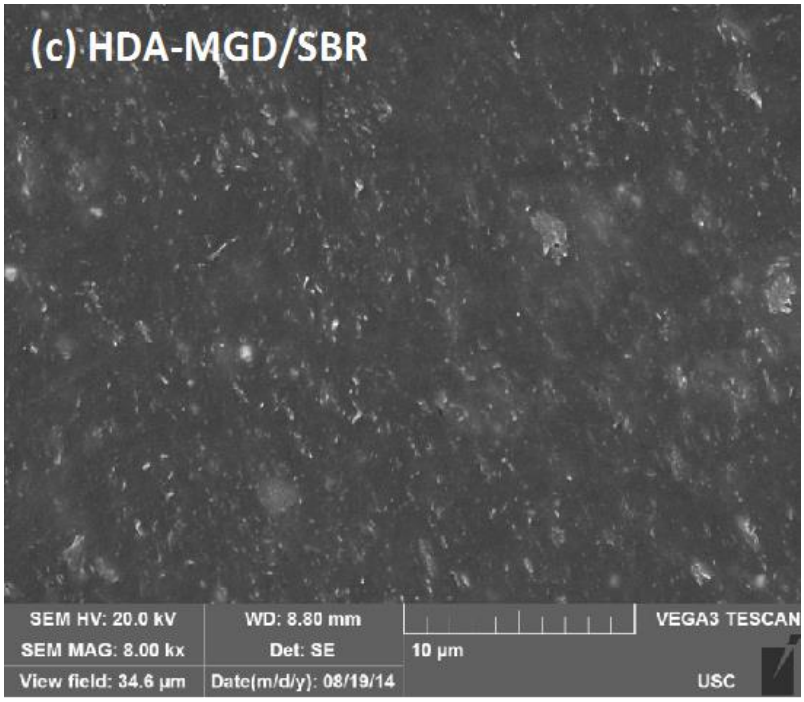

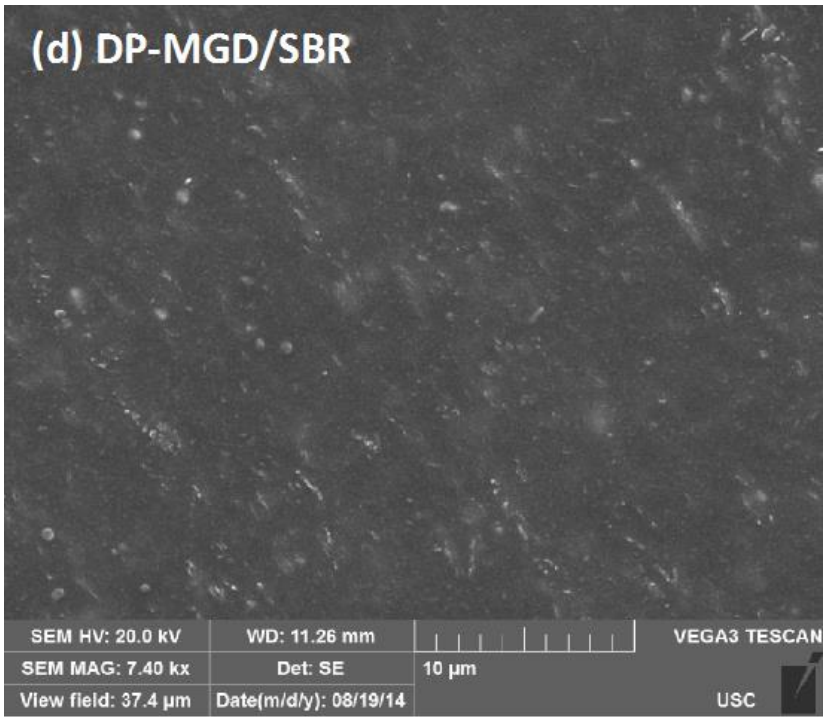

Figure 3.10 SEM images of (a) silica/SBR, (b) CTA-MGD/SBR-1, (c) HDA-MGD/SBR, and (d) DP-MGD/SBR composites.

Figure 3.11 shows the topography of CTA-MGD/SBR-1 cross-section measured by the nSpec® 3D system using a 50× objective. A dispersion rating was calculated by nSpec® software based on the topography (Table 3.9). A lower dispersion rating value corresponds to better filler dispersion. In the rest of the work, we show only the dispersion rating values and do not include the topography figure for each sample.

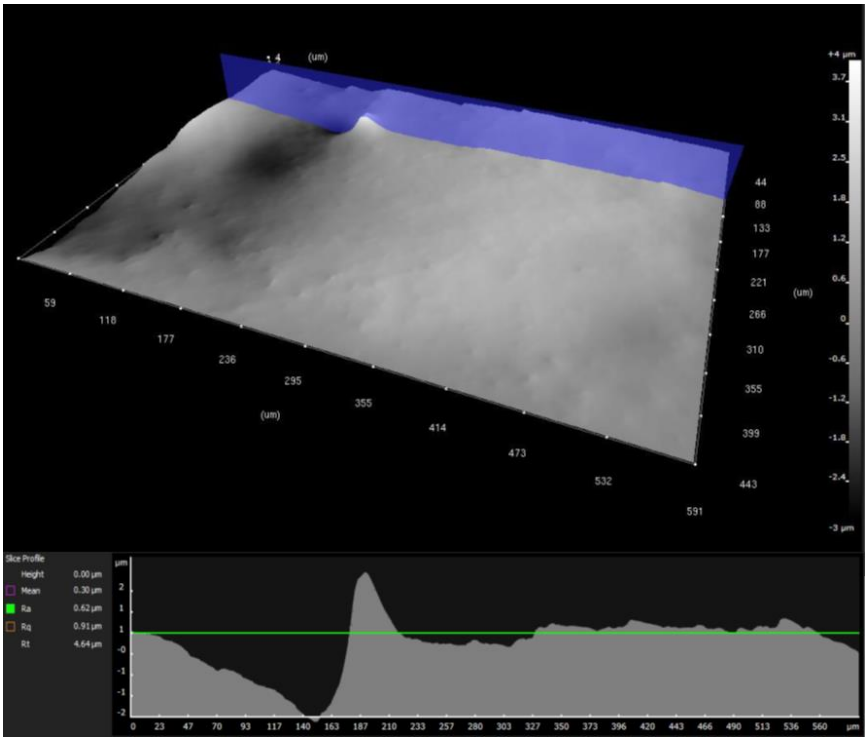

Figure 3.11 3D topography of CTA-MGD/SBR-1 composite.

DP-MGD/SBR shows the lowest dispersion rating, 0.006, which correlates with the largest interlayer spacing (4.37 nm) measured by XRD. CTA-MGD/SBR has a higher dispersion rating of 0.011, which is consistent with the smaller interlayer spacing of CTA-MGD after each stage (Figure 3.7 and 3.9). HDA-MGD/SBR shows the worst filler dispersion with a dispersion rating of 0.019, in accordance with the collapse of the

interlayers in HDA-MGD/SBR. The MGD dispersion rating results are consistent with the final interlayer spacings in all of the MGD/SBR composites.

Silica has a dispersion rating of 0.020 which is comparable to that of HDA-MGD/SBR (0.019). One must remember that silica has a different primary particle shape and aggregate structure compared to HDA-MGD. Therefore we should not draw any conclusions from the dispersion rating values about the quality of silica particle dispersion in SBR compared to HDA-MGD.

Table 3.9 Crosslink densities, M_c values and dispersion ratings of various OMGD/SBR and silica/SBR samples.

Sample	Sample ID	Dispersion Rating	Crosslink density (10^{-4} mol/cm^3)	M_c (10^4 g/mol)
DP-MGD/SBR	YM1263	0.006	0.95±0.01	1.24±0.01
HDA-MGD/SBR	YM1264	0.019	1.24±0.02	0.94±0.01
CTA-MGD/SBR-1	YM2003	0.011	0.94±0.01	1.25±0.01
silica/SBR	YM2022	0.020	1.23±0.02	0.95±0.01

The rubber crosslink densities and M_c values are listed in Table 3.9 as well. DP-MGD/SBR has crosslink density and M_c values comparable to CTA-MGD/SBR-1. Though DP-MGD/SBR shows an interlayer spacing 0.46 nm more than that of CTA-MGD/SBR-1, both composites are fully expanded by SI-69 and SBR. Thus, the same amount of SI-69 and added S results in similar amounts of crosslinks.

DP-MGD/SBR and CTA-MGD/SBR-1 have about 23% lower crosslink density and 32% higher M_c values than those of HDA-MGD/SBR and silica/SBR. In DP-MGD/SBR and CTA-MGD/SBR, the interlayer surfaces are well-exposed, based on

XRD results. During mixing, SI-69 and SBR prepolymer enter the interlayer space. After vulcanization, the intercalated SI-69 produces many SBR-S-MGD crosslinks inside the interlayers. However, the "free sulfur" released from SI-69 may be trapped in the MGD interlayer space. If the freed sulfur does not escape into the SBR, it does not contribute to SBR-SBR crosslinking. This may explain why the crosslink densities in both CTA-MGD/SBR and DP-MGD/SBR composites are comparatively smaller than those in HDA-MGD/SBR and silica/SBR composites.

For HDA-MGD/SBR, XRD shows that most HDA-MGD interlayers collapsed after batch mixing. XRD also indicates that little SI-69 and SBR prepolymer migrates into the interlayer space. Free sulfur released from SI-69 is able to produce many SBR-SBR crosslinks outside the interlayers, which leads to the higher crosslink density and smaller M_c value for HDA-MGD/SBR compared to CTA-MGD/SBR and DP-MGD/SBR.

In the silica/SBR composites, the crosslink density and M_c value are very close to those of HDA-MGD/SBR. Silica does not have a layered structure; if consists of spheroidal primary particles aggregated into fractal aggregates with a relatively open morphology.[125,126] When SI-69 grafts onto the silica surface, it remains exposed to the SBR prepolymer matrix. Upon vulcanization, most (or all) of the released "free sulfur" can escape to help form SBR-SBR crosslinks. This is similar to the situation in HDA-MGD/SBR due to the collapsed HDA-MGD interlayers. This explains why silica/SBR and HDA-MGD/SBR have similar crosslink densities.

With the use of SI-69, SBR is bound to fillers via strong covalent bonds. The bound rubber does not dissolve in toluene and therefore the grafted SBR contributes to

the crosslink density. For expanded MGD, some SBR enters the MGD interlayers and is trapped there by physical forces and SBR-SBR crosslinks. The physically trapped SBR also contribute to the crosslink density. Especially for DP-MGD/SBR and CTA-MGD/SBR (Figure 3.7 and 3.9), the larger interlayer expansions indicate more trapped SBR. The physically trapped SBR contributes to reinforcement but is not reflected in the measurements of crosslink density. Both bound and trapped SBR behaves like the filler and provides extra reinforcement to platelet-filled elastomer composites. The "effective filler concentration" consists of the actual filler concentration plus covalent-bound and physically trapped SBR. The concept of effective filler concentration can help rationalize measured mechanical properties.

Tensile testing can be used to characterize quantitatively the strength of polymer composites under finite deformations. As stress increases with tensile strain, modulus values at various strain levels can tell us about different contributions to mechanical strength. The modulus at 10% strain (M10) depends primarily on the effective filler concentration. As the strain increases, the corresponding moduli (e.g., M100 and M250) provide information on the disruption of particle aggregates and, ultimately, the stretching of the crosslinked polymer network. In essence, moduli at low (M10) and higher strains (M100 and M250) quantify the filler-filler and filler-matrix interactions. The area under the stress-strain curve gives the strain energy (also known as toughness), the total energy per unit volume stored by the material during the deformation. The number of testing samples is denoted as "N".

Figure 3.12 compares stress-strain behavior for three OMGD/SBR composites and silica/SBR. The corresponding stress-strain data are shown in Table 3.10. At M10,

CTA-MGD/SBR-1 (4.66 MPa) has 53% and 47% higher modulus than silica/SBR (3.04 MPa) and HDA-MGD/SBR (3.16 MPa), respectively. At M10, the modulus is mostly determined by the effective filler concentration. CTA-MGD/SBR-1 has superior interlayer expansion and filler dispersion compared to HDA-MGD/SBR and silica/SBR, indicating more SBR crosslinked or trapped in the interlayer space. The resulting higher filler effective concentration explains the higher tensile modulus of CTA-MGD/SBR-1. For similar reasons, DP-MGD/SBR (4.67 MPa) shows 54% and 48% higher modulus than silica/SBR (3.04 MPa) and HDA-MGD/SBR (3.16 MPa), respectively.

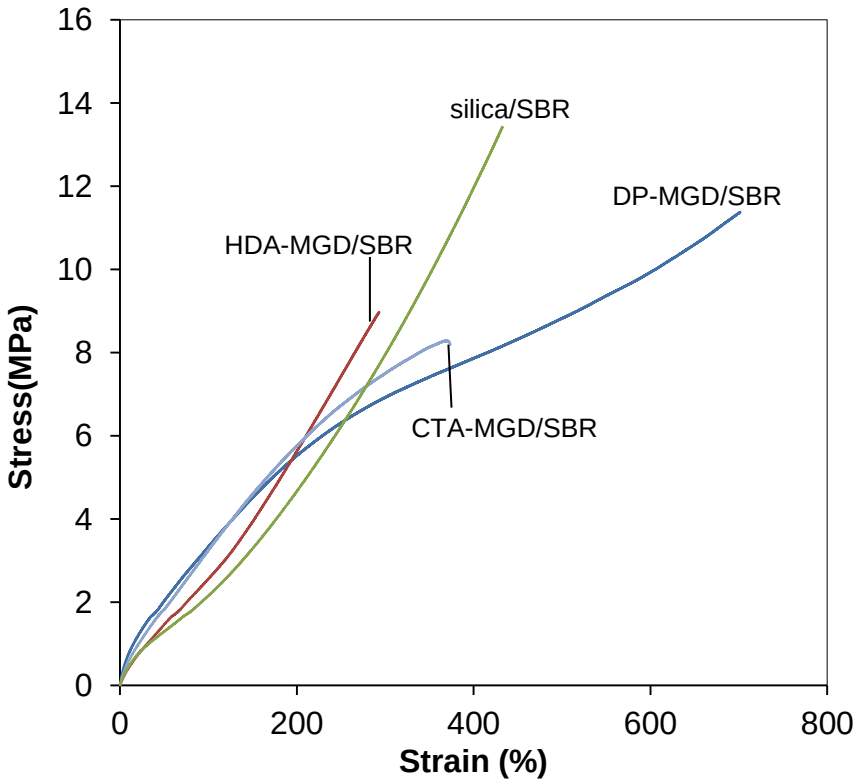

Figure 3.12 Representative stress-strain curves for various OMGD/SBR and silica/SBR composites.

Table 3.10 Tensile testing results for OMGD/SBR and silica/SBR composites.

Sample	ID	N	M10 (MPa)	M100 (MPa)	M250 (MPa)	Strain energy density (MJ/m^3)	Tensile strength (MPa)	Strain at break (%)
CTA-MGD/SBR-1	YM2003	5	4.66±0.49	2.56±0.21	1.72±0.14	22.3±4.16	8.37±0.48	424±55.4
silica/SBR	YM2022	4	3.04±0.85	1.49±0.88	2.52±0.80	28.2±4.25	12.7±2.12	518±109
DP-MGD/SBR	YM1263	5	4.67±0.35	2.40±0.33	1.36±0.06	42.2±7.84	8.52±3.11	669±99.5
HDA-MGD/SBR	YM1264	4	3.16±0.22	2.40±0.80	3.06±0.63	12.7±2.84	8.63±0.26	316±67.5

At M10, DP-MGD/SBR and CTA-MGD/SBR-1 have comparable tensile moduli due to the similar intercalated structures and filler dispersion. DP-MGD/SBR has an interlayer spacing of 4.37 nm, which is only 0.46 nm larger than that of CTA-MGD/SBR-1. The filler dispersion ratings in both composites are also comparable. Thus, both DP-MGD/SBR and CTA-MGD/SBR-1 have similar tensile moduli at 10% strain. Silica/SBR and HDA-MGD/SBR have comparable tensile moduli, which is also explained by their similar effective filler concentration. Due to the collapse of HDA-MGD interlayers, SBR only crosslinks (via SI-69) to the exterior surfaces of HDA-MGD particles. Consequently, HDA-MGD/SBR has similar effective filler concentration to silica/SBR, resulting in comparable tensile moduli (M10) in both composites.

At 100% strain, the modulus (M100) is influenced mostly by the disruption of filler aggregate structure. There is no significant difference (95% confidence) in the M100 values for all three OMGD/SBR composites (Table 3.10). The MGD are modified by various organo-modifiers, but the resulting OMGD have similar aggregate structures, which may explain the similar M100 values. Silica/SBR has lower M100 value than

CTA-MGD/SBR-1, DP-MGD/SBR, and HDA-MGD/SBR with 90%, 85% and 81% confidence, respectively. This can be attributed to MGD having 162 % more CTAB surface area compared to silica, resulting in greater filler reinforcement.

At high strains, crosslink density governs the modulus. HDA-MGD/SBR and silica/SBR have the greatest M250 values (Table 3.10, no significant difference between them) and the highest crosslink density values (Table 3.9). In these composites, all of the sulfur from SI-69 is released and can contribute to SBR-SBR crosslinking. Both CTA-MGD/SBR-1 and DP-MGD/SBR have lower M250 values due to their lower crosslink densities. In these composites, most of the SI-69 is sequestered in the MGD interlayer space, so freed sulfur may not escape and contribute as much to SBR crosslinking. Comparing CTA-MGD/SBR-1 and DP-MGD/SBR, the former has a higher M250 value than the latter. This could be explained by greater SI-69 grafting in DP-MGD, which sequesters more of the freed sulfur. However, the crosslink density values (Table 3.9) are the same for these two composites, so this explanation may not be complete.

Due to its high tensile strength and elongation at break, DP-MGD/SBR has the highest strain energy (42.2 MJ), which is about 50% more than that of silica/SBR (28.2 MJ). Silica/SBR shows outstanding tensile strength and moderate elongation at break; the resulting strain energy (28.2 MJ) is 26% higher than that of CTA-MGD/SBR (22.3 MJ). HDA-MGD/SBR shows the lowest strain energy (12.7 MJ), which is 70% less than that of DP-MGD/SBR (42.2 MJ).

Among all of these composites, DP-MGD/SBR appears to have the best combination of high tensile strength and elongation at break, resulting in superior

toughness. At low to moderate strains, DP-MGD/SBR behaves like CTA-MGD/SBR: both kinds of composites have high effective filler concentrations resulting from significant binding of SBR to the MGD surface. This is in contrast to HDA-MGD/SBR and silica/SBR, which have lower effective filler concentrations due to their lower surface area (exposed to SBR) per unit mass of filler. At high strain levels (>250%), DP-MGD/SBR manifests enhanced ductility compared to CTA-MGD/SBR, leading to superior tensile strength and elongation at break. The greater expansion of MGD in the cured DP-MGD/SBR composite, presumably due to greater SBR intercalation, crosslinking, and binding to MGD within the interlayer space, seems to have a favorable impact on the crosslinked network structure, leading to the superior stress-strain behavior.

We used DMA to measure the dynamic mechanical properties of SBR composites as a function of temperature from -80°C to 100°C. We compare mechanical properties of various OMGD/SBR and silica/SBR composites to evaluate the influence of interlayer spacing on elastic energy storage (storage modulus, E') and energy dissipation (loss tangent, tan δ). In the glassy regime at low temperatures, all of the composites have no apparent difference in the E' values (Figure 3.13, Table 3.11). A statistical comparison of average E' value at -60°C confirms this conclusion with greater than 95% confidence. Below the glass transition temperature (T_g), the elastomer does not have enough energy to move around. The elastomer chains are interlocked and immobilized in a glassy state, resulting in higher modulus than that in the rubbery regime above T_g.

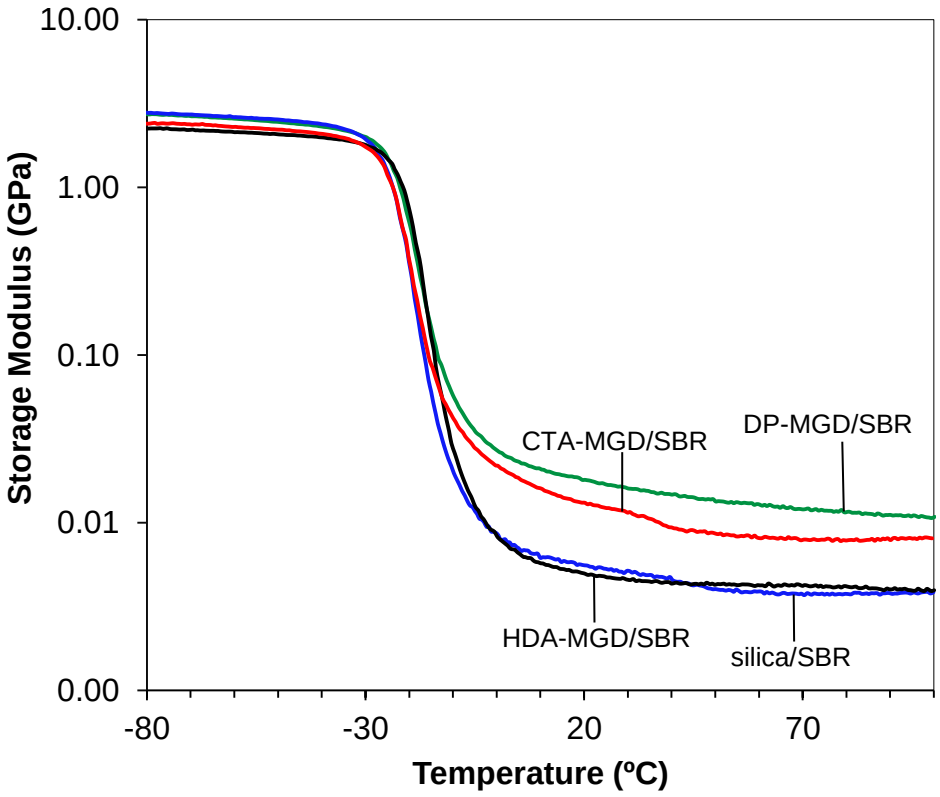

Figure 3.13 Storage modulus as a function of temperature for silica/SBR and various OMGD/SBR composites.

Table 3.11 Dynamic mechanical properties of silica/SBR and various OMGD/SBR composites measured by DMA.

Sample	N	E' at -60 ºC (GPa)	E' at 0 ºC (MPa)	E' at 60 ºC (MPa)	Avg. T_g (ºC)	Avg. value of tan δ peak	tan δ at 60 ºC
DP-MGD/SBR	3	2.60±0.10	27.43±1.82	12.63±1.07	-15.43±0.46	0.95±0.01	0.12±0.010
HDA-MGD/SBR	3	2.65±0.07	8.57±0.26	3.89±0.09	-14.06±0.81	1.43±0.05	0.06±0.004
CTA-MGD/SBR-1	2	2.38±0.12	21.80±0.28	8.40±0.31	-16.59±0.44	1.01±0.03	0.11±0.008
Silica/SBR	3	1.95±0.34	8.75±1.50	4.32±0.49	-12.83±0.38	1.26±0.05	0.05±0.006

As temperature increases through the glass transition, the storage modulii of CTA-MGD/SBR-1 and DP-MGD/SBR undergo a more gradual transition to the rubbery state (Figure 3.13), resulting in lower tan δ peak values (Figure 3.14) compared to those for HDA-MGD/SBR and silica/SBR. The T_g values of the OMGD/SBR composites do

not differ from each other (95% confidence). The T_g of silica/SBR is higher than those of the OMGD/SBR composites (86% confidence). The differences in the temperatures of the peak maxima (T_g) might be due to the plasticizing effect of organic modifier.[2]

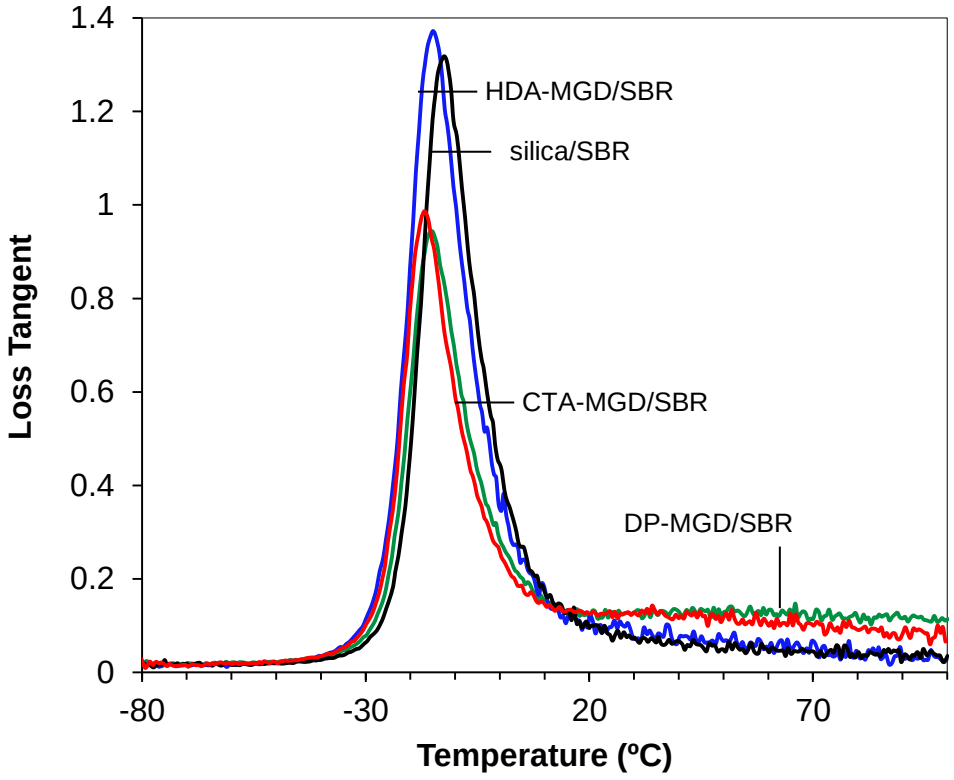

Figure 3.14 Loss tangent as a function of temperature for silica/SBR and various OMGD/SBR composites.

We observe more significant property differences in the rubbery regime at temperatures above T_g. The E' value at 60ºC for DP-MGD/SBR (12.63 MPa) is 50% higher than that of CTA-MGD/SBR-1 (8.40 MPa, Table 3.11). This is rationalized in terms of the larger initial interlayer spacing of DP-MGD (4.96 nm, Figure 3.9) compared to CTA-MGD (3.10 nm, Figure 3.6), which presumably enables a greater amount of SBR

and SI-69 intercalation into the MGD interlayer during the initial mixing stage. Comparing Figures 3.7 and 3.9, the DP-MGD interlayer spacing remains greater than that of CTA-MGD throughout the milling and curing stages. This permits greater SI-69 and SBR intercalation, as indicated by the difference in the final interlayer spacing of the cured composites (4.37 nm for DP-MGD/SBR versus 3.91 nm for CTA-MGD/SBR), resulting in more SI-69 grafting onto MGD, enhanced filler-matrix bonding, and increased mechanical reinforcement.

Table 3.11 shows that at 60 ºC, the E' value of silica/SBR (4.32 MPa) is lower than that of DP-MGD/SBR (12.63 MPa) and CTA-MGD/SBR-1 (8.40 MPa) by 66% and 49%. The significant difference is attributed to 162% more surface area in MGD than silica. DP-MGD and CTA-MGD are well dispersed and expanded by SBR after curing. The interlayer surface is crosslinked with the intercalated SBR, resulting in greater effective filler concentration and thus higher storage moduli. Compared to OMGD, silica has less surface area and therefore lower effective filler concentration, which leads to the lower storage moduli.

Although HDA-MGD started with the largest interlayer spacing (5.81 nm, Figure 3.6), XRD patterns (Figure 3.8) indicate that the interlayer structure collapsed during mixing with SBR. Consequently we believe that little or no SBR and SI-69 intercalation occurred in the HDA-MGD/SBR composite. If this picture is correct, then the structure within the HDA-MGD/SBR composite resembles that of silica/SBR, in the sense that it consists of non-intercalated particles interacting with the SBR matrix via SI-69 linkages on external particle surfaces. The composites differ primarily in the shape of the filler particles and their surface area (per g) exposed to SBR. Figure 3.13 indicates that in the

rubbery regime, the E' values for HDA-MGD/SBR are similar to those for silica/SBR, and considerably less than those for CTA-MGD/SBR and DP-MGD/SBR. In fact, comparing storage modulii at 60°C (Table 3.11), the E' value for HDA-MGD/SBR (3.89 MPa) is about 10 % less (73% confidence) than that of silica/SBR (4.32 MPa). This demonstrates that the lack of SI-69 and SBR intercalation in HDA-MGD results in mechanical reinforcement no better than that in silica/SBR, and perhaps even worse. With little intercalation of SI-69 or SBR into the HDA-MGD interlayer space, the amount of filler-SBR interfacial area (m^2/g) for HDA-MGD/SBR may be less than that in silica/SBR.

With respect to energy dissipation at temperatures relevant to tire performance, we compare the tan δ values at 60°C. Silica/SBR has a tanδ value (0.05) less than that of HDA-MGD/SBR (0.06) with 89% confidence. DP-MGD/SBR and CTA-MGD/SBR have similar tan δ values, which are ~100% higher than those of silica/SBR and HDA-MGD/SBR. This can be explained based on the observation that silica/SBR and HDA-MGD/SBR have higher crosslink densities and lower M_c values than those of DP-MGD/SBR and CTA-MGD/SBR-1 (Table 3.9), resulting in less mobile SBR chains and therefore less energy dissipation in silica/SBR and HDA-MGD/SBR composites.

3.3.1.3 Discussion

Section 3.3.1 considers the influence of starting MGD interlayer spacing on the mechanical properties of MGD/SBR composites. HDA-MGD has the largest starting interlayer spacing, but the collapse of the interlayers during mixing limits the intercalation of SBR prepolymer. This results in reduced amount of filler-SBR crosslinking and low effective filler concentrations. Consequently, HDA-MGD/SBR has

the poorest mechanical reinforcement. DP has a smaller initial interlayer spacing than HDA-MGD. However, the interlayers are still well expanded by SI-69 and SBR after vulcanization, which results in better filler dispersion and higher effective filler concentration. This explains why DP-MGD/SBR shows the best mechanical properties.

Although HDA-MGD started with a much larger interlayer spacing (5.81 nm) than CTA-MGD (3.10 nm), mixing with SBR resulted in the collapse of the interlayer structure, perhaps due to extraction of HDA^+ by the green rubber mix. After mixing, the HDA-MGD filler was well-dispersed in the SBR. Except for particle shape, HDA-MGD resembles silica in the sense that only the external particle surface interacts with the SBR matrix. Because SI-69 and SBR cannot access the internal interlayer surface area in HDA-MGD, the overall amount of MGD-SBR interfacial area in the HDA-MGD/SBR composite may be about the same or slightly lower than that in silica/SBR. For this reason, the mechanical properties of HDA-MGD/SBR are comparable to those of silica/SBR.

The tensile test results (Table 3.10) and DMA results (Table 3.11) clearly show that CTA-MGD/SBR and DP-MGD/SBR composites have much higher elastic moduli at low strain than HDA-MGD/SBR and silica/SBR. CTA-MGD/SBR and DP-MGD/SBR manifested considerable SBR intercalation in the MGD interlayers, presumably accompanied by interlayer SBR-MGD grafting and SBR-SBR crosslinking. These results lead to the conclusion that SBR intercalation and interlayer grafting, via SI-69, lead to much higher effective filler concentrations than comparable MGD loading in HDA-MGD/SBR, or silica loadings in silica/SBR. In essence, CTA-MGD and DP-MGD are

better active filler than HDA-MGD on silica for enhancing low strain mechanical properties in SBR composites.

The initial interlayer spacing in DP-MGD (4.96 nm) is also greater than that of CTA-MGD. During mixing with SBR, the DP-MGD interlayer spacing decreases but does not collapse. The DP-MGD interlayer spacing in the final cured composite (4.37 nm) is greater than that in cured CTA-MGD/SBR (3.91 nm). This demonstrates that greater initial interlayer spacing leads to greater levels of SI-69 and SBR intercalation in OMGD composites. This has several consequences, presumably including higher effective filler concentration and better filler dispersion.

Mechanical property measurements establish the superiority of DP-MGD over CTA-MGD as an active filler in SBR, especially at low to moderate strain values. The storage modulus (from DMA), elastic moduli (from tensile testing), tensile strength, elongation at break, and strain energy are all greater in DP-MGD/SBR compared to CTA-MGD/SBR, at the same levels of inorganic MGD loading (26.34 phr) and SI-69 (7.25 phr). We believe these results are directly attributable to more extensive SI-69 and SBR intercalation and grafting to MGD interlayer surfaces as a result of the greater initial DP-MGD spacing.

3.3.2 Influence of SI-69 and Mixing Time on CTA-MGD/SBR Composites

3.3.2.1 Results

In previous work[75], XRD showed that interlayer spacing of CTA-MGD expanded after compounding with SI-69 and SBR. However, the distinct roles of SI-69 and SBR were not elucidated. In current work, we prepared CTA-MGD/SBR with and without SI-

69 added during mixing and collected the XRD patterns after each composite synthesis step (mixing, milling and curing). CTA-MGD/SBR-1 was prepared with added SI-69 and 2 min batch mixing (Figure 3.6). Figure 3.7 shows that the starting CTA-MGD had an interlayer spacing of 3.10 nm. After mixing with SI-69 and SBR prepolymer, the interlayer spacing increased to 4.01 nm. Afterwards, the interlayer spacing did not change much during milling and curing: the interlayer spacings were 4.01 nm and 3.91 nm respectively. For CTA-MGD/SBR-1, all of the intercalation took place during batch mixing. The interlayer space expansion was due to the intercalation of a combination of SI-69 and SBR prepolymer during mixing.

We also prepared CTA-MGD/SBR composites with added SI-69, using 6 min of batch mixing time (Table 3.6, CTA-MGD/SBR-3) instead of just 2 min (Table 3.6, CTA-MGD/SBR-1). For CTA-MGD/SBR-3 (Figure 3.15), the MGD interlayer spacing values after mixing, milling, and curing steps were 4.05, 4.05, and 3.98 nm, respectively – essentially the same values found for CTA-MGD/SBR-1 (2 min mixing, Figure 3.7). This shows that extended mixing time does not result in greater levels of SI-69 or SBR prepolymer intercalation. In light of this conclusion, the XRD results for CTA-MGD/SBR-3 basically replicate those of CTA-MGD/SBR-1, demonstrating reproducibility of the synthesis process.

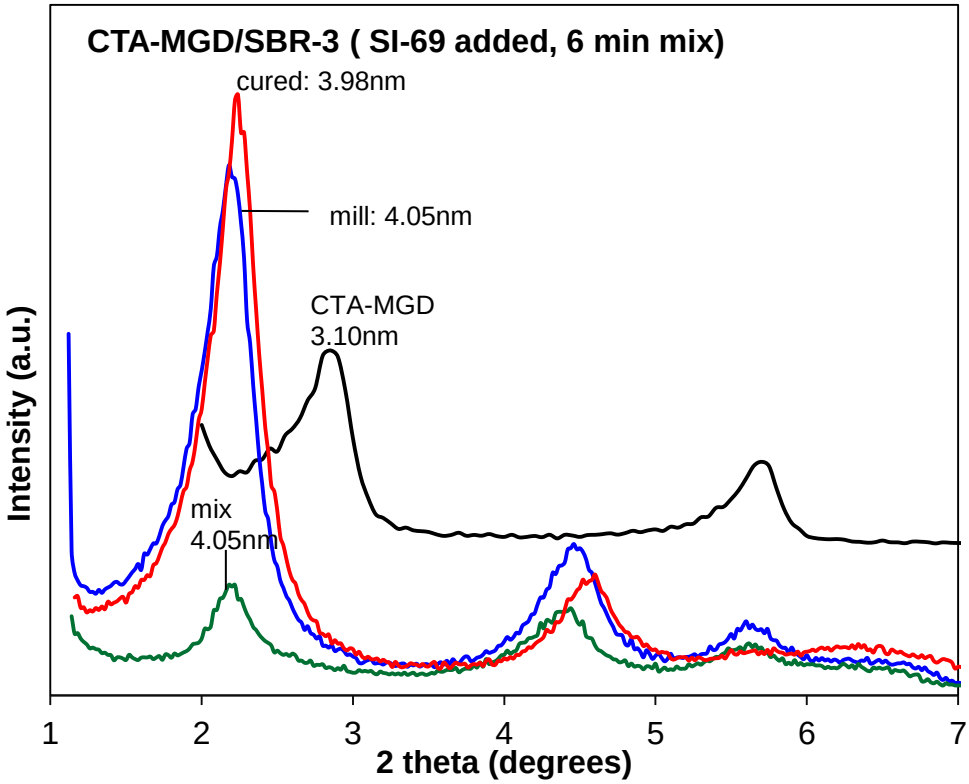

Figure 3.15 XRD patterns for CTA-MGD/SBR-3 composite after batch mixing, milling, and thermal curing (curves labeled "mixed", "milled", and "cured"). Composite was prepared with SI-69 added prior to 6 min of batch mixing.

Figure 3.16 shows XRD patterns for CTA-MGD/SBR-2 composite prepared without any added SI-69 and 2 min batch mixing. During mixing, the MGD interlayer spacing expands from 3.10 to 3.62 nm, indicating intercalation of SBR prepolymer. However, the expansion amount, 0.52 nm, is only about 60% of that found when SI-69 was included in the mix (0.91 nm for CTA-MGD/SBR-1, Figure 3.7). The smaller post-mixing expansion seen in CTA-MGD/SBR-2 may be due to the absence of SI-69, which results in less overall intercalation. Alternately, it may indicate that when SI-69 is included in the mix, it facilitates SBR intercalation into CTA-MGD interlayer spaces.

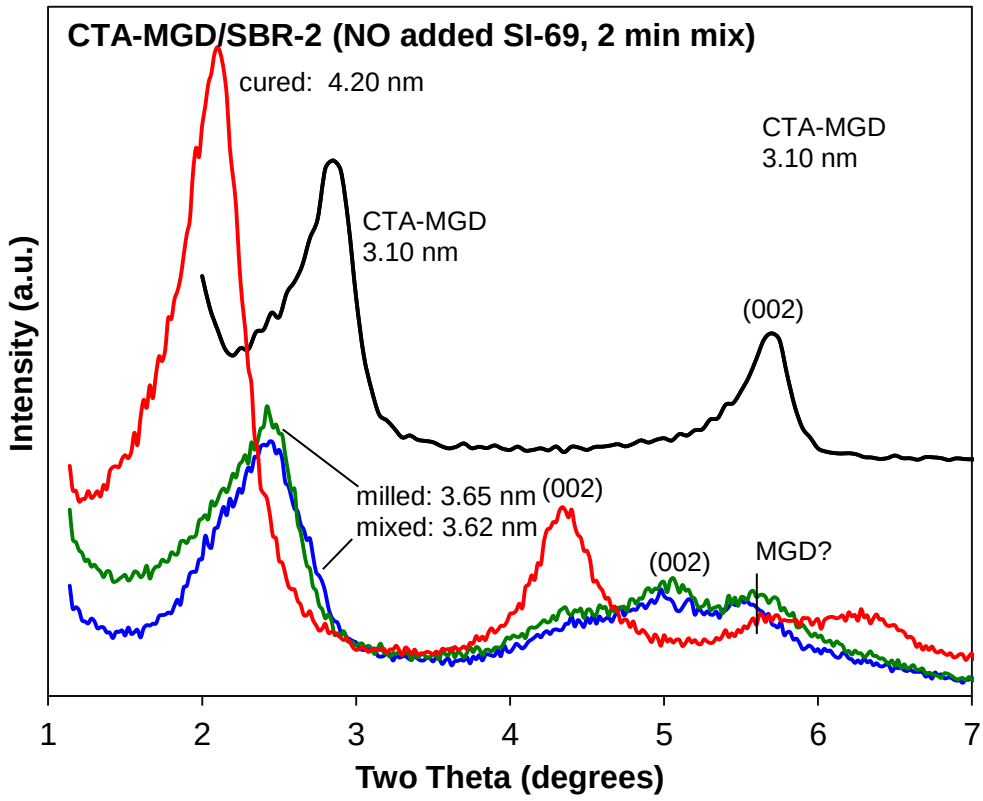

Figure 3.16 XRD patterns for CTA-MGD/SBR-2 composite after batch mixing, milling, and thermal curing (curves labeled "mixed", "milled", and "cured"). Composite was prepared with no added SI-69 but with 2 min of batch mixing.

In CTA-MGD/SBR-2 (Figure 3.16), for the mix without added SI-69, the XRD pattern shows little change after milling. This tells us that the addition of curatives (sulfur and CBS) does not alter the CTA-MGD interlayer spacing. After curing, XRD indicates that the MGD interlayer spacing increased to 4.20 nm, an expansion of 0.58 nm relative to the pre-cured state. This shows that either additional SBR enters the MGD interlayer space during the curing stage, or that the crosslinking process results in expansion of the SBR that had already intercalated during the mixing stage. The final interlayer spacing in cured CTA-MGD/SBR-2 (4.20 nm) is somewhat larger than that in CTA-MGD/SBR-1 (3.91 nm); we do not know if this is significant.

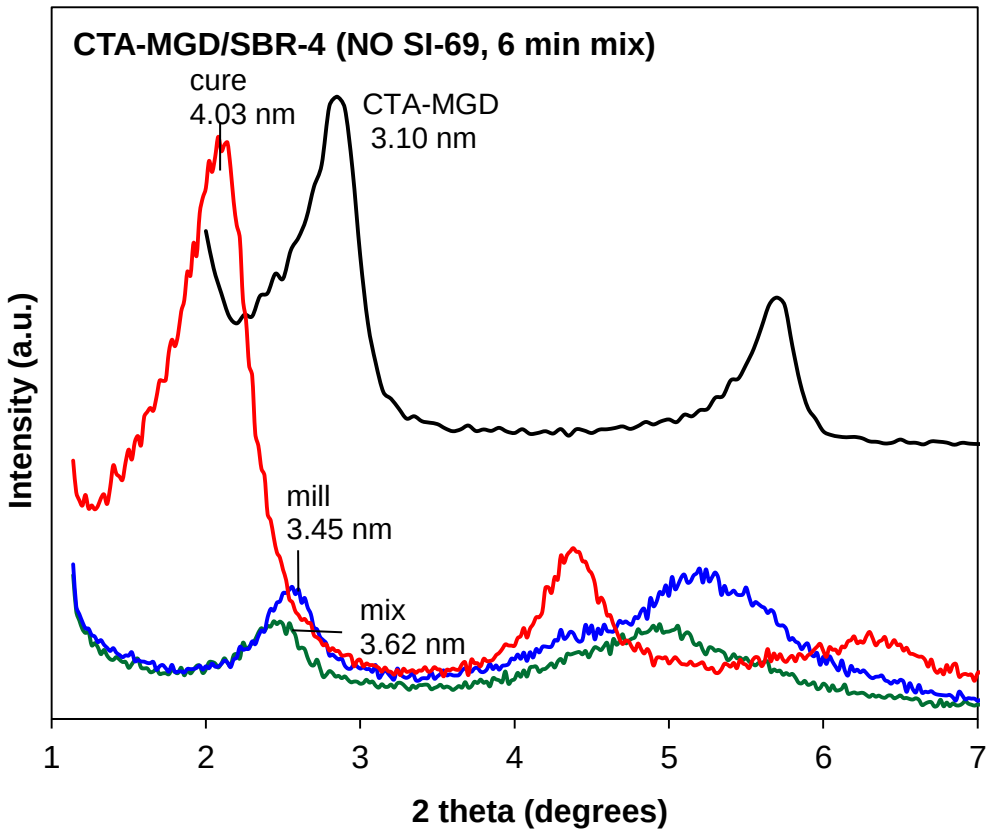

Figure 3.17 XRD patterns for CTA-MGD/SBR-4 composite after batch mixing, milling, and thermal curing (curves labeled "mixed", "milled", and "cured"). Composite was prepared with no added SI-69 but with 6 min batch mixing.

For CTA-MGD/SBR prepared without SI-69, but mixed for 6 min (Figure 3.17, CTA-MGD/SBR-4), the XRD patterns are essentially the same as those found with 2 min mixing time; MGD interlayer spacing values are 3.62, 3.45, and 4.03 nm after mixing, milling and curing stages. These results again show that mixing time has little influence on the degree of SBR intercalation. Moreover, the MGD spacing in cured CTA-MGD/SBR-4 (4.03 nm, no SI-69, mixed 6 min) is only 0.05 nm larger than that for cured

CTA-MGD/SBR-3 (3.98 nm, with Si-69, mixed 6 min), which probably is not a significant difference.

None of the composite XRD patterns in Figures 3.7, 3.15-3.17 have a peak at about 2.9° (3.10 nm spacing), which indicates uniform intercalation throughout the CTA-MGD filler. On the other hand, the appearance in the composite patterns of a small peak at 5.5-5.7° suggests restacking of a small amount of "bare" MGD with interlayer spacing of approximately 1.54 nm. Previous research attributed this to the formation of Zn-sulfur-amine complexes, which may extract long chain surfactants out of the interlayer spaces, resulting in interlayer collapse.[127] In our system, Zn and stearic acid may be facilitating CTA extraction from MGD interlayer spaces; Figure 3.7 and 3.15-3.17 provide evidence of this independent of the presence of SI-69 and length of mixing time. However, the intensity of this peak is weak in all XRD patterns for CTA-MGD/SBR composites, so the significance of interlayer collapse in CTA-MGD fillers should be minimal.

Overall, the results show that including SI-69 in the mix results in greater CTA-MGD interlayer expansion during the mixing process. However, the magnitude of CTA-MGD interlayer expansion in cured SBR composites (about 0.9 to 1.1 nm) is about the same regardless of whether or not SI-69 is included in the mix. Since the MGD interlayer spacing increases during mixing/milling and curing stages without added SI-69, we conclude that SBR prepolymer enters the MGD interlayer spaces during composite synthesis. SI-69 appears to facilitate this process during the mixing stage.

SEM images of various MGD/SBR composites provide qualitative information on the degree of MGD particle dispersion in SBR and the nature of MGD/SBR adhesion. Figure 3.18 shows SEM images for various CTA-MGD/SBR composites. In the four composites, the MGD particles are uniformly dispersed throughout the field of the images. The MGD particles have apparent sizes of less than 1 μm and appear to be elongated, as expected for aggregates of plate-like particles.

The difference in particle/matrix contrast in CTA-MGD/SBR-1 can be explained by the presence (or lack) of SI-69 and its role in interfacial adhesion in the two composites. In CTA-MGD/SBR-1, the added SI-69 grafts onto the MGD surface and crosslinks with the SBR, leading to strong MGD-SBR adhesion. Upon microtoming, the MGD particles remain substantially covered by SBR, resulting less particle-matrix contrast in the SEM image [Figure 3.18(1)]. The converse is found in CTA-MGD/SBR-2: in the absence of SI-69, no covalent bonds are formed between MGD and SBR, so only physical adhesion occurs. When this sample is microtomed, SBR may be pulled away from the MGD particles, and some MGD particles may be pulled out of the matrix, resulting in higher particle-matrix contrast in the SEM image [Figure 3.18(2)]. However, in the SEM images of CTA-MGD/SBR-1 and-3 (or -2 and -4), it is not clear whether longer mixing time promotes MGD platelet dispersion in the composites.

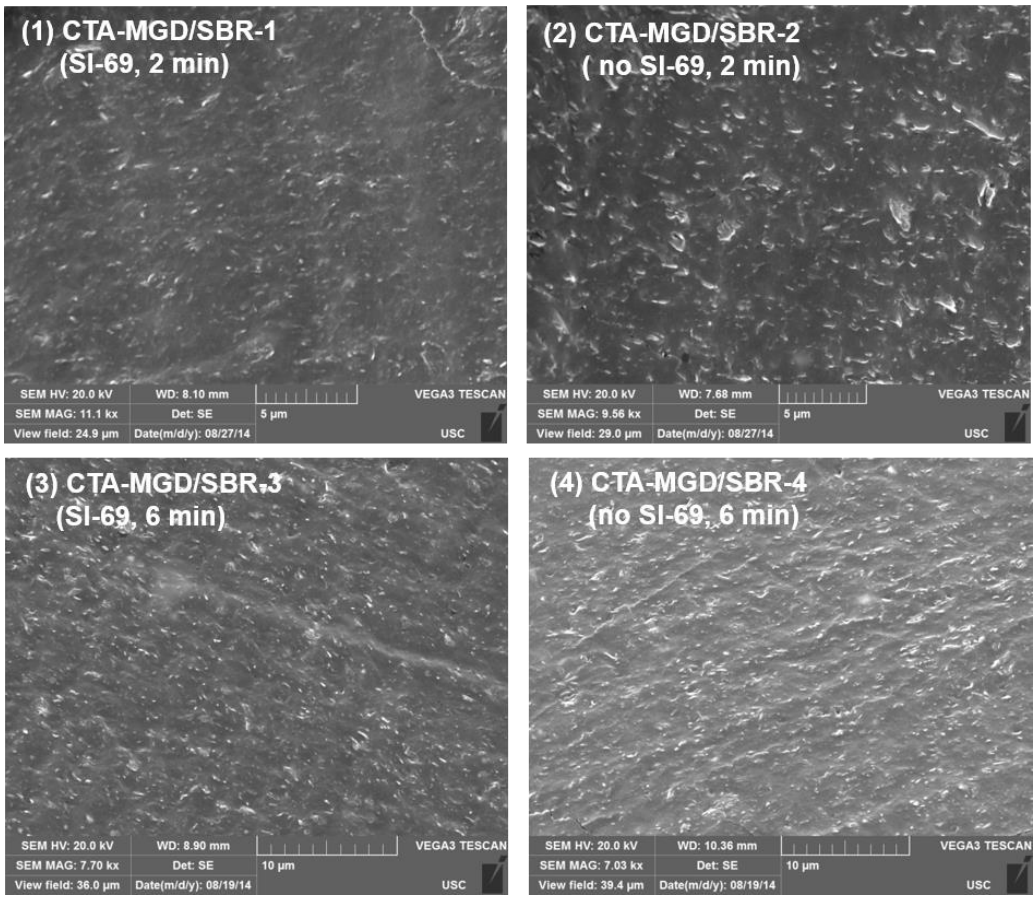

Figure 3.18 SEM images of (1) CTA-MGD/SBR-1 (2) CTA-MGD/SBR-2 (3) CTA-MGD/SBR-2 (4) CTA-MGD/SBR-4 composites with and without added SI-69 and for varying mixing times as indicated.

Quantitative filler dispersion values based on nSpec measurements are shown in Table 3.12. All CTA-MGD/SBR composites show comparable filler dispersion ratings with low values indicating better filler dispersion. It is not surprising that CTA-MGD/SBR-2 has slightly poorer filler dispersion than the other three. The lack of SI-69 and shorter mixing time (2 min) may contribute to the poor filler dispersion. The filler dispersion rating of silica is apparently higher than that of the OMGD/SBR composites. This could be due to differences in the morphology of filler particle aggregates as well as particle shape.

Table 3.12 Crosslink density and Mc values for CTA-MGD/SBR and silica/SBR composites.

Sample	ID	Filler Dispersion	Crosslink Density (10^{-4} mol/cm^3)	M_c (10^4 g/mol)
CTA-MGD/SBR-1	YM2003	0.011	0.94±0.01	1.25±0.01
CTA-MGD/SBR-2	YM2007	0.016	0.62±0.05	1.90±0.15
CTA-MGD/SBR-3	YM2010	0.014	0.98±0.01	1.19±0.01
CTA-MGD/SBR-4	YM2012	0.011	0.48±0.01	2.44±0.08
silica/SBR	YM2022	0.020	1.23±0.02	0.95±0.01

Table 3.12 also contains the crosslink densities and average molecular weight between crosslinks (M_c) for CTA-MGD/SBR composites. Composites prepared with SI-69 (CTA-MGD/SBR-1 and -3, silica/SBR) show apparently high crosslink densities and low M_c values compared to composites without SI-69 (CTA-MGD/SBR-2 and -4). CTA-MGD/SBR-1 has 52% higher crosslink density and 34% lower M_c values than CTA-MGD/SBR-2. The increase of crosslink densities (CTA-MGD/SBR-1 and -3 compared to -2 and -4) is due to the addition of SI-69. SI-69 binds SBR molecules to MGD surfaces as well as produces SBR crosslinking by releasing free sulfur.

When SI-69 is added, longer mixing time does not improve crosslink density. CTA-MGD/SBR-1 and -3 show crosslink densities of 0.94×10^{-4} mol/cm^3 and 0.98×10^{-4} mol/cm^3, respectively. When SI-69 is not added to the mix, we find that the crosslinking density decreases with the increase of mixing time. CTA-MGD/SBR-4 shows 23% lower crosslink density than CTA-MGD/SBR-2. In the absence of SI-69, longer mixing time improves CTA-MGD dispersion, and the better-dispersed MGD particles appear to disrupt SBR crosslinking.

Silica/SBR shows higher crosslinking density than all the CTA-MGD/SBR composites, which might be due to the filler aggregate structure. In the silica/SBR composite, the open aggregate structure and lack of interlayer spaces enables all of the freed sulfur from SI-69 to be released for SBR-SBR crosslinking. Moreover, compared to MGD, silica has less surface area to produce silica-SBR crosslinking. The CTAB surface area of silica is 150 m^2/g, versus 393 m^2/g for MGD. Thus in silica/SBR, more SBR-SBR crosslinks are formed compared to silica-SBR crosslinks, which explains the high crosslink density and lower M_c values for silica/SBR.

We next consider stress-strain behavior of CTA-MGD/SBR composites prepared with and without SI-69, and with varying batch mixing time (Figure 3.19). The data plotted in Figure 3.19, as well as statistical analysis based on multiple measurements, indicate that mixing time has no significant impact on the stress-strain behavior of CTA-MGD/SBR composites. On the other hand, including SI-69 in the recipe has a remarkable effect. Table 3.13 shows that CTA-MGD/SBR composites prepared with SI-69 have larger moduli values at all strains, larger tensile strength values, but smaller elongation at break compared to composites prepared without added SI-69. The increase in tensile strength in composites with SI-69 is offset somewhat by the decrease in elongation at break: consequently the strain energy increases by only about 25% in the composites with SI-69 relative to those without added SI-69. Adding SI-69 makes composites more rigid and less ductile, as observed in many other silica-elastomer composites containing silane crosslinkers.[128]

Table 3.13 Tensile testing results for CTA-MGD/SBR and silica/SBR samples.

Sample	ID	N	M10 (MPa)	M100 (MPa)	M250 (MPa)	Strain Energy density (MJ/m^3)	Tensile Strength (MPa)	Strain at break (%)
CTA-MGD/SBR-1	YM2003	5	4.66±0.49	2.56±0.21	1.72±0.14	22.3±4.16	8.37±0.48	424±55.4
CTA-MGD/SBR-2	YM2007	5	2.77±0.23	0.23±0.05	0.20±0.05	17.4±4.19	3.49±0.48	1,020±165.0
CTA-MGD/SBR-3	YM2010	5	4.48±1.02	2.58±0.44	1.84±0.25	22.3±2.16	8.79±0.29	418±45.8
CTA-MGD/SBR-4	YM2012	4	2.54±0.15	0.20±0.04	0.14±0.03	16.7±1.31	2.96±0.09	1,010±52.0
Silica/SBR	YM2022	4	3.04±0.85	1.49±0.88	2.52±0.80	28.2±4.25	12.70±2.12	518±109.0

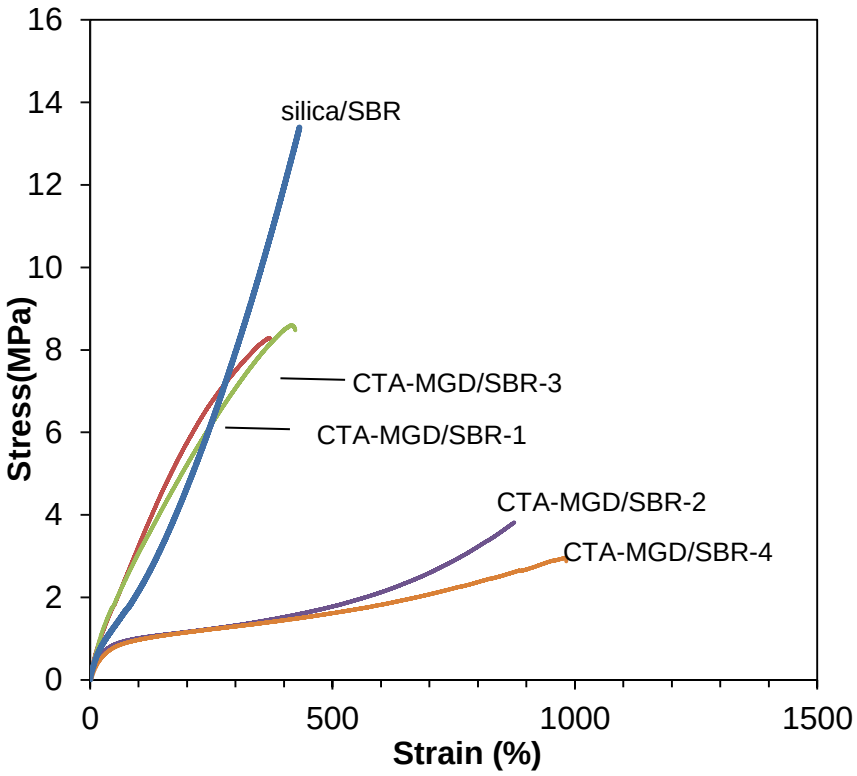

Figure 3.19 Representative stress-strain curves for CTA-MGD/SBR and silica/SBR composites.

These observations are rationalized in terms of the roles of SI-69 in these composites. First, SI-69 delivers additional sulfur to the composite, which increases the density of crosslinks. Second, SI-69 serves as the linking agent between the MGD filler

and the SBR matrix. The greater modulus and tensile strength of CTA-MGD/SBR composites prepared with SI-69 (Figure 3.19) could be due, in part, to the additional crosslinking resulting from the extra sulfur coming from SI-69. Moreover, in composites with MGD-SBR crosslinking mediated by SI-69, de-aggregation of MGD requires more stress at moderate strains. Extension of the SBR network at large strains also requires more stress due to the additional network crosslinking associated with covalent bonding with the MGD. In the absence of SI-69, MGD more readily separates from the SBR under moderate to large strains, as seen in the SEM images of microtomed composites in Figure 3.18.

We also compare the tensile properties of silica/SBR with CTA-MGD/SBR composites. With the addition of SI-69, CTA-MGD/SBR-1 and -3 have higher modulii than that of silica/SBR at 10% and 100% strain. The higher reinforcement is explained by the greater MGD surface area and concomitant increase in SBR-MGD crosslinking. However, the elastic modulus of silica/SBR increases much faster than for CTA-MGD/SBR composites when strain is higher than 270%. The tensile strength of silica/SBR is 52% higher than that of CTA-MGD/SBR-1. When the elastomer composite is stretched to higher strains, the tensile modulus is determined by the crosslink density. Silica/SBR has a higher crosslink density than CTA-MGD/SBR composites (Table 3.12), resulting in higher moduli at higher strains (>270%) and higher tensile strength. Silica/SBR has 26% higher strain energy than that of CTA-MGD/SBR-1 due to the higher tensile strength.

We compare the dynamic mechanical properties of various CTA-MGD/SBR composites (Figure 3.20 and 3.21, Table 3.14) to evaluate the effect of SI-69 and mixing

time on mechanical reinforcement. Among the CTA-MGD/SBR and silica/SBR composites, Figure 3.20 indicates little apparent difference in the *E*' values in the low temperature regime below the glass transition (T_g) with 95% confidence. Considering the magnitude of the tanδ peak (Figure 3.21), compared to all the CTA-MGD/SBR composites, silica/SBR has the highest tan δ peak. CTA-MGD/SBR composites prepared without SI-69 (CTA-MGD/SBR-2 and -4) have higher tan δ peaks than the corresponding composites prepared with SI-69 (> 90% confidence). The addition of SI-69 lowers the energy dissipation of the composites by promoting SBR-MGD and SBR-SBR crosslinking.

Table 3.14 Dynamic mechanical properties of CTA-MGD/SBR-1~4 and silica/SBR composites measured by DMA.

Sample	ID	N	E' at -60 ºC (GPa)	E' at 60 ºC (MPa)	Avg. T_g (ºC)	Avg. value of tan δ peak	tan δ at 60 ºC
CTA-MGD/SBR-1	YM2003	2	2.38±0.12	8.40±0.31	16.59±0.44	1.01±0.03	0.11±0.008
CTA-MGD/SBR-2	YM2007	2	2.41±0.17	6.97±0.53	17.65±0.21	1.11±0.03	0.11±0.010
CTA-MGD/SBR-3	YM2010	2	2.05±0.05	14.69±1.17	17.21±0.03	0.93±0.02	0.08±0.029
CTA-MGD/SBR-4	YM2012	2	2.63±0.13	8.49±0.31	17.71±0.17	1.05±0.02	0.08±0.017
Silica/SBR	YM2022	3	1.95±0.34	4.32±0.49	12.83±0.38	1.26±0.05	0.06±0.008

At temperature above the glass transition, E' values for all CTA-MGD/SBR composites are greater than that of the silica/SBR composite (Figure 3.20). Table 3.14 shows average E' values at 60ºC to explore the role of SI-69 and mixing time on the rubbery moduli of CTA-MGD/SBR composites. The E' value for CTA-MGD/SBR-1 (8.40 MPa) is 21% higher than that of the corresponding composite without SI-69, CTA-MGD/SBR-2 (6.97 MPa, 81% confidence). E' for CTA-MGD/SBR-3 with SI-69 is 73% higher than that of CTA-MGD/SBR-4 without SI-69 (91% confidence). This is explained by the role of SI-69, which not only provides free sulfur for SBR crosslinking, but also

produces crosslinking between MGD and SBR. The higher levels of crosslinking result in greater elastic energy storage (E' values, Figure 3.12).

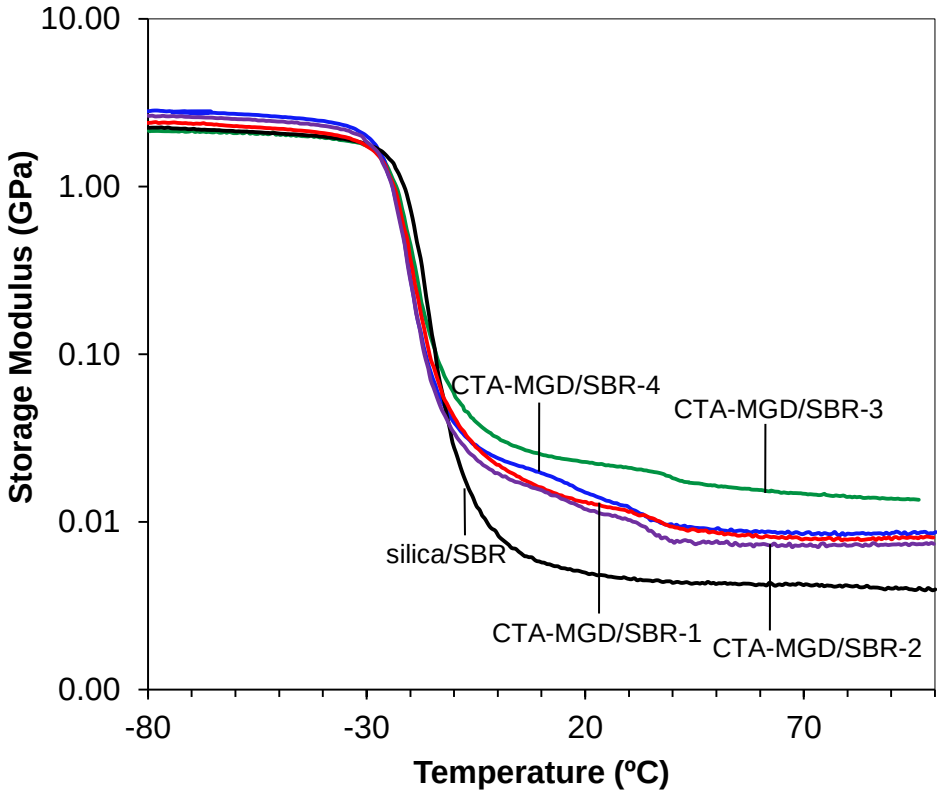

Figure 3.20 Storage modulus as a function of temperature for silica/SBR and CTA-MGD/SBR composites.

Compared to CTA-MGD/SBR composites, silica/SBR has much lower E' at 60ºC. This value (4.32 MPa) is 38% lower (> 95% confidence) than that of CTA-MGD/SBR-2 (6.97 MPa), which has the lowest E' among all the CTA-MGD/SBR composites. This can be attributed to the higher specific surface area of MGD (393 m^2/g) compared to silica (150 m^2/g). In the CTA-MGD/SBR composites, the large interlayer expansion indicates that the interlayer surface area of MGD interacts with SBR to boost the effective filler concentration, resulting in higher E' values. In contrast, less filler surface

area interacts with SBR in silica/SBR composites, producing lower effective filler concentration and thus lower storage modulus.

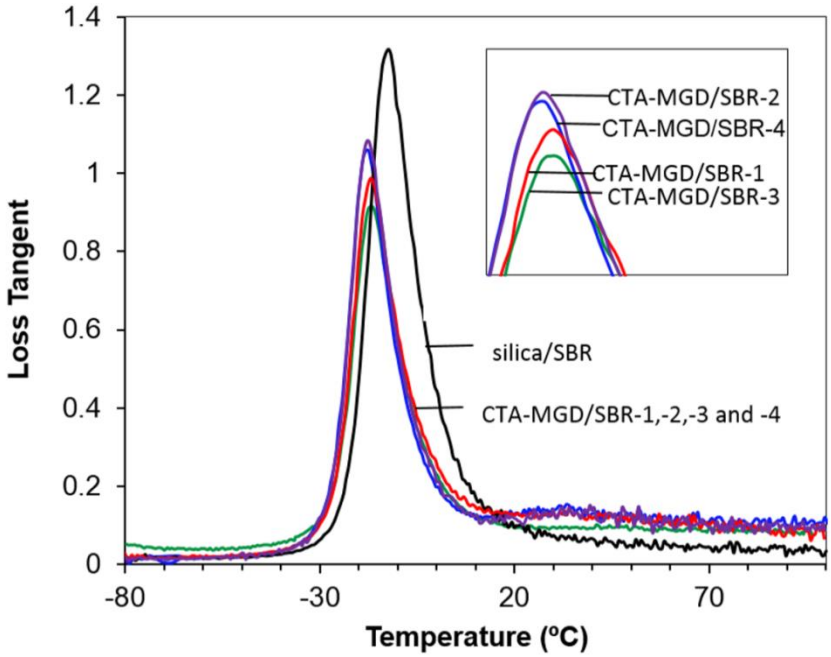

Figure 3.21 Loss tangent as a function of temperature for silica/SBR and CTA-MGD/SBR composites.

With respect to mixing time, for composites prepared without added SI-69 (CTA-MGD/SBR-2 and -4), longer mixing time seems to improve the E' value at 60°C (only 82% confidence). XRD results (Figure 3.16 and 3.17) do not indicate a greater interlayer spacing in CTA-MGD/SBR-4 compared to CTA-MGD/SBR-2. However, nSpec results (Table 3.12) suggest that CTA-MGD particles may be better dispersed in CTA-MGD/SBR-4. When comparing CTA-MGD/SBR-3 and -1, longer mixing time increases E' at 60°C by 75% (91% confidence). CTA-MGD/SBR-1 and -3 composites show comparable filler dispersion (Table 3.12) and MGD interlayer spacing in the final composites. The presence of SI-69 and longer mixing time seems to work together to

enhance the reinforcing effect of MGD. It is possible that longer mixing time promotes the dispersion of both filler and SI-69, which results in improvement of crosslink density (Table 3.12) and the enhanced mechanical properties. Longer mixing time and the addition of SI-69 appear to produce a synergistic effect on mechanical reinforcement in CTA-MGD/SBR composites. It is interesting to mention that CTA-MGD/SBR-4 has about the same E' as CTA-MGD/SBR-1 at 60 ºC. It seems that longer mixing time may compensate the lack of SI-69 to produce comparable E' values in the rubbery regime.

Considering energy dissipation, at temperatures above at 60°C, all CTA-MGD/SBR composites have tan δ values higher than that for the silica/SBR composite (> 90% confidence, Figure 3.21 and Table 3.14). We speculate that in CTA-MGD/SBR, free sulfur from SI-69 is trapped in the interlayer space and does not contribute to produce SBR-SBR crosslinking. In contrast, in silica/SBR, free sulfur from SI-69 leads to more SBR-SBR crosslinking. These observations are supported by the crosslink density values in Table 3.12. The tighter crosslinking in silica/SBR leads to lower tanδ values (lower energy dissipation) in the rubber regime. Longer mixing time does not change the energy dissipation of CTA-MGD/SBR in the rubbery regime, either with or without SI-69. All four CTA-MGD/SBR composites show comparable tan δ values at 60 ºC.

3.3.2.2 Discussion

In section 3.3.2.1, we explored the influence of mixing time and the addition of SI-69 on the mechanical reinforcement of CTA-MGD/SBR composites. Several composites were prepared with varying mixing time and with and without SI-69. XRD patterns were collected after each stage of composite synthesis to identify the distinct role of SI-69 in material reinforcement.

According to the DMA results and tensile properties, SI-69 increases the elastic modulus and storage modulus, and decreases the tan δ peak values. The addition of SI-69 to CTA-MGD/SBR also increases the crosslink density and promotes filler dispersion. SI-69 presumably helps MGD reinforce the composite by releasing free sulfur to produce more SBR-SBR crosslinks and by grafting SBR to MGD. XRD results show that composites prepared with SI-69 showed expansion of the interlayer space entirely during mixing. For composites without SI-69, the interlayer expansion starts during mixing and is not completed until curing. SI-69 seems to facilitate the intercalation of SBR prepolymer.

The influence of longer mixing time is not significant in filler dispersion or tensile properties. The interlayer expansions after each synthesis stage do not change much after longer initial mixing for CTA-MGD/SBR. Longer mixing time does not change the crosslink density of CTA-MGD/SBR with added SI-69. However, crosslink density decreases with increasing mixing time when no SI-69 was added to the mix. CTA-MGD/SBR-2 (no SI-69 and 2 min mixing) shows the worst filler dispersion. Longer mixing time increases the rubbery storage modulus E' value at 60º by 75% and 22% for composites prepared with and without SI-69, respectively. We speculate that SI-69 and longer mixing time show a synergistic effect in improving the reinforcing effect of MGD in CTA-MGD/SBR composites. Longer mixing time may compensate the lack of SI-69 to increase the storage modulus at temperatures in the rubbery regime.

Silica/SBR has a higher filler dispersion rating than all the CTA-MGD/SBR composites, which is possibly due to the different particle shape and morphology of

aggregates. Silica/SBR shows the highest tensile modulus at higher strains (>270%) and ultimate tensile strength, which are attributed to the higher crosslink density.

3.3.3 Influence of Sulfur Source on MGD/SBR Composites

3.3.3.1 Results

Based on the chemical structure of SI-69, it produces rubber composite crosslinks in two ways. Each SI-69 molecule has four sulfur atoms. Upon vulcanization, two are bound to carbon atoms and create crosslinks between filler and elastomer. The other two are released to produce elastomer crosslinking. This "freed" sulfur should act like the bulk sulfur added as a curative in the recipe. This hypothesis has not been tested. Understanding the influence of sulfur source on elastomer crosslinking, composite structure, and mechanical reinforcement will help us to formulate MGD/SBR composites with well-controlled structure and mechanical properties.

CTA-MGD/SBR-1 and -2 were prepared with and without SI-69 respectively. Results in Section 3.3.2 showed that CTA-MGD/SBR-1 had higher crosslink density and better mechanical reinforcement than CTA-MGD/SBR-2. Better reinforcement was attributed to the role of SI-69. It produces crosslinks between MGD and SBR, and it also releases free sulfur to create SBR-SBR crosslinking. In CTA-MGD/SBR-1, two sulfur sources (SI-69 and bulk sulfur) are contributing to crosslinking. We are interested in comparing the roles of these sulfur sources in mechanical reinforcement.

To do this, we prepared additional CTA-MGD/SBR composites with varying amounts of added bulk sulfur (Table 3.15). CTA-MGD/SBR-1 follows the standard

recipe, and CTA-MGD/SBR-2 omits the SI-69. The omitted SI-69 contains 1.73 phr of sulfur. Half of the sulfur, 0.87 phr, is released (freed) during vulcanization. The rest is bound to carbon atoms. CTA-MGD/SBR-5 was prepared with an extra 1.73 phr of bulk sulfur to make up for all of the omitted SI-69 sulfur. Thus the sulfur in the formula of CTA-MGD/SBR-5 includes 3.08 phr bulk sulfur (1.35+1.73). CTA-MGD/SBR-6 was prepared with an additional 0.87 phr of bulk sulfur to make up for only the "freed sulfur" from the omitted SI-69. Thus the bulk sulfur in this recipe is 2.22 phr (1.35+0.87).

Table 3.15 Crosslink density, Mc values, and dispersion ratings of CTA-MGD/SBR-1,-2, -5, and -6 samples.

Sample	ID	Added Sulfur (phr)	SI-69 (phr)	Dispersion Rating	Crosslink density (10^{-4} mol/cm^3)	M_c (10^4 g/mol)
CTA-MGD/SBR-1	YM2003	1.35	7.25	0.011	0.94±0.01	1.25±0.01
CTA-MGD/SBR-2	YM2007	1.35	0	0.016	0.62±0.05	1.90±0.15
CTA-MGD/SBR-5	YM2059	3.08	0	0.007	0.82±0.01	1.42±0.01
CTA-MGD/SBR-6	YM2061	2.22	0	0.021	0.62±0.02	1.89±0.08

We first discuss the three CTA-MGD/SBR composites with no added SI-69: CTA-MGD/SBR-2, -6 and -5. They contain 1.35 phr, 2.22 phr and 3.08 phr of free sulfur, respectively. With the increase in sulfur amount, the crosslink density is 0.62 for CTA-MGD/SBR-2 and -6, with an increase to 0.82 for CTA-MGD/SBR-5. The increase in crosslink density in CTA-MGD/SBR-5 is due to the addition of more sulfur. However, we are not sure why CTA-MGD/SBR-6 does not show an increase in crosslink density compared to -2, even though the added free sulfur increased by 64%.

To compare the reinforcing influence of the two sulfur sources in crosslinking, CTA-MGD/SBR-1 may be compared directly with CTA-MGD/SBR-5 and -6. The latter

two composites are prepared without SI-69, but with extra sulfur to compensate the sulfur from SI-69. CTA-MGD/SBR-1 has a crosslink density 0.94×10^{-4} mol/cm^3, which is 15% and 52% more than that of CTA-MGD/SBR-5 and -6, respectively. CTA-MGD/SBR-1 and -5 have the same amount of sulfur, 3.08 phr. The only difference is that 1.73 phr sulfur in CTA-MGD/SBR-1 is bound to carbon atoms, while in CTA-MGD/SBR-5 it is in the form of free sulfur. The greater crosslinking in CTA-MGD/SBR-1 is from the fixed sulfur atoms that produce MGD-SBR crosslinks and decrease the mobility of elastomer chains. CTA-MGD/SBR-5 features elastomer crosslinking that forms a cage around the MGD interlayers, but does not build any covalent bonds between MGD and SBR. Thus, compared to CTA-MGD/SBR-1, the crosslink density of CTA-MGD/SBR-5 is slightly lower. CTA-MGD/SBR-6 contains 0.87 phr less sulfur than -5, so the crosslink density is even lower in CTA-MGD/SBR-6.

Another speculation about the improved crosslink density in CTA-MGD/SBR-1 is that free sulfur from SI-69 is more effective for reinforcement than the sulfur added on the mill. We learned in Section 3.3.2 that SI-69 facilitates the intercalation of elastomer chains into the MGD interlayer space. In CTA-MGD/SBR-1, SBR prepolymer and SI-69 enter the MGD interlayer space during mixing when SI-69 is added. SI-69 releases free sulfur both inside and outside the MGD interlayers. This results in crosslinking inside the interlayer spaces. In contrast, when no SI-69 is added, based on our XRD results about when elastomer intercalation occurs (Figure 3.16), CTA-MGD/SBR-5 and -6 have only partially penetration of SBR into the interlayer space during mixing.

XRD results show that milling does not change the interlayer spacing much, regardless of whether SI-69 is added. It is speculated that the two roll mill does not

impart enough shear force to drive more SBR intercalation into the interlayers. Very little material exchange between the inside and outside of the MGD interlayers occurs during milling. Thus, curing agents (sulfur and CBS) added in this processing step do not intercalate, either. With less SBR and little or no sulfur in the MGD interlayer spaces, we believe very little interlayer scrosslinking occurs in CTA-MGD/SBR-5 or -6 composites.

In Figure 3.22, SEM images of four MGD/SBR composites provide qualitative information on filler dispersion and MGD/SBR interaction. In all the composites, the MGD particles are evenly dispersed. It is apparent that CTA-MGD/SBR-2 appears to have greater contrast with the surrounding SBR matrix compared to the other three composites. The low contrast in CTA-MGD/SBR-1 is due the addition of SI-69, because it improves the interfacial interaction between the MGD and SBR. The particle/matrix contrast is also low in CTA-MGD/SBR-5 and -6 due to the increased elastomer crosslinking by compensating sulfur. Even though there are no filler-polymer crosslinks, greater sulfur produces stronger "cages" of elastomer around the MGD particles. Upon microtoming, the MGD particles are still entrapped by elastomers, leading to less particle-matrix contrast in the SEM images.

The high filler/matrix contrast seen in CTA-MGD/SBR-2 is explained by the absence of SI-69 and make-up free sulfur. There are no covalent bonds formed between MGD and SBR, thus only physical adhesion occurs. The lack of compensating free sulfur results in less crosslinked elastomer. Some MGD particles are pulled out of the matrix by microtoming, resulting higher filler/matrix contrast in SEM images.

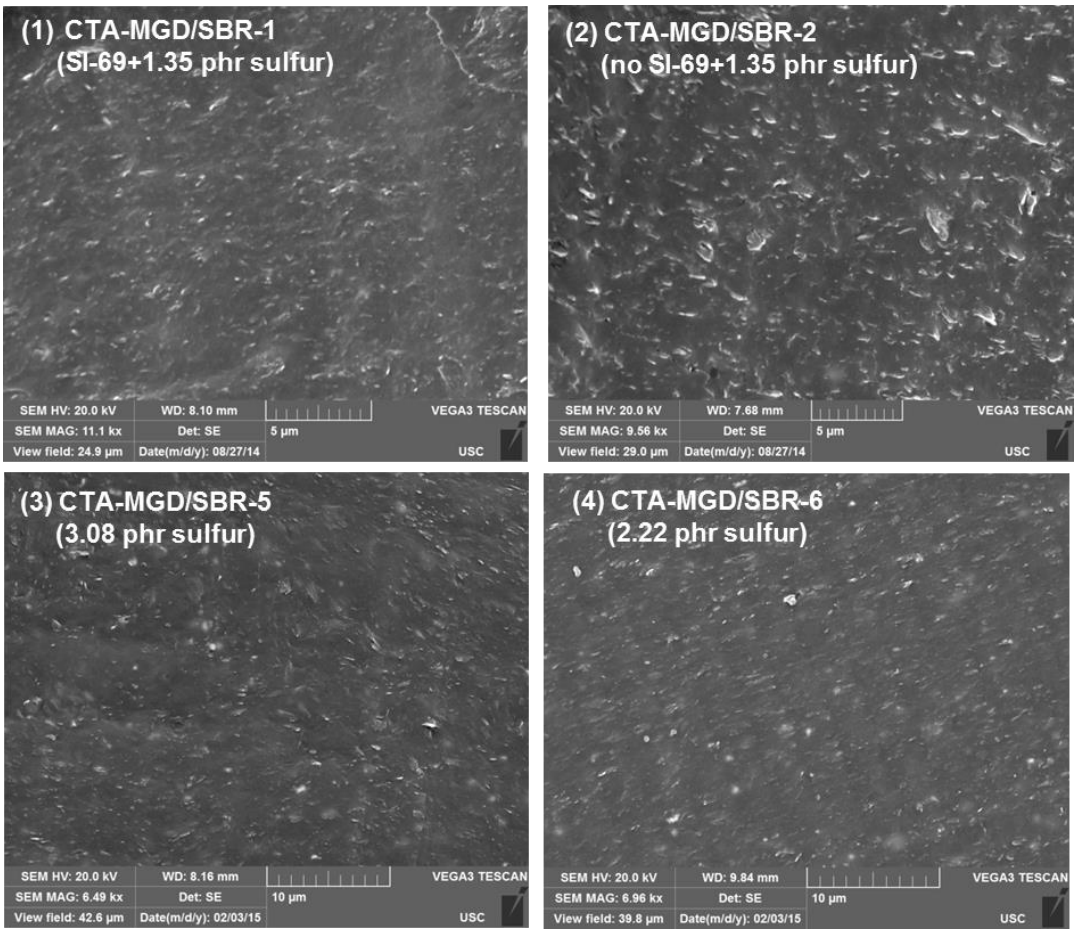

Figure 3.22 SEM images of (1) CTA-MGD/SBR-1, (2) CTA-MGD/SBR-2, (3) CTA-MGD/SBR-5 and (4) CTA-MGD/SBR-6 composites. The sulfur sources for each composite are indicated on the image labels.

Table 3.15 shows quantitative filler dispersion ratings of these four CTA-MGD/SBR composites. CTA-MGD/SBR-1 and -5 show filler dispersion values of 0.011 and 0.007 respectively, which were lower than the other two composites. Both SI-69 and extra free sulfur are effective in promoting dispersion of MGD particles. CTA-MGD/SBR-2 and -6 are prepared without SI-69 or with less compensating sulfur than the other two, which resulted in higher dispersion values corresponding to poorer MGD particle dispersion.

Figure 3.23 shows the stress-strain curves for CTA-MGD/SBR-1, -2, -5, and -6 composites. The figure shows that composites with SI-69 have qualitatively different stress-strain behavior than ones prepared with bulk sulfur. The four CTA-MGD/SBR composites have similar tensile moduli up to around 40% strain. Then, as strain increases, the tensile modulus of CTA-MGD/SBR-1 is obviously larger than those of CTA-MGD/SBR-2, -5, and -6, due to the extra reinforcement resulting from MGD-SBR crosslinking by SI-69. The resulting ultimate tensile strength of CTA-MGD/SBR-1 is higher than the others. However, the corresponding elongation at break of CTA-MGD/SBR-1 is lower. The stress-strain curves for the CTA-MGD/SBR composites clearly show that the presence of SI-69 in the recipe results in a crosslinked structure, certainly involving MGD-SBR crosslinks, that has a profound effect on enhancing mechanical reinforcement by the active MGD filler.

Besides the effect of SI-69, Figure 3.23 also indicates that the reinforcement increases with an increasing amount of free sulfur (CTA-MGD/SBR-2, -6, -5). This is true despite the observation that measured crosslink density (based on bound rubber fraction) does not depend strongly on free sulfur amount in the formulation.

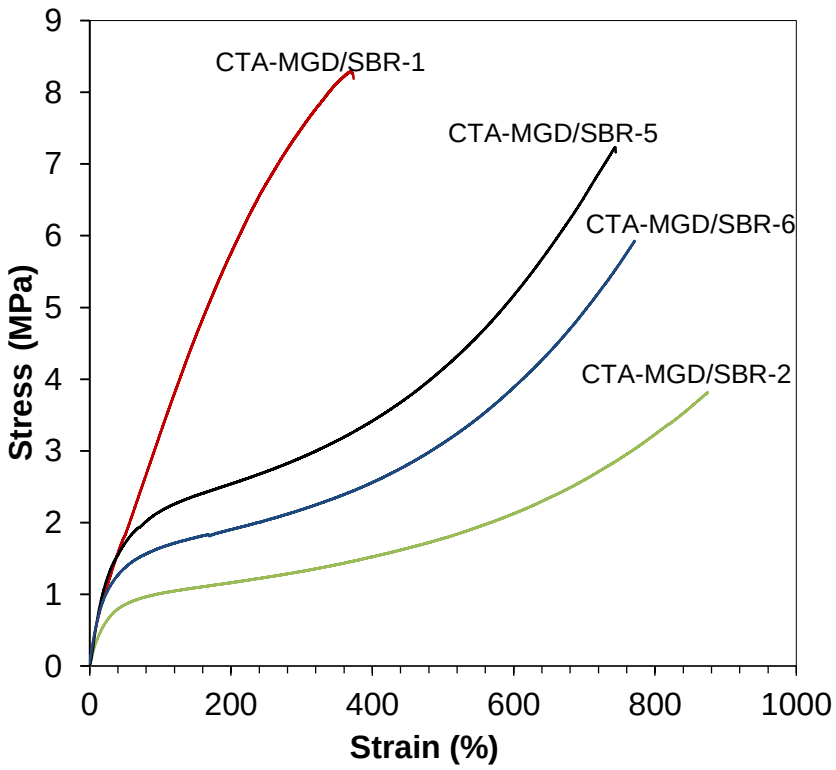

Figure 3.23 Representative stress-strain curves for CTA-MGD/SBR-1, -2, -5, and -6 composites.

Table 3.16 shows mechanical property data derived from tensile stress-strain measurements. The elastic moduli at 10%, 100%, and 250% are denoted as M10, M100, and M250, respectively. As discussed earlier, M10 depends primarily on effective filler concentration, M100 on the effect of strain in disrupting filler aggregates, and M250 on the nature of the crosslinked elastomer network. First, we compare three composites with no added SI-69 and varying amounts of free sulfur. For CTA-MGD/SBR-2, -6 and -5, as the free sulfur amount increases, the moduli at all strains increase. With the greatest amount of added free sulfur, CTA-MGD/SBR-5 has the highest modulus values at all strains, highest tensile strength and highest strain energy. However, with increasing

addition of sulfur, the composite becomes more rigid, thus decreasing the elongation at break. This is often observed in conventional filled rubber composites.[2] The tensile test results are consistent with the crosslink density measurements in Table 3.15. Greater moduli and tensile strength are attributed to higher crosslink density due to the increase in added free sulfur.

Table 3.16 Tensile testing results for MGD/SBR-1, -2, -5, and -6 samples.

Sample	ID	N	M10 (MPa)	M100 (MPa)	M250 (MPa)	Strain Energy density (MJ/m^3)	Tensile Strength (MPa)	Strain at break (%)
CTA-MGD/SBR-1	YM2003	5	4.66±0.49	2.56±0.21	1.72±0.14	22.3±4.16	8.37±0.48	424±55.4
CTA-MGD/SBR-2	YM2007	5	2.77±0.23	0.23±0.05	0.20±0.05	17.4±4.19	3.49±0.48	1,020±165
CTA-MGD/SBR-5	YM2059	5	5.86±0.89	0.56±0.05	0.41±0.04	26.8±2.21	7.22±0.43	745±71.2
CTA-MGD/SBR-6	YM2061	4	4.67±0.50	0.44±0.05	0.30±0.05	24.0±2.79	6.11±0.26	811±85
Silica/SBR	YM2022	4	3.04±0.85	1.49±0.88	2.52±0.80	28.2±4.25	12.7±2.12	518±109

Next we compare the effects of adding SI-69 versus free sulfur on tensile properties by comparing CTA-MGD/SBR-1 and -5 composites. For M10, tensile modulus of CTA-MGD/SBR-5 (5.86 MPa) is 26% greater than CTA-MGD/SBR-1 (4.66 MPa). All of the sulfur in CTA-MGD/SBR-5 is free and responsible for producing SBR-SBR crosslinking during vulcanization. In CTA-MGD/SBR-1, some of the sulfur is bonded to carbon atoms that couple MGD to SBR. Also the freed sulfur released by SI-69 may react more with SBR in the interlayer. This may reduce the effective filler concentration in CTA-MGD/SBR-1 compared to -5.

As strain increases to 100% and 250%, the tensile modulus is dominated by the interaction between filler and polymer. In CTA-MGD/SBR-1, “bound” sulfur enhances

the adhesion between MGD and SBR, so the M100 and M250 values are much higher than for CTA-MGD/SBR-5. The M100 and M250 values for CTA-MGD/SBR-1 are 357% and 320% higher than those of CTA-MGD/SBR-5. These data, as well as the shapes of the stress-strain curves in Figure 3.23, demonstrate the profound effect of silane coupling by SI-69 on the large strain properties of CTA-MGD/SBR composites.

Figure 3.24 compares the dynamic mechanical properties of these four CTA-MGD/SBR composites. In the glassy regime at low temperatures (Figure 3.24 (a), Table 3.17), all of the composites have similar *E*' values. As temperature increases through the glass transition, the storage modulii of four CTA-MGD/SBR composites show a similar transition to the rubbery state.

Table 3.17 compares the storage modulus values at various temperatures, T_g values, and the value of tan δ peak. The four composites have similar storage moduli at -60°C. When the temperature is below T_g, the SBR molecules are trapped by cohesive forces due to low thermal energy, and so the materials behave similarly independent of sulfur source. When temperatures increase to 0°C and 60°C, the trends are similar to these seen in the tensile stress-strain data at low strain. Comparing CTA-MGD/SBR-2, -6, and -5 (increasing amount of free sulfur, no added SI-69), E' values increase with sulfur content, as does T_g. This can be explained by the increase in crosslinking with increasing added free sulfur. Comparing CTA-MGD/SBR-5 (3.08 phr free sulfur) with CTA-MGD/SBR-1 (1.73 phr sulfur from SI-69, 1.35 phr free sulfur), T_g is higher for the former. As the temperature increases above T_g, the SBR chains gain enough energy to move locally. Thus the value of T_g tells us about mechanical reinforcement. The difference in T_g for CTA-MGD/SBR-1 and -5 indicates that SBR needs more thermal

energy to generate chain motion in CTA-MGD/SBR-1 than -5, because MGD/SBR crosslinking immobilizes the SBR more effectively than SBR-SBR crosslinking. However, the E' values at 0°C and 60°C do not differ significantly between CTA-MGD/SBR-1 and -5. These results indicate that the reinforcing effects of both sulfur sources are comparable in terms of their effect on storage modulus above T_g.

With regards to energy dissipation, all four CTA-MGD/SBR composites show similar values of tan δ peak and tan δ at 60 ºC (95% confidence, Table 3.17 and Figure 3.25), indicating similar levels of energy dissipation.

Table 3.17 Dynamic mechanical properties of CTA-MGD/SBR-1, -2, -5, and -6 composites measured by DMA.

Sample	ID	N	E' at -60 ºC (Gpa)	E' at 0 ºC (Mpa)	E' at 60 ºC (Mpa)	Avg. T_g (ºC)	Avg. value of tan δ peak	tan δ value at 60 ºC
CTA-MGD/SBR-1	YM2003	2	2.38±0.12	21.8±0.28	8.40±0.31	-16.6±0.44	1.01±0.03	0.11±0.008
CTA-MGD/SBR-2	YM2007	2	2.41±0.17	18.8±1.12	6.97±0.53	-17.7±0.21	1.11±0.03	0.11±0.010
CTA-MGD/SBR-5	YM2059	2	2.27±0.08	22.4±2.81	8.68±0.56	-13.6±0.04	1.00±0.03	0.08±0.029
CTA-MGD/SBR-6	YM2061	2	2.16±0.30	21.3±3.19	7.72±0.51	-15.5±0.09	0.99±0.01	0.08±0.017

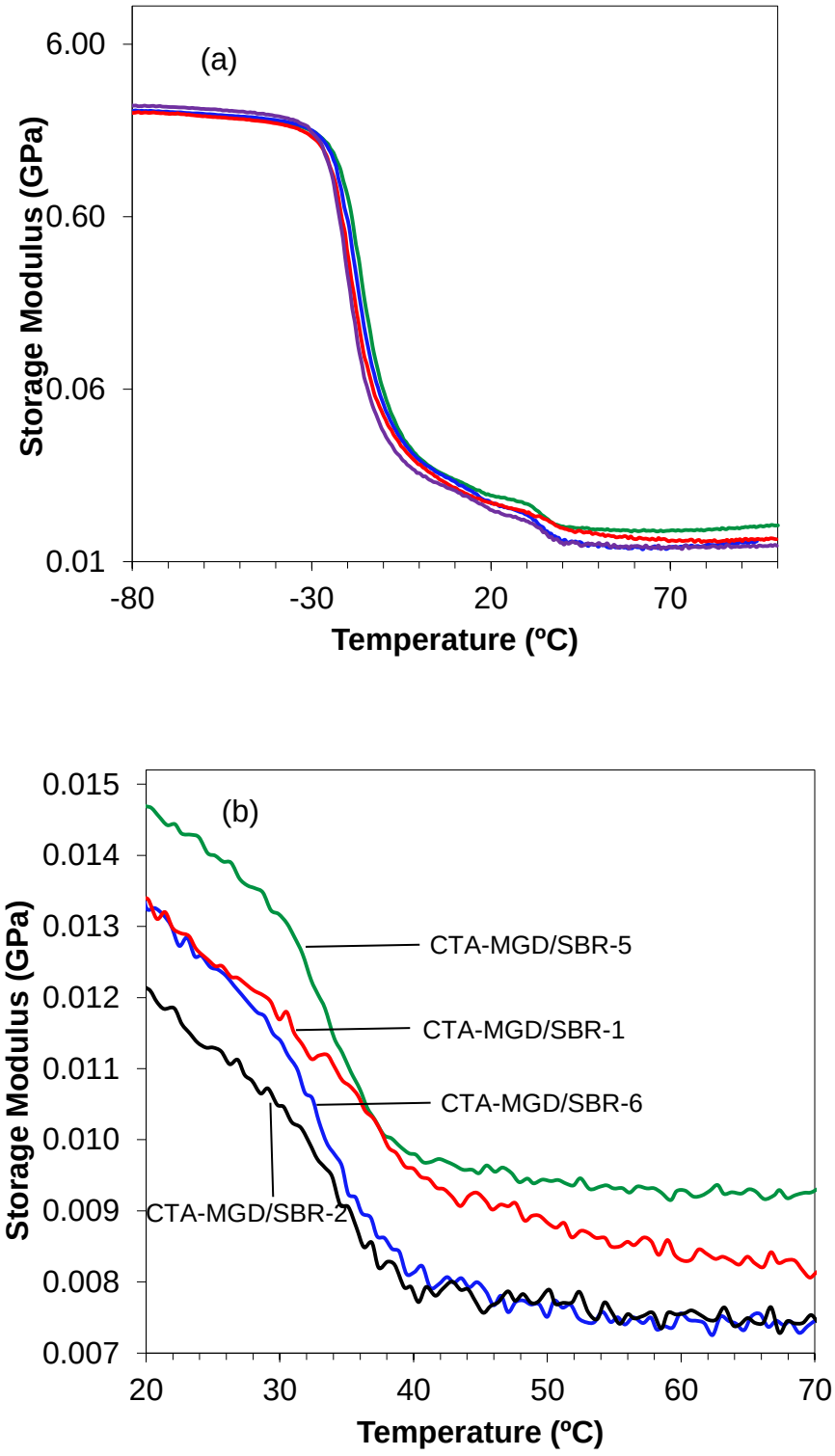

Figure 3.24 Storage modulus as a function of temperature for CTA-MGD/SBR-1, -2, -5, and -6 composites. Panel (a) shows the full temperature range, and (b) emphasizes the rubbery regime.

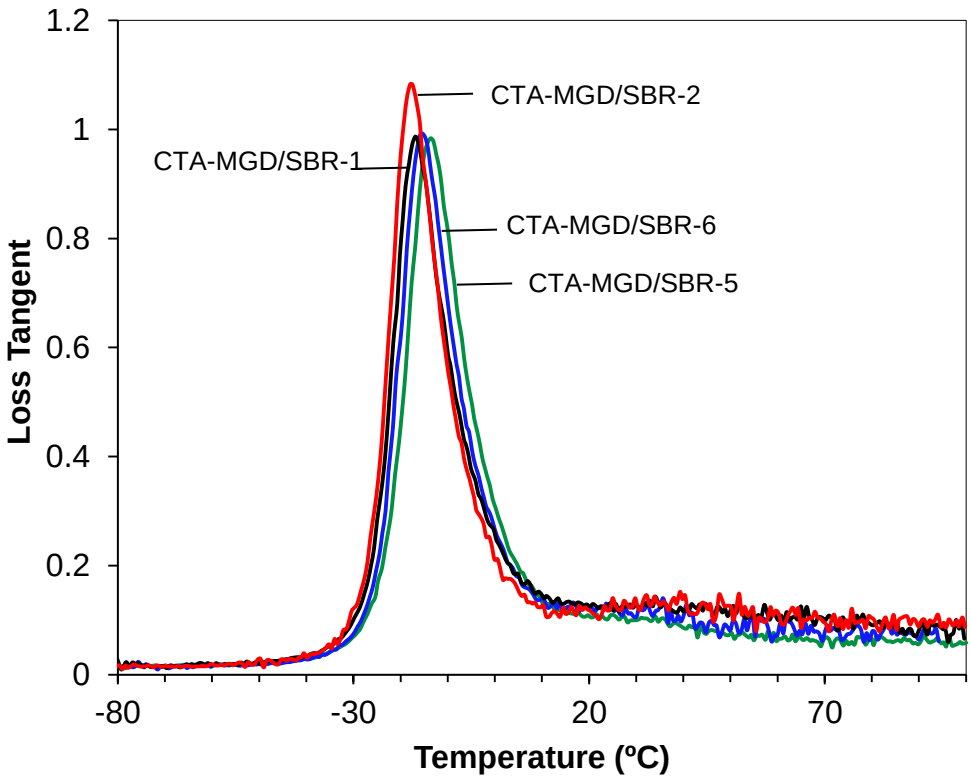

Figure 3.25 Loss tangent as a function of temperature for CTA-MGD/SBR-1, -2, -5, and -6 composites.

3.3.3.2 Discussion

SI-69 provides two kinds of sulfur sources: two sulfur atoms that are released to produce SBR-SBR crosslinking, and two that are attached to carbon atoms for coupling MGD with SBR. In order to understand how the reinforcement mechanisms vary due to the two sources, CTA-MGD/SBR-5 was prepared with extra sulfur to make up for all the sulfur that would have been introduced by SI-69. CTA-MGD/SBR-6 was prepared with extra sulfur to make up the free sulfur that would have been released by SI-69.

CTA-MGD/SBR-1 has the highest crosslink density, which is 15% higher than that of CTA-MGD/SBR-5 having the second highest crosslink density. The higher crosslink density of the former is attributed to the role of SI-69, which produces both SBR-SBR and MGD-SBR crosslinking. The effect of SI-69 is also observed in tensile properties. CTA-MGD/SBR-1 has obviously high tensile moduli at high strains (M100 and M250). This kind of reinforcement is not seen in the other CTA-MGD/SBR composites prepared with only bulk sulfur. Quantitive filler dispersion measurements show that bulk sulfur and SI-69 both promote CTA-MGD dispersion in SBR. There is no apparent difference in storage modulus and energy dissipation values for CTA-MGD/SBR-1, -2, -5 and -6 composites. The difference in T_g values shows that SI-69 seems to be more effective in immobilizing the SBR with MGD. So, the addition of SI-69 in CTA-MGD/SBR increases the crosslinking density and tensile modulus at high strains, promotes MGD platelet dispersion, and immobilizes the SBR by forming covalent bonds with MGD. The influences upon storage modulus and energy dissipation by SI-69 and bulk sulfur in CTA-MGD/SBR are comparable.

Based on the results in section 3.3.3.1, the presence of sulfur in the MGD interlayer space appears to play an important role in reinforcing the intercalated elastomer, resulting in better composite mechanical performance. Scheme 3.1 shows a proposed picture of the crosslinked structure in these composites. Scheme 3.1(a) shows elastomer fully crosslinked fully both inside and outside MGD platelets (CTA-MGD/SBR-1). In Scheme 3.1(b), even though the elastomer outside the interlayers is crosslinked well and fully covers the fillers, the incomplete crosslinking between the interlayers may

inadvertently create defects that could possibly cause material failure under stress with poor reinforcement.

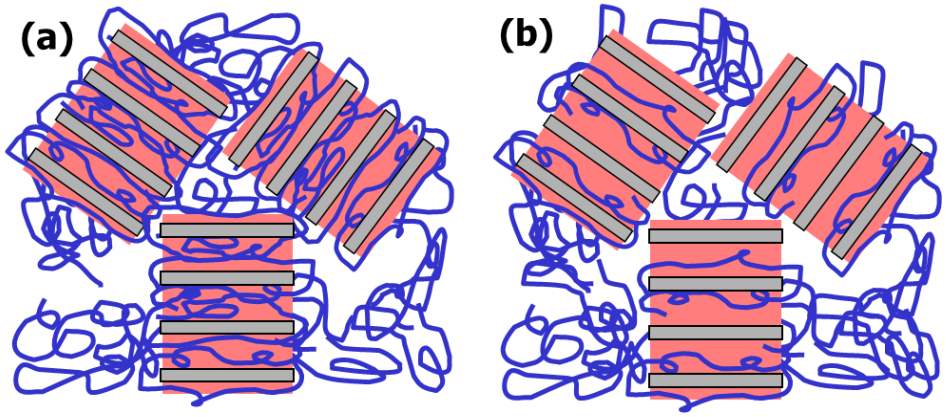

Scheme 3.1 (a) sulfur released by SI-69 in the interlayers produced fully crosslinked structure, (b) no sulfur released by SI-69 in the interlayers and the intercalated polymer interlayers are not well crosslinked.

In future work, it will be interesting to study CTA-MGD/SBR with silane containing only bound sulfur. This kind of silane, 3-mercaptopropyltriethoxysilane (MPTES), was introduced in previous work.[75] The resulting CTA-MGD/SBR should be compared with CTA-MGD/SBR prepared with SI-69, which will help us to understand the reinforcing effect of two kinds of free sulfur.

3.3.4 Influence of Varying Elastomer Chemistry on MGD/Elastomer Composites

Some research papers[111,118,119] reported that layered silicates produced different reinforcing effects in various elastomers depending on the elastomer chemistry. So far, we studied the reinforcement mechanism of MGD only in SBR composites. It will help us to understand how MGD reinforces elastomer composites by preparing composites containing MGD dispersed in other elastomers. In this section, we compare elastomer

composites prepared with BR and SBR to explore the influence of different elastomer chemistry on MGD reinforcement mechanisms.

3.3.4.1 Results

Figure 3.26 shows the XRD patterns for CTA-MGD, CTA-MGD/SBR and CTA-MGD/BR. In CTA-MGD/SBR, the MGD interlayer spacing increased from 3.100 nm in CTA-MGD to 3.943 nm in the final cured composite. The interlayer expansion of CTA-MGD is 0.843 nm. In CTA-MGD/BR, the MGD interlayer spacing increases from 3.100 nm to only 3.297 nm in the cured CTA-MGD/BR composite. The interlayer expansion is only 0.197 nm. The small expansion indicates that only a limited amount of BR chains are intercalated into the CTA-MGD interlayers. The expansion in CTA-MGD/BR composite is 0.646 nm less than that in CTA-MGD/SBR composite, indicating that SBR intercalates more readily than BR into the CTA-MGD interlayer space.

We speculate that the difference in intercalation behavior is due to the aromatic group in the SBR. For ammonium surfactants like CTA^+, some research shows that an additional attraction exists between the cationic head group of the surfactant and the pi electrons in aromatic compounds.[129,130] It is possible that in SBR composites, the styrene groups experience cation-pi interaction with the ammonium head group of CTAB, creating an attractive force between SBR and CTA^+. This extra attraction may help to draw the SBR prepolymer into the MGD interlayers. The additional SBR intercalation, along with the bulky styrene groups in SBR, make SBR more effective in expanding the MGD interlayer space, explaining the larger MGD interlayer spacing compared with CTA-MGD/BR composites.

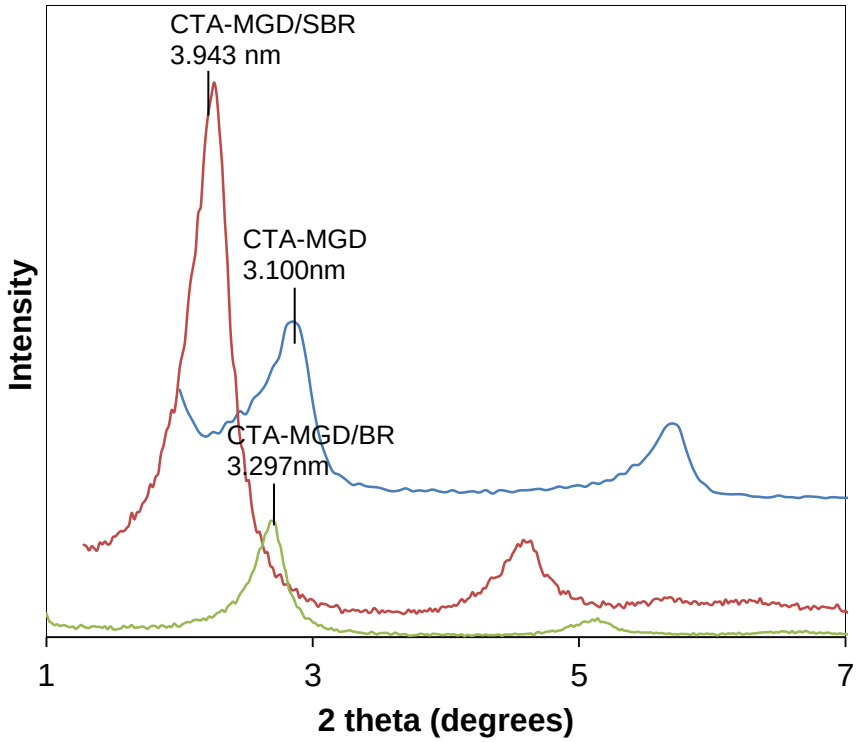

Figure 3.26 XRD patterns for starting CTA-MGD and CTA-MGD in BR and SBR composites.

During batch mixing, blade torque is recorded by a computer. Figure 3.27 shows that torque changes as a function of mixing time for SBR and BR green mixes. CTA-MGD/SBR shows a much lower torque value than the other three composites, which might be related to the filler-elastomer compatibility. Because of the interaction between CTA^+ head groups and styrene groups in SBR, CTA-MGD interlayers may be more compatible with SBR prepolymer, resulting lower torque values and better material processability. In contrast, in the two BR composites and silica/SBR, the lack of this extra interaction may result in greater mixing torque. The higher mixing torque in CTA-MGD/BR indicates a low compatibility between CTA-MGD and BR, which is consistent with the comparatively small MGD interlayer expansion.

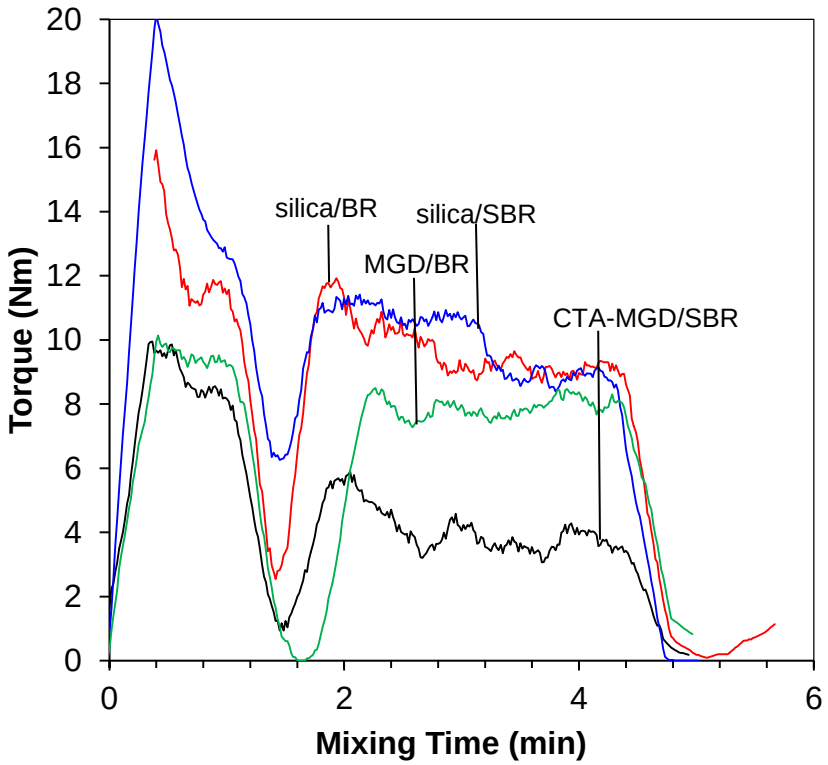

Figure 3.27 Torque profiles for mixing CTA-MGD and silica with SBR and BR.

According to SEM images in Figure 3.28, all of the fillers are dispersed uniformly in these elastomer composites. Silica/SBR and silica/BR appear to have similar silica dispersion and aggregation, consistent with the similar dispersion rating of both composites (Table 3.18). In MGD/elastomer composites, MGD particles are also well dispersed in the composites. CTA-MGD/BR appears to show more particle aggregation and longer MGD filler particles than CTA-MGD in SBR. This observation is consistent with poor filler dispersion rating value for CTA-MGD/BR and its low interlayer expansion. The particle dispersion of CTA-MGD/BR is the poorest among all the OMGD/elastomer samples we prepared in our current work.

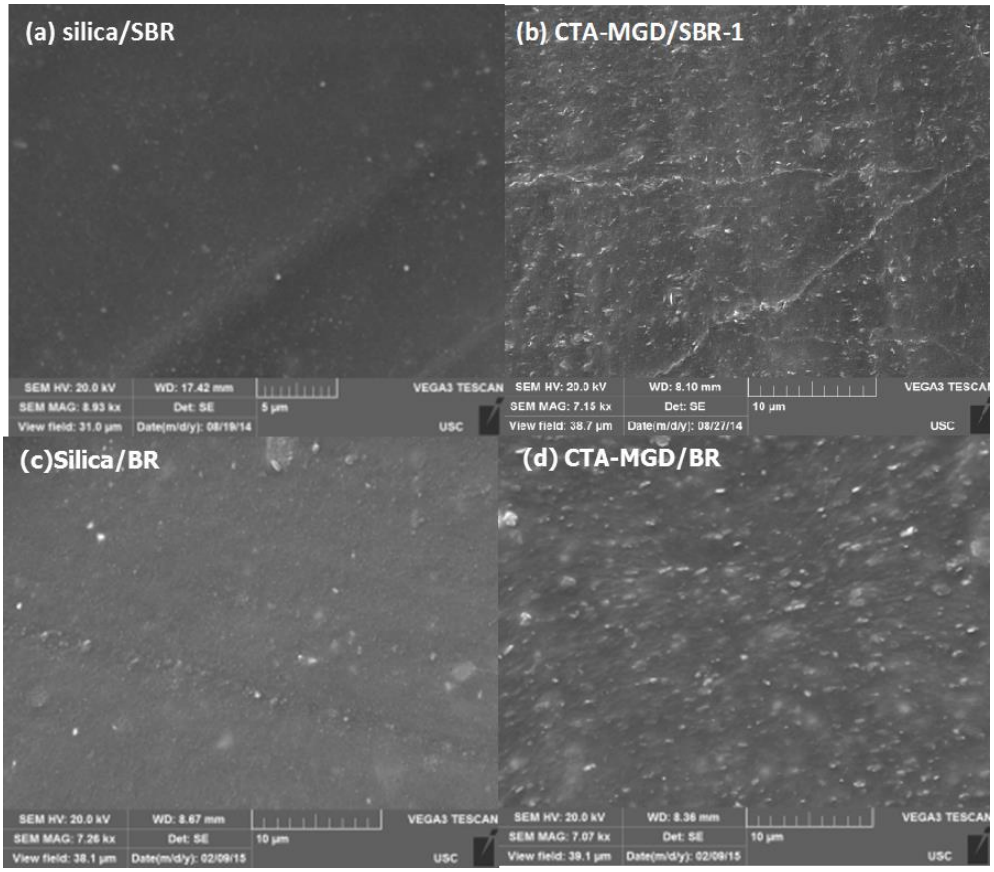

Figure 3.28 SEM images of (a) silica/SBR, (b) CTA-MGD/SBR-1, (c) silica/BR, and (d) CTA-MGD/BR composites.

Table 3.18 Crosslink density, Mc values and dispersion rating values of SBR and BR composites.

Sample	Sample ID	Dispersion Rating	Crosslink density (10^{-4} mol/cm^3)	M_c (10^4 g/mol)
silica/SBR	YM2022	0.020	1.23±0.02	0.95±0.01
silica/BR	YM2072	0.019	1.75±0.03	0.67±0.01
CTA-MGD/SBR	YM2003	0.011	0.94±0.01	1.25±0.01
CTA-MGD/BR	YM2065	0.020	0.31±0.02	3.83±0.20

Table 3.18 shows that silica/BR has a 42% higher crosslink density and 42 % lower M_c value than silica/SBR. This may be due to the difference in polymer chemistry

between BR and SBR: for a given chain length between crosslinks, the SBR chain will have a higher molecular weight due to the bulky styrene side groups. However, in CTA-MGD composites, the trend is opposite. CTA-MGD/SBR has 203% higher crosslink density and 67% lower M_c value than those of CTA-MGD/BR. Considering the poor filler dispersion and low interlayer expansion in CTA-MGD/BR, the low crosslink density might be expected. If BR does not intercalate into the CTA-MGD interlayers, there would be much less MGD-BR crosslinking by SI-69. Moreover, SI-69 might be sequestered in the CTA-MGD interlayer space, making all of the SI-69 sulfur unavailable for BR crosslinking.

Similar to discussion about CTA-MGD/SBR and silica/SBR composites, CTA-MGD/BR has a much lower crosslink density and higher M_c value than silica/BR. As explained above and previously in Section 3.3.1.2, sulfur from SI-69 may be trapped in the MGD interlayers, resulting in poor crosslinking densities. All of the SI-69 sulfur in silica/SBR can contribute to crosslinking: the carbon-bound S can produce covalent silica-BR crosslinks, and the freed S may be released to produce BR-BR crosslinking, resulting in much higher crosslink densities and lower M_c values in silica/BR compared to CTA-MGD/BR composites.

Representative stress-strain curves for SBR and BR composites are shown in Figure 3.29. SBR composites show higher tensile strength and strain energy than the corresponding BR composites. This can be attributed to the presence of styrene groups in SBR. Generally, SBR composites are stiffer than BR composites.

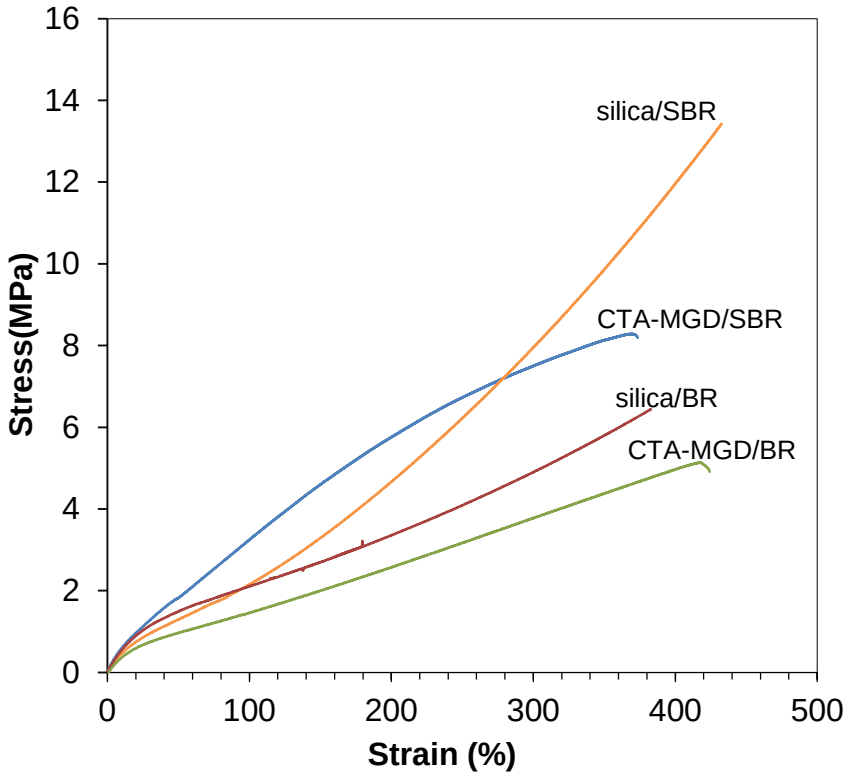

Figure 3.29 Representative stress-strain curves for SBR and BR composites.

More tensile testing results are shown in Table 3.19. We first compare two silica filled elastomer composites. Silica/SBR has an M10 value 32% lower than that of silica/BR. The stress and tensile modulus of silica/SBR increase with strain more rapidly than in silica/BR. When strain increases to 100%, two composites have approximately the same M100 value. As the composites are stretched to 250% strain, silica/SBR has an M250 value 63% higher than that of silica/BR. Tensile modulus at M250 is dominated by the composites' crosslink density. However, silica/SBR has a lower crosslink density than that of silica/SBR (Figure 3.18). We think that even though the silica/SBR composite has a lower crosslink density, the modulus is higher due to the stiffer chemical

structure resulting from the styrene groups in SBR. Consequently the tensile strength, elongation at break, and strain energy of silica/SBR are superior to those of silica/BR.

Table 3.19 Tensile testing results for various BR and SBR composites.

Sample	ID	N	M10 (MPa)	M100 (MPa)	M250 (MPa)	Strain Energy Density (MJ/m^3)	Tensile Strength (MPa)	Strain at Break (%)
silica/SBR	YM2022	4	3.04±0.85	1.49±0.88	2.52±0.80	28.2±4.25	12.70±2.12	518±109.0
silica/BR	YM2072	6	4.45±0.54	1.17±0.18	1.55±0.17	9.21±2.80	5.20±1.02	324±46.7
CTA-MGD/SBR	YM2003	5	4.66±0.49	2.56±0.21	1.72±0.14	22.3±4.16	8.37±0.48	424±55.4
CTA-MGD/BR	YM2065	5	2.64±0.20	1.06±0.10	1.25±0.17	9.9±1.42	4.76±0.41	404±33.4

We next compare the two CTA-MGD filled elastomer composites. CTA-MGD/SBR has higher tensile moduli than those of CTA-MGD/BR at all of the strains. CTA-MGD/SBR has more elastomer intercalation than CTA-MGD/BR, due to the extra attraction between cationic head group in CTA^+ and the styrene aromatic rings in SBR. CTA-MGD/SBR therefore has a higher effective filler concentration, which dominates the tensile modulus at low strains. At high strains, the higher tensile moduli of CTA-MGD/SBR are rationalized by the corresponding higher crosslink density than that of CTA-MGD/BR. Due to the higher effective filler concentration and the stiff structure of SBR, CTA-MGD/SBR has higher tensile strength, elongation at break, and strain energy than CTA-MGD/BR.

3.3.4.2 Discussion

Preparing MGD rubber composites in various elastomers helps us to understand more about MGD reinforcement mechanisms. According to XRD results, in final cured CTA-MGD/BR composites, the MGD interlayers are barely expanded. In contrast, in CTA-MGD/SBR, the expansion of interlayer spacing indicates the intercalation of SBR.

The filler dispersion ratings are consistent with the interpretation of XRD results. CTA-MGD/SBR has much better filler dispersion than CTA-MGD/BR. The differences between SBR and BR composites are believed to be due to the favorable interaction of the ammonium head group of CTA^+ with the styrene aromatic rings of SBR. In addition to the bulky structure of SBR, CTA-MGD is more readily intercalated by SBR. The absence of the attractive interaction and less-bulky structure of BR results in CTA-MGD/BR having the worst filler dispersion rating among all the OMGD rubber composites prepared in our current work. The crosslink density of silica/SBR is lower than that of silica/BR. However, silica/SBR has higher moduli at high strains, higher tensile strength and other tensile properties compared to silica/BR, probably due to the stiffer structure of SBR. CTA-MGD/SBR has higher tensile properties and crosslink density than those of CTA-MGD/BR. CTA-MGD and silica show different reinforcement mechanisms in SBR and BR, depending on the elastomer chemistry. This exploration of reinforcement mechanism provides us with some insight into formulating better rubber composites and improving mechanical properties.

3.3.5 Influence of CTA^+ on MGD/SBR and Silica/SBR Composites

Much research has reported that ammonium cations, such as CTA^+, are efficient in accelerating rubber vulcanization and increasing crosslink density. In previous work[75], the influence of CTA^+ on MGD/SBR curing was mentioned, but not explored in detail. In MGD/SBR composites, the layered structure brings more varying factors into the system, such as accessible filler surface area and interlayer spacing. In this work, we now compare CTA-silica/SBR and silica/SBR directly to study the influence of CTA^+ on vulcanization, crosslinking and mechanical properties. The results will shed some light

on results from previous work[75] and help us to understand more about the influence of organic surfactants like CTA^+ on vulcanization and mechanical reinforcement.

3.3.5.1 Organically-Modified Silica Fillers

Figure 3.30 shows the TGA weight loss of silica and CTA-silica. For silica, the water loss up to 150 ºC is 4.22%. The total weight loss is 7.04%, and the residue weight is 92.96%. Thus the dehydroxylation loss is 2.82%. Similar to the discussion about MGD, we think that there is a constant ratio of dehydroxylation loss (2.82%) to residue weight (92.96%). In silica, this ratio is 0.030. For CTA-silica (Figure 3.30), the water loss up to 150 ºC is 4.26%. The total weight loss is 20.49%, thus the residue weight is 79.51%. Assuming a constant ratio of dehydroxylation loss to residue weight (0.030), the dehydroxylation loss is 2.39%. Subtracting dehydroxylation and water loss from total weight loss, the CTA^+ loss is 13.83%. This indicates that CTA-silica contains 1.91 moles of CTA^+ per mole of $Si_{14}O_{29}$ unit cells (Table 3.20).

Table 3.20 TGA results for silica and organically-modified silica samples.

Sample	Total Weight Loss (%)			Residue (%)	moles of cations per $Si_{14}O_{29}$ mole
	Water (%)	Dehydroxylation (%)	Cations (%)		
silica	7.04			92.96	NA
	4.22	2.82	NA		
CTA-silica	20.49			79.51	1.91
	4.26	2.39	13.83		

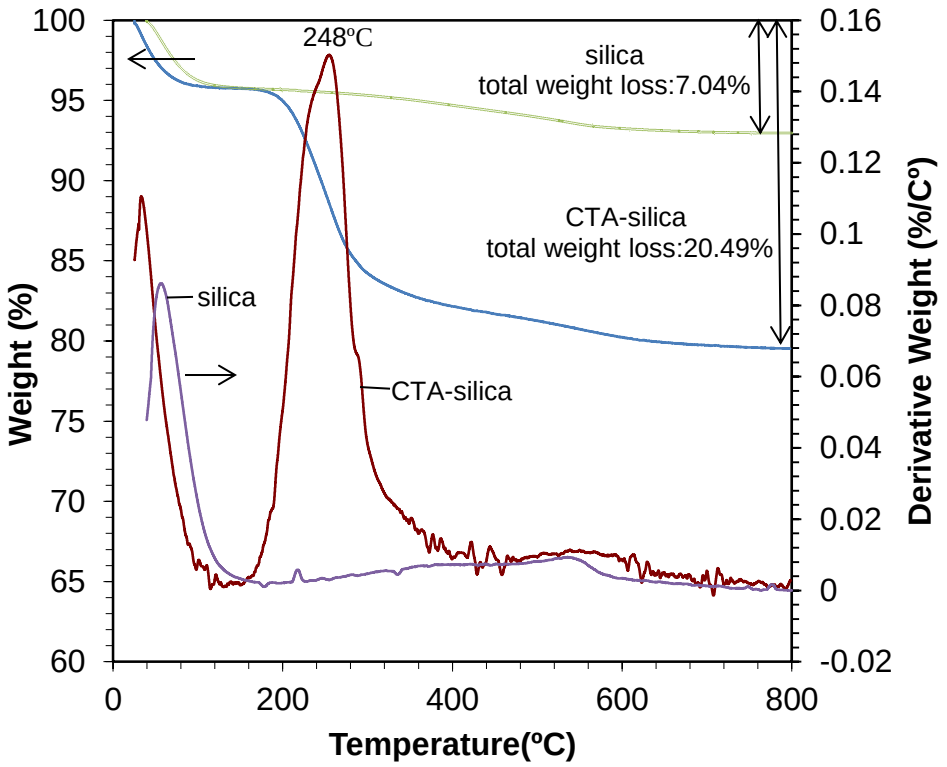

Figure 3.30 TGA weight loss and rate of change (derivative weight) as functions of temperature for silica and CTA-silica. The heating rate is 5°C/min.

3.3.5.2 Silica/SBR Composites

Figure 3.31 shows cure curves for silica/SBR composites as characterized by RPA. More information about the vulcanization characteristics is shown in Table 3.21. The addition of CTA^+ to the silica/SBR mix decreases the scorch delay time from 7.80 min to 2.60 min. This observation is consistent with much work reporting that the ammonium modifier serves as a catalyst to accelerate the vulcanization rate and decrease the scorch delay time. Short scorch delay time causes processing or control problems, which is not beneficial in industry for rubber production.

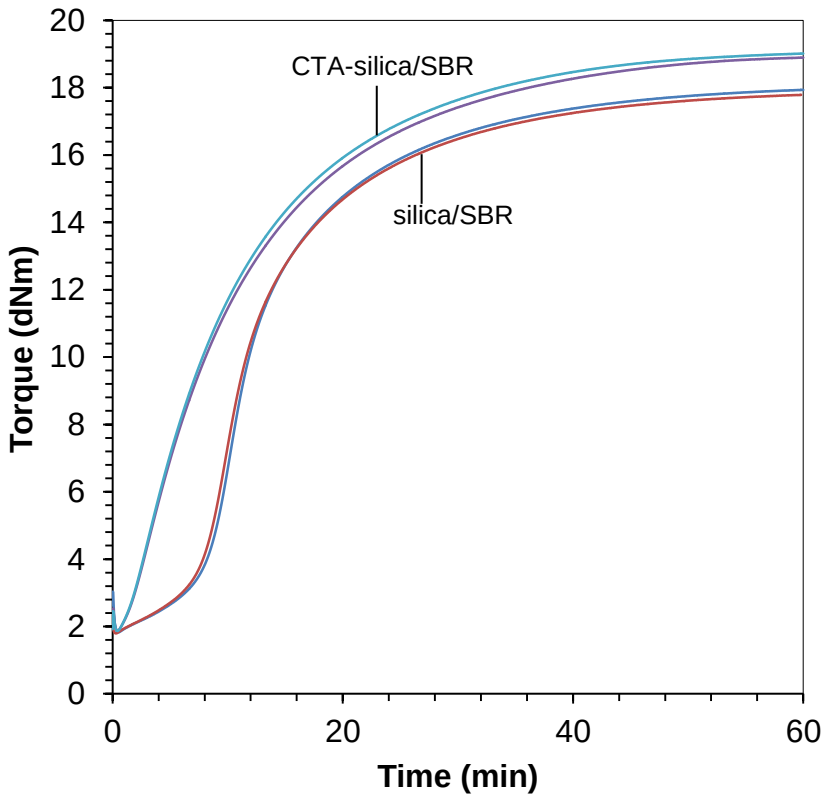

Figure 3.31 Cure curves of CTA-silica/SBR and silica/SBR

With the addition of CTA^+ to silica/SBR, the scorch delay was shortened considerably. For CTA-silica/SBR, T_{S2} was 5.2 min shorter than that for silica/SBR. However, the optimum cure time T_{C90} was not changed much. Cure Rate Index (CRI) is commonly used as a measure of the rate of the cure reaction. The addition of CTA^+ decreases the CRI by 1.03 min^{-1} (Table 3.21), which suggests that the vulcanization is deactivated by the presence of CTA^+. This contradiction can be explained by looking at the definition of the CRI (Table 3.21 heading or Equation 3.4). The lower CRI for CTA-silica/SBR is entirely due to its lower T_{s2}, or shorter scorch delay; T_{c90} remains the same. From the shape of the cure curves (Figure 3.31), it appears that CTA^+ accelerates the initial vulcanization rate, but after 10 minutes, the reaction rates are similar.

Table 3.21 Vulcanization characteristics of silica/SBR and CTA-silica/SBR

Sample	S' Max (dNm)	S' Min (dNm)	ΔS=S'Max-S'Min (dNm)	T_{S2} (min)	T_{C90} (min)	CRI=100/(T_{c90}-T_{s2}) (min^{-1})
silica/SBR	17.86	1.82	16.05	7.80	27.75	5.01
CTA-silica/SBR	18.95	1.87	17.08	2.60	27.74	3.98

The maximum torque values are 17.86 dNm and 18.95 dNm for silica/SBR and CTA-silica/SBR, respectively. The presence of CTA^+ results in about 6% increase in the maximum torque. The increase in maximum torque correlates with an increase in crosslink density (Table 3.22). CTA-silica/SBR has 29 % larger crosslink density and 22% lower M_c value compared to these of silica/SBR. This may be explained by the catalytic effect of CTA^+ in accelerating the vulcanization. The amine groups activate functional groups of the accelerators, resulting in a more highly crosslinked structure.

Table 3.22 Crosslink density, Mc values and filler dispersion ratings of silica/SBR and CTA-silica/SBR.

Sample	Crosslink Density (10^{-4} mol/cm^3)	M_c (10^{-4} g/mol)	Dispersion Rating
silica/SBR	1.23±0.02	0.95±0.01	0.020
CTA-silica/SBR	1.58±0.02	0.74±0.01	0.014

SEM images of both silica/SBR and CTA-silica/SBR are shown in Figure 3.32. Silica is dispersed uniformly in both composites. There is no notable difference in filler dispersion observed in the SEM images. Quantitative information about filler dispersion is provided in Table 3.22. CTA-silica/SBR has a dispersion rating of 0.014, which is about 30% smaller than that of silica/SBR. The improvement in filler dispersion is consistent with the increases in torque value and crosslink density. The improved silica

dispersion in CTA-silica/SBR may be explained by the surface activity of CTA^+, which helps break up silica aggregates.

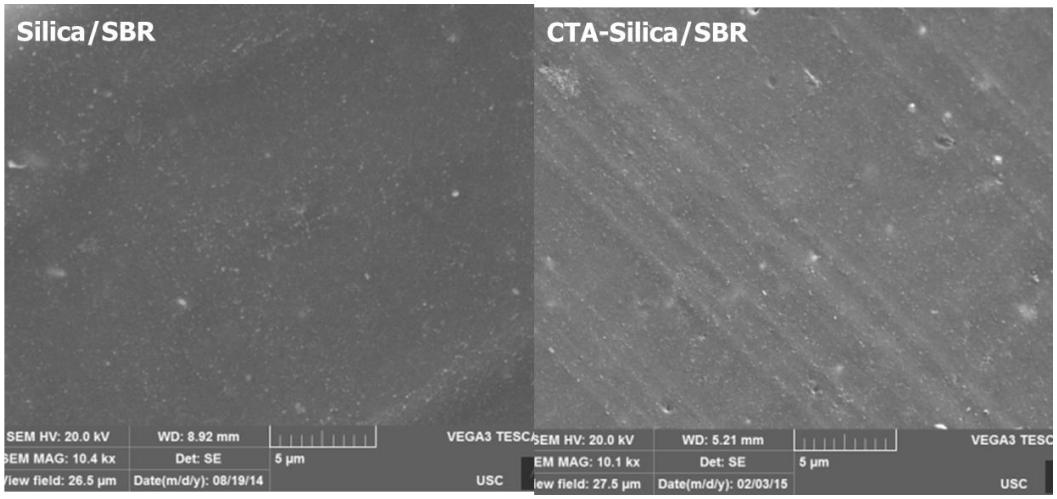

Figure 3.32 SEM images of (a) silica/SBR and (b) CTA-silica/SBR composites.

In terms of tensile properties, there is not much apparent difference between silica/SBR and CTA-silica/SBR as shown in Figure 3.33 and Table 3.23. At 10% strain, CTA-silica/SBR has a 30% larger M10 value (82% confidence). The presence of CTA^+ may promote better silica dispersion and thus effective filler concentration, which may explain the larger M10 value for CTA-silica/SBR. At larger strains, the differences in the M100 and M250 values are not statistically significant. CTA-silica/SBR and silica/SBR have comparable tensile strength and strain at break. The larger strain at break for CTA-silica/SBR (83% confidence) results in higher strain energy for CTA-silica/SBR. We conclude that CTA^+ does not have a significant effect on the tensile properties of CTA-silica/SBR composites, other than perhaps promoting better silica dispersion that results in better low strain tensile modulus.

Table 3.23 Tensile testing results for silica/SBR and CTA-silica/SBR composites.

Sample	ID	N	M10 (MPa)	M100 (MPa)	M250 (MPa)	Strain Energy Density (MJ/m^3)	Tensile Strength (MPa)	Strain at break (%)
silica/SBR	YM2022	4	3.04±0.85	1.49±0.88	2.52±0.80	28.2±4.25	12.70±2.12	518±109
CTA-silica/SBR	YM2074	4	3.96±0.15	1.81±0.24	2.80±0.37	20.7±2.59	11.00±1.18	414±30.4

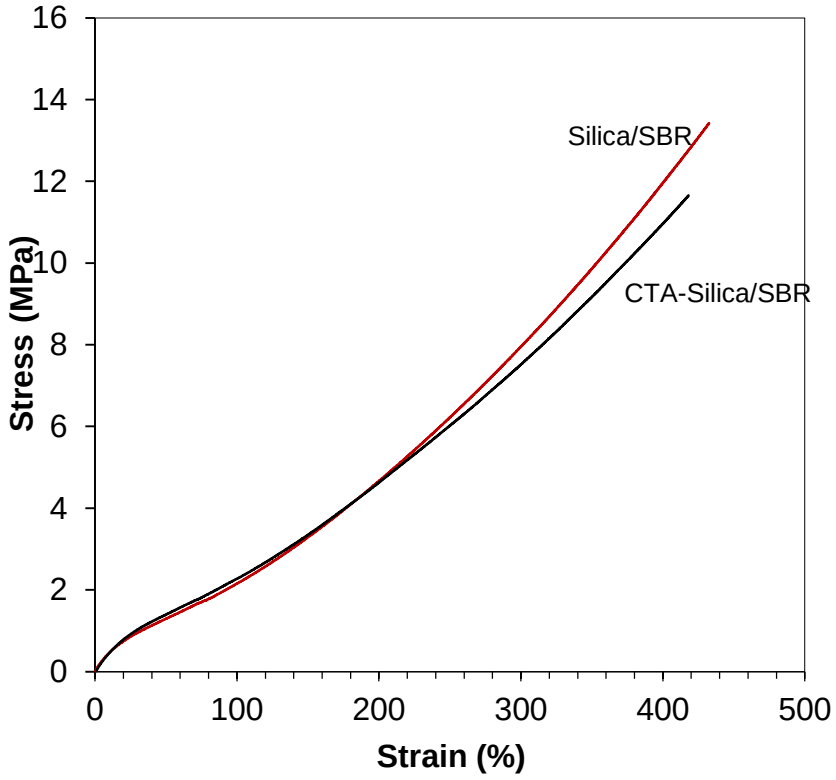

Figure 3.33 Representative stress-strain curves for CTA-silica/SBR and silica/SBR composites.

Dynamic mechanical properties are characterized by DMA. Figures 3.34 and 3.35 show the storage modulus and loss tangent as functions of temperature. The storage modulus values at -60 ºC, 0 ºC and 60 ºC, tan δ peak values and T_g are shown in Table 3.24. CTA-silica/SBR and silica/SBR show almost the same values of these properties. The addition of CTA^+ does not result in any change in dynamic mechanical properties.

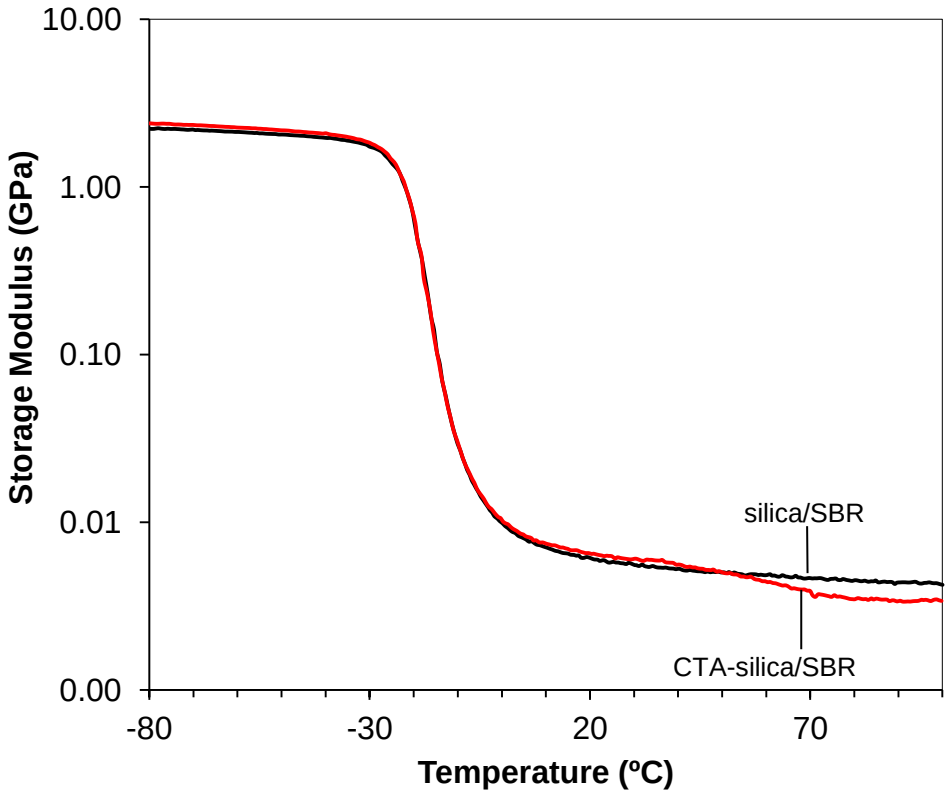

Figure 3.34 Storage modulus as a function of temperature for silica/SBR and CTA-silica/SBR composites.

Table 3-24 Dynamic mechanical properties of silica/SBR and CTA-silica/SBR composites measured by DMA.

Sample	ID	E' at -60 ºC (Gpa)	E' at 0 ºC (Mpa)	E' at 60 ºC (Mpa)	Avg. T_g (ºC)	Avg. value of tan δ peak
Silica/SBR	YM2022	1.95±0.34	8.75±1.50	4.32±0.49	-12.83	1.26
CTA-Silica/SBR	YM2074	2.20±0.09	10.37±0.30	4.32±0.20	-13.50	1.23

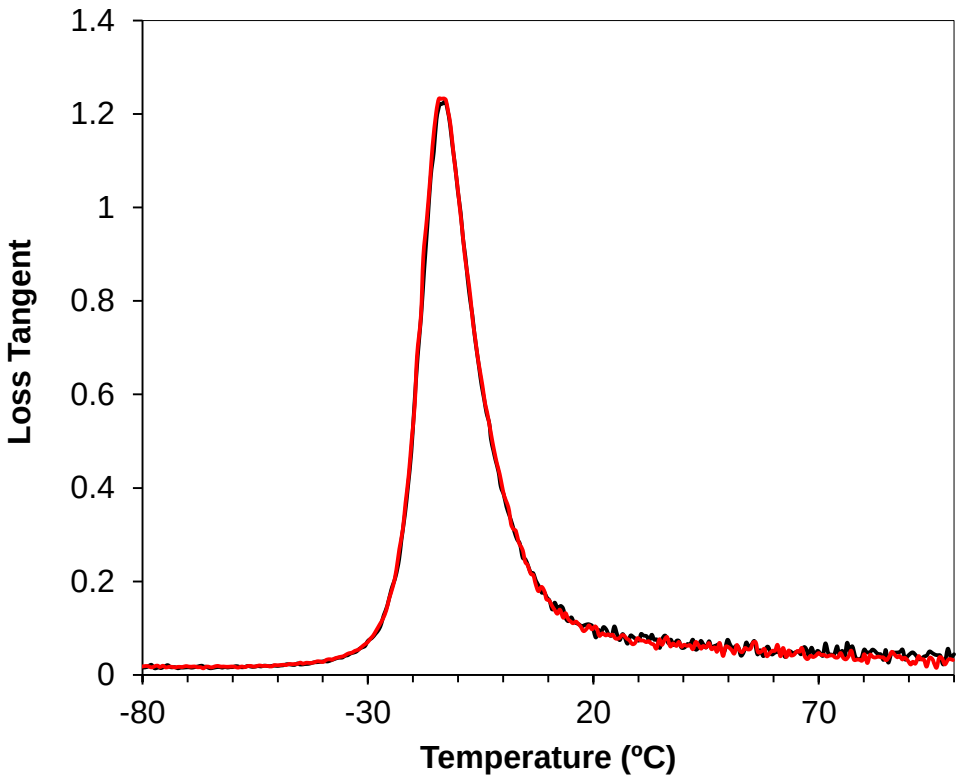

Figure 3.35 Loss tangent as a function of temperature for silica/SBR and CTA-silica/SBR composites.

3.3.5.3 MGD/SBR Composites

This section is a discussion of results from previous work of our group[75], and so we do not analyze them in depth here. After studying the influence of CTA^+ in silica/SBR composites, we reflect on previous results and explore the influence of CTA^+ on mechanical reinforcement and crosslinking in MGD/SBR composites.

In CTA-MGD/SBR mixes, the scorch delay was significantly shortened compared to MGD/SBR mixes, which is what we expected.[75] The addition of CTA^+ accelerates the vulcanization reaction and decreases the time before vulcanization onset.

However at the same time, the torque decreased considerably, suggesting a negative impact on crosslink density in the composite. CTA-MGD/SBR has 63% lower crosslink density than that of MGD/SBR.[75] Previously, this was attributed to the failure of SI-69 to intercalate in Na-MGD, resulting in more sulfur available for forming SBR-SBR crosslinks. Now we believe that the presence of CTA^+ may also play a role.

Previous work[75] compared two CTA-MGD/SBR composites with varying filler loadings. In CTA-MGD/SBR with 60 phr of inorganic MGD, the composite includes 24.35 phr of CTA^+. This composite has a crosslink density of 0.84×10^{-4}mol/cm^3. Another CTA-MGD/SBR prepared with 26.34 phr of inorganic MGD includes only 15.33 phr of CTA^+. The resulting crosslink density is 1.33×10^{-4}mol/cm^3. The crosslink density of the latter CTA-MGD/SBR is 58.3% higher than that of former one. We speculate that the excessive amount of CTA^+ may decrease the crosslink density. Similar results are observed in another work in EPDM and silicone rubber systems.[131] When the amount of the amine-containing compound is above the optimum value, the elastomer may be degraded or depolymerized, producing poor crosslink density and mechanical properties.

The catalytic influence on the rubber system is determined by the amount of CTA^+. If the amount of surfactant is too low, it leads to small starting MGD interlayer spacing and promotes the vulcanization with low efficiency. However, excessive CTA^+ decreases the crosslink density, which is not favorable for mechanical reinforcement.

3.3.5.4 Discussion

This section continues previous work in exploring the influence of CTA^+ on SBR composites. Here, we prepared silica/SBR and CTA-silica/SBR composites in order to

explore the influence of CTA^+ on composite properties. Then, we went back to re-compare CTA-MGD/SBR and MGD/SBR and explore the role of CTA^+ in MGD/SBR composites.

Compared with silica/SBR, CTA^+ decreases the scorch delay in CTA-silica/SBR. However, the addition of CTA^+ does not affect the optimum cure time. CTA-silica/SBR has higher crosslink density than that of silica/SBR. Both composites show comparable tensile properties, except that CTA-silica/SBR has higher M10 value, higher elongation at break and higher strain energy density. The addition of CTA^+ to silica/SBR has almost no influence on dynamic mechanical properties.

Then, we compared MGD/SBR and CTA-MGD/SBR composites. Those experimental results are from dissertation research by Dr. Li.[75] As for silica, with the addition of CTA^+, CTA-MGD/SBR has a shorter scorch delay time than MGD/SBR. The negative impact of CTA^+ might be another reason for the lower crosslink density of CTA-MGD/SBR compared to MGD/SBR, besides the discussion in previous work.[75] A similar conclusion, based on the negative effect of excessive CTA^+, explains differences in crosslink density when comparing another two CTA-MGD/SBR composites with varying amounts of MGD and CTA^+.

CHAPTER 4
Comparison of MMT/SBR and MGD/SBR Composites

4.1 Introduction

Since Toyota prepared organoclay/nylon-6 composites with improved thermal and mechanical properties,[3,132] much research has been done to prepare nanocomposites with layered smectite clays. Montmorillonite (MMT) is the most widely studied clay in the smectite family. The alkali-metal-ion forms of layered silicates have similar intercalation chemistry, but they have not been used in polymer nanocomposites as often. The members of the layered silicate family are magadiite, ilerite, kenyaite, kanemite, makatite and octosilicate.[43] Various layered silicates can be synthesized via hydrothermal reactions, resulting high purity materials. The purity of synthetic layered silicates gives them an advantage over smectic clays, like MMT, that are impure natural products. Layered silicates also possess more hydroxyl sites on face surfaces, which may promote stronger interaction with intercalated organic modifiers.[43] For these reasons, it is interesting to compare, head-to-head, the performance of MGD (a layered silicate) and MMT (a smectic clay) as active fillers in elastomer composites. The knowledge will shed more light on the relative merits of using other members of the two mineral families for preparing rubber composites.

Several publications[84,133] reported comparisons of membrane gas permeability and mechanical properties for MGD and MMT polymer composites. Wang et al's work[78,79] shows the most detailed direct comparison of mechanical properties between MGD and MMT/epoxy composites. When the filler loadings were low, the reinforcing performances in both composites were comparable. At high loadings, the organo-MMT (OMMT) showed superior reinforcing performance compared to organo-MGD (OMGD). The weaker reinforcement by OMGD was speculated to be caused by movement of the long alkylammonium and alkylamine chains, leading to the deterioration of rubber crosslink network. The advantage of MGD nanocomposites was better optical transparency than MMT nanocomposites.

To date, there has not been a direct comparison of mechanical properties in elastomer composites reinforced with MGD and MMT. In this chapter, we report on the preparation of OMGD/SBR and OMMT/SBR nanocomposites, their characterization, and their mechanical properties. Comparison of mechanical properties may be rationalized in terms of filler and composite structure.

4.2 Materials and Experimental Methods

4.2.1 Material Preparation

4.2.1.1 Magadiite

Sodium magadiite (Na-MGD) was synthesized using the hydrothermal method[83] and treated with cetyltrimethylammonium bromide (CTAB, Sigma-Aldrich, used as received), resulting in cation exchange of CTA^+ for interlayer protons to produce CTA-

MGD.[75] The synthesis procedures and characterization results for CTA-MGD were described in Chapter 3.

4.2.1.2 Montmorillonite

Montmorillonite (MMT, Cloisite Na^+, Southern Clay Products, Inc.) was treated with CTAB, resulting in cation exchange of CTA^+ to produce CTA-MMT. The procedure is similar to that used to prepare CTA-MGD.[75] CTAB (8.46g) was added to 500 mL of deionized water. CTAB was dissolved at 50-60ºC with a vigorous stirring to produce a deep vortex without foaming. MMT (20 g) was added to the stirred CTAB solution. The ratio of CTAB to MMT was 1.16 mmol/g. The CTA-MMT suspension was filtered and rinsed with deionized water to remove the excess CTAB. The CTA-MMT product was dried at 60ºC overnight for further use.

4.2.1.3 Elastomer Composites

Table 4.1 shows the recipes for CTA-MGD/SBR and CTA-MMT/SBR composites, which is the same as that used in Chapter 3.[75] The filler weight loadings of CTA-MMT and CTA-MGD were fixed at 26.34 phr based on the inorganic residue weight. Table 4.2 outlines the procedure for preparing for CTA-MGD/SBR and CTA-MMT/SBR composites. The linking agent SI-69, ZnO, stearic acid, and an accelerator/activator (diphenyl guanidine, DPG) were added during the mixing process. The curative (sulfur) and an accelerator (N-cyclohexyl-2-benzothiazole sulfonamide, CBS) were added to the green rubber mixture via processing on a four-roll Brabender mill. Finally, the green rubber mixture was cured in a mold under 20,000 lb compression

at 150°C for 1 hour to crosslink the SBR chains. The details of the rubber composite preparation procedures were introduced in Section 3.2.1.1.

Table 4.1 Recipes for CTA-MGD/SBR and CTA-MMT/SBR composites.

	phr basis	weight (g)
S-SBR	100.00	36.04
Wax	10.00	3.56
CTA-MGD	26.34 (a), 40.11(b)	14.50 (b)
CTA-MMT	26.34 (a), 40.55(b)	14.56 (b)
SI-69	7.25	2.61
ZnO	1.75	0.63
Steric Acid	1.75	0.63
Sulfur	1.35	0.49
CBS	1.20	0.43
DPG	1.30	0.47

(a) Filler loading based on inorganic content, not including surface modifier CTA^+.
(b) Filler loading including organic cationic modifier CTA^+.

Table 4.2 Mixing procedure for preparation of CTA-MGD/SBR and CTA-MMT/SBR composites.

Initial Temp: 105°C; Mixing Speed: 70 rpm	
	Mixing Step
1	After preheated to 105 °C, add elastomer, DPG and 1/2 filler. After piston was down, mix for 1 min.
2	Add ZnO, Stearic acid, and the other 1/2 filler. After piston was down, mix for 1min.
3	Raise and lower piston. Mix for 2 min.
4	Stop mixer

(1) Filler: CTA-MGD, CTA-MMT
(2) Curatives (CBS and sulfur) were added on the mill.

4.2.2 Characterization Methods

Due to the bulky structure of SBR, the filler surface area of MMT and MGD might not be entirely accessible. The CTAB molecule has a relatively bulky head group structure. In composite research, CTAB is used to measure the filler surface area, denoted

as “CTAB surface area”. In this work, the CTAB surface areas of MGD and MMT were measured according to ASTM D6845-02.

Fourier transform infrared spectroscopy (FTIR) measurements utilized a Shimadzu FTIR-8400 spectrometer with a diffuse reflectance solid state attachment (Pike Technologies). FTIR was used to characterize the organic functional groups in CTA-MGD and CTA-MMT. Powder samples were placed on the sample stage for measurement.

Thermogravimetric analysis (TGA) data were obtained using a model Q600 TGA (TA Instruments) employing a heating rate of 5ºC/min from room temperature to 800ºC in air. The TGA results were to quantify the amounts of CTA^+ exchanged into MGD and MMT.

The structures of fillers (CTA-MGD, CTA-MMT) and composites (CTA-MGD/SBR, CTA-MMT/SBR) were characterized by X-ray diffraction (XRD). Uncured rubber XRD samples were prepared using a heated Carver press with the help of Dr. Hongying Zhao. XRD patterns were acquired using an X-ray diffractometer (Rigaku Ultima IV, Cu Kα radiation, $\lambda = 1.5418$ Å), typically over the 2θ range of 1-60º with a step size of 0.02º and a scan speed of 1º/min. The XRD measurements were carried out by Dr. Michael Chance and Allison Latshaw from Dr. zur Loye’s research group in the Department of Chemistry and Biochemistry.

The structures of fillers and SBR composites were also characterized by scanning electron microscopy (SEM). SEM images, obtained using a Tescan Vega 3 SBU Variable Pressure SEM, were used to observe the quality of filler dispersion in cured composites.

nSpec® 3D is an automated, rapid optical microscope that provides surface topographies and quantitative roughness measurements. In this work, three dimensional topography images were generated using an nSpec® 3D system using a 50x objective. Samples were cross-sectioned using a cutter loaded with a fresh razor blade prior to measurement. The scans were measured on the cross-section surface. The dispersion rating takes into account the volume of the agglomerates while ignoring basic surface roughness. The dispersion rating also depends on the applied thresholds for peaks and valleys. A lower dispersion rating value corresponds to higher dispersion. All filler dispersion ratings were measured by collaborators at Nanotronics Imaging, the manufacturer of nSpec® 3D.

Mechanical properties of elastomer composites were evaluated using dynamic mechanical analysis (DMA) and tensile testing. DMA measurements (model RSA III, TA Instruments Inc.) were carried out at constant frequency (1.0 Hz) and strain amplitude (0.05%) with temperature ranging from -80ºC to 60ºC ramped at 3ºC/min. Tensile properties were measured at room temperature with dumbbell specimens (4.80 mm wide and 2.20 mm thick in the cross-section) on a tensile tester (Instron model 5566) with a crosshead speed of 25 mm/min. The strain was measured by crosshead separation distance. Reported tensile test values represent the average of four to six specimens.

The crosslink density in our elastomer composites was measured using a method reported previously.[75] Cured rubber samples were cut into 1.0 g pieces and immersed into 100 mL toluene and stored in darkness for 72 h. The solvent was replaced every day. Just after immersion, the rubber sample weight was W_{sw}. After 72 h immersion, the sample

was moved to a vacuum oven to dry for 48 h. After drying, the sample weight was $W_{\text{dry.}}$ The volume fraction of rubber $\phi_r$was calculated using

$$\frac{1}{\phi_r} = 1 + \frac{W_{sw}\rho_r}{W_{dry}\rho_t} \tag{4.1}$$

In this equation, ρ_r and ρ_t are densities of rubber and toluene, 1.17 g/cm^3 and 0.87 g/cm^3 respectively.

The crosslink density n is calculated according to Flory-Rehner equation,[120,121,122]

$$\ln(1-\phi_r) + \phi_r + \chi\phi_r^2 = V_t n\left(\frac{\phi_r}{2} - \phi_r^{1/3}\right) \tag{4.2}$$

where V_t denotes the molar volume of toluene 106.29 mL/mol. χ denotes the Flory-Huggins interaction coefficient for rubber-toluene. In this work we use χ=0.39.[123,124]

M_c is the average molecular weight between two crosslinks per primary rubber chain. It is calculated using

$$M_c = \frac{\rho_r}{n} \tag{4.3}$$

where ρ_r denotes density of rubber, 1.17 g/cm^3, and n is the measured crosslink density.

4.3 Results and Discussion

4.3.1 Characterization of MMT and CTA-MMT

The CTAB surface areas of MGD and MMT were measured as 393±8 m^2/g and 335±14 m^2/g, respectively. MGD possesses 17% more surface area than MMT per unit mass; this area should be available to molecules like CTAB or SBR prepolymer.

Figure 4.1 shows the weight percentage and derivative weight loss curves of MMT and CTA-MMT. For MMT, the total weight loss is 13.31%, and the residue weight is 86.69%. The water loss is 6.97% up to 150ºC. Subtracting water weight from the total weight loss, MMT has additional weight loss of 6.34% between 150ºC and 800ºC. Although the reason for this weight loss is not clear, we shall refer it as "dehydroxylation" loss by analogy with MGD. We assume that the ratio of MMT dehydroxylation loss to MMT residue weight is constant at 0.073. For CTA-MMT, the total weight loss is 34.90%, and the residue weight is 65.10%. Up to 150 ºC, the weight loss is 3.00% due to water. Assuming a constant ratio of dehydroxylation loss to residue weight, the dehydroxylation loss is 4.75%. Subtracting the water loss and dehydroxylation loss from the total weight loss, the loss due to CTA^+ is 27.15%. The peak at 242 ºC is mainly due to the loss of CTA^+. Based on TGA results, there is 1.31 mmol CTA^+ per gram of MMT. For CTA-MGD, this value is 1.43 mmol CTA^+/g MGD.

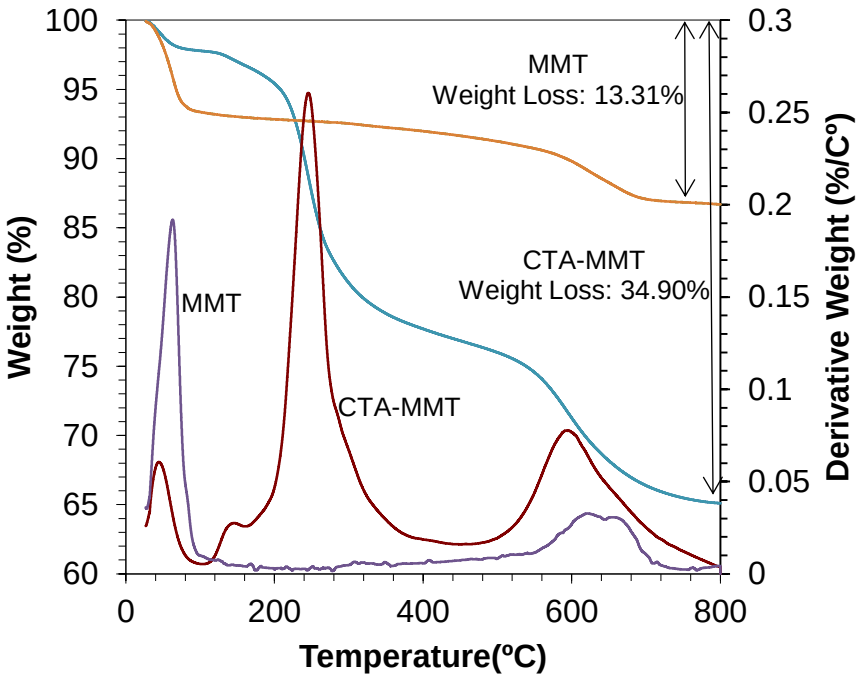

Figure 4.1 Weight loss and rate of change (derivative weight) as functions of temperature for Na-MMT and CTA-MMT. The heating rate was 5 °C/min.

Figure 4.2 shows the FTIR spectra of CTAB, MMT and CTA-MMT. After MMT undergoes cation exchange with CTA^+, the characteristic peaks of CTA^+ appear in CTA-MMT at 2916 cm^{-1} and 2849 cm^{-1} due to the CH stretching vibration, and at 1467 cm^{-2} due to CH_2 scissoring.[134] This indicates that CTA cations were adsorbed onto the surface of MMT. The peak at 1018 cm^{-1} in CTA-MMT is a characteristic of phyllosilicate minerals.[135]

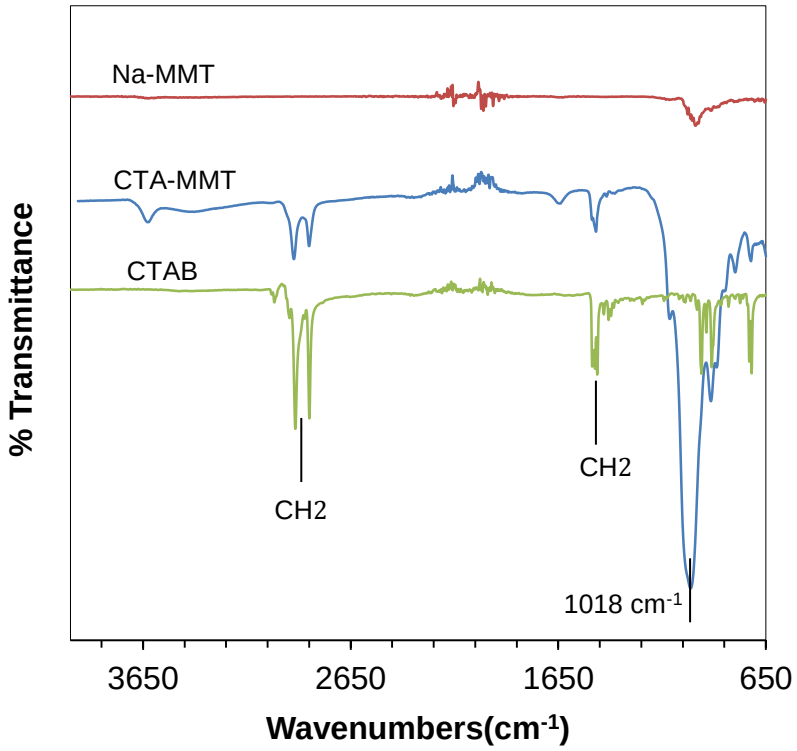

Figure 4.2 IR spectra of CTAB, MMT, and CTA-MMT.

Figure 4.3 shows XRD patterns for MMT and CTA-MMT. The interlayer spacing of MMT is 1.18 nm, which is consistent with our published work.[45] After cation exchange with CTA^+, the interlayer spacing increases to 2.21 nm in CTA-MMT, an increase of 1.03 nm. This increases in due to CTA^+ cations adsorbed onto MMT surface. The XRD pattern for CTA-MMT also shows a small peak at 8º, consistent with the (001) peak for non-expanded MMT. The presence of a small fraction of non-exfoliated MMT is consistent with expectations based on past AFM studies of MMT exfoliation.[45]

After reacting with CTA^+, the interlayer spacing of MGD increases from 1.56 nm to 3.10 nm, a change of 1.54 nm. The increase in MGD interlayer expansion is clearly

greater than that for CTA-MMT. This may be explained by the higher cation exchange capacity (CEC) of MGD compared to MMT. The CEC value for MMT is 92 meq/100 g as reported by the supplier (Southern Clay Products) and 83 meq/100 g as measured by our group.[136] The CEC for MGD has a theoretical value of 188 meq/100g (based on two cations per unit cell) and a measured value of 169 meq/100 g.[137] On the other hand, TGA results indicate only slightly more CTA^+ in CTA-MGD (29 wt%, section 3.3.1.1) than in CTA-MMT (27 wt%). The tighter packing of CTA^+ in CTA-MGD may result in more ordered chain packing and a larger angle of inclination of the chains from the MGD surface, resulting in the greater CTA-MGD interlayer spacing.

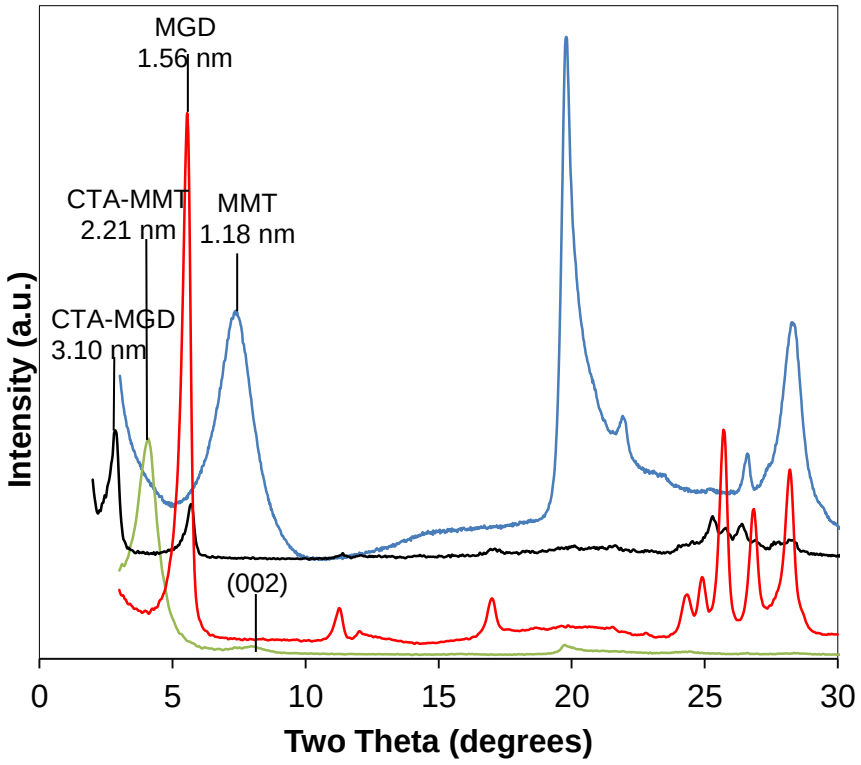

Figure 4.3 XRD patterns of Na-MMT and CTA-MMT composites.

4.3.2 CTA-MGD/SBR and CTA-MMT/SBR Composites

XRD patterns (Figure 4.4) were measured after each stage (mixing, milling and curing) for CTA-MMT/SBR samples. The interlayer spacing for CTA-MMT is 2.21 nm based on the location of the (001) peak at 2.4°. After mixing, milling, and curing, the interlayer spacings were 3.68 nm, 3.74 nm, and 3.65 nm respectively. For the patterns after each stage, (001), (002), and (003) peaks were clearly indexed. Most of the interlayer expansion occurred during mixing. The interlayer spacing values did not change during the milling or curing stages, as was found for CTA-MGD/SBR (Figure 3.2). By analogy with CTA-MGD/SBR, most intercalation occurs during the mixing stage.

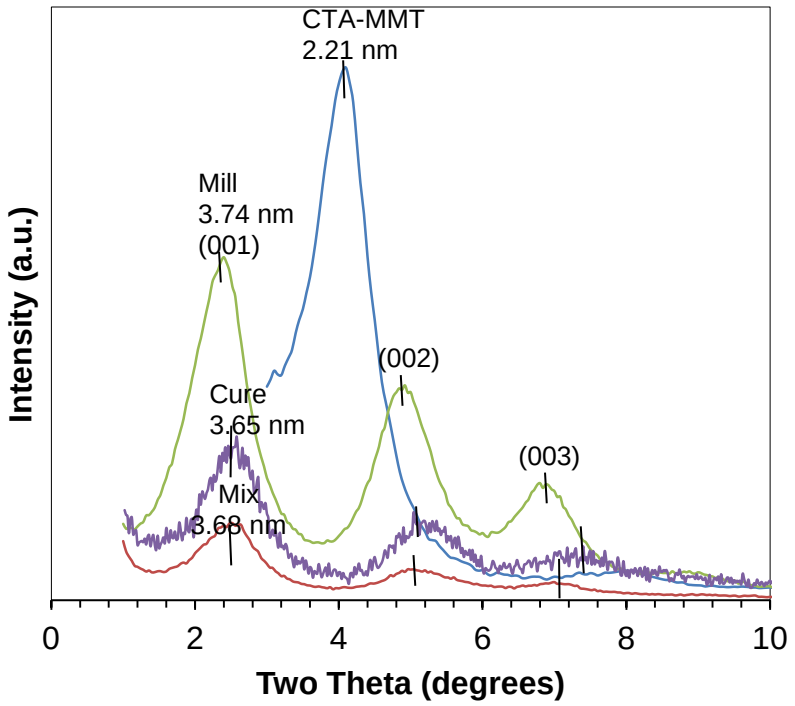

Figure 4.4 XRD patterns for CTA-MMT/SBR composites after batch mixing, milling, and thermal curing (curves labeled “mix”, “mill”, and “cure”). The intensity values for cured CTA-MMT/SBR were multiplied by a factor of 30 for clarity.

It is interesting to compare the XRD pattern evolution of CTA-MGD/SBR (Figure 3.7) and CTA-MMT/SBR (Figure 4.5). From CTA-MMT filler to CTA-MMT/SBR composite, the interlayer spacing increased from 2.21 nm to 3.65 nm, a change of 1.44 nm. For CTA-MGD/SBR, the interlayer spacing of CTA-MGD (3.10 nm) increased 0.84 nm in CTA-MGD/SBR (3.94 nm). These results indicate that for both fillers, some combination of SBR and SI-69 occupy the fillers interlayer spaces. Comparing with the starting filler materials, the layer spacing expands by 2.47 nm between Na-MMT and CTA-MMT/SBR (3.65-1.18 nm), and by 2.40 nm comparing Na-MGD and CTA-MGD/SBR (3.94-1.54 nm). Thus the amounts of interlayer expansion are almost the same for the two fillers.

Despite this similarity, the pathways that resulted in the final intercalation of SBR (and SI-69) may be different for the two composites. The indexed (001), (002), (003) and (110)[138] peaks of CTA-MMT/SBR indicate that the layered structure of MMT was not destroyed by the intercalation of SBR prepolymer and SI-69. If unscaled, the peaks of CTA-MMT/SBR are relatively broad and appear insignificant. We speculate that prior to and after curing, a considerable amount of CTA-MMT was exfoliated, with co-existence of both intercalated and exfoliated platelets. Both exfoliation and exfoliation/intercalation of OMMT in rubber composites by melt blending have been reported widely.[139,104,140] Previous work from our group reported that in MMT/levan composites (same MMT as in this work), the onset of nematic (stacking) ordering is 1.6 vol% MMT.[141] In this work, the MMT loading in CTA-MMT/SBR is 6.10 vol% (see supporting information). Thus, the (001) peak at 2.2° for CTA-MMT/SBR (Figure 4.5) is likely due to the nematic ordering of MMT. Based on the likely exfoliated state of CTA-MMT in the starting

suspension, it is also possible that CTA-MMT is partially exfoliated, or at least highly delaminated and then restacked in a less-ordered state (e.g., turbostratic stacking), in the final composite. Each delaminated MMT platelet contributes distinctly to reinforcing the material. Exfoliated MMT platelets are regarded as the most desirable state of layered clay in nanocomposites.[78]

In contrast, CTA-MGD/SBR shows a relatively sharp (001) peak in the XRD results (Figure 4.5), suggesting the presence of an expanded, yet well-ordered layered structure with little or no exfoliated CTA-MGD platelets in CTA-MGD/SBR composites. To our knowledge, there have been no previous reports of exfoliation of MGD in elastomers by melt blending methods. Even though CTA-MGD shows a slightly larger interlayer spacing in the final SBR composites compared to CTA-MMT, the presence of some exfoliated CTA-MMT, or at least delaminated and restacked MMT platelets, probably plays an important role in crosslinking and reinforcement in CTA-MMT/SBR composites.

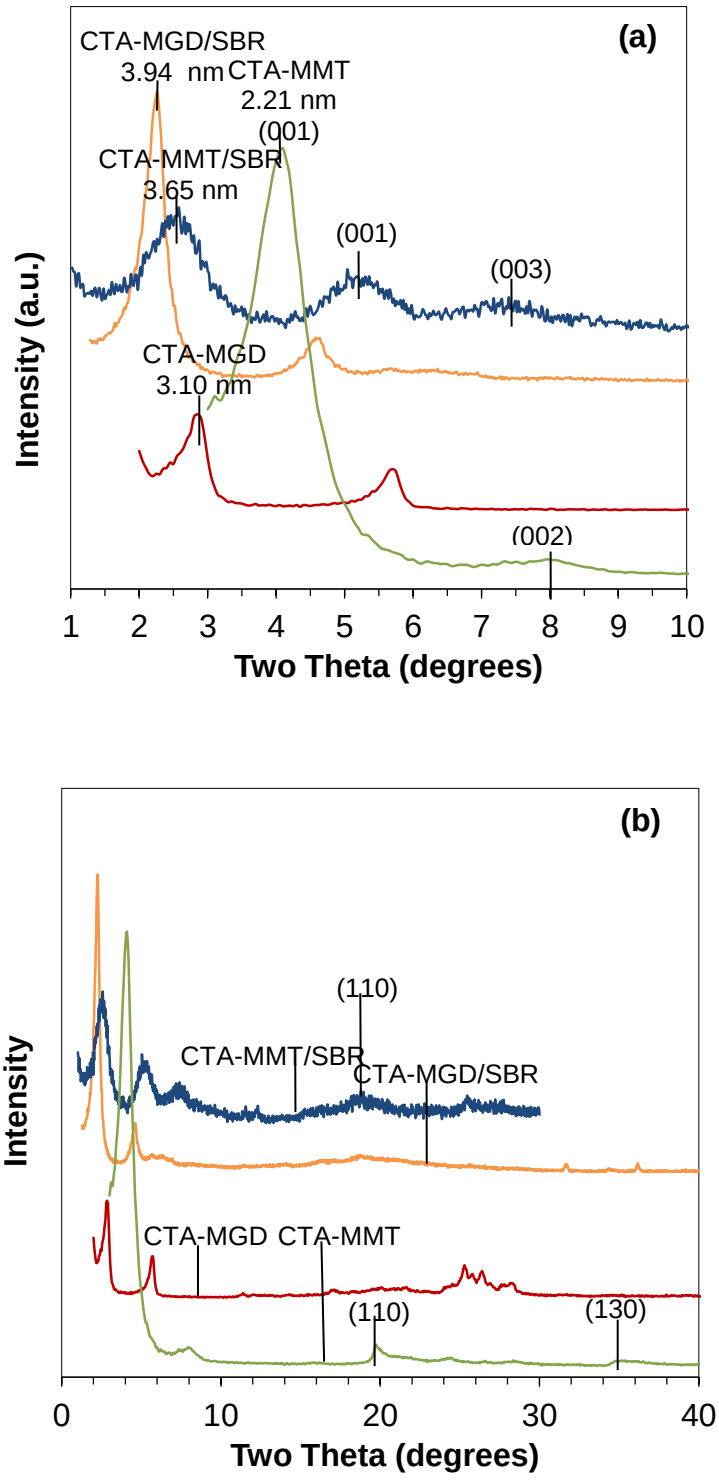

Figure 4.5 XRD patterns for organo-fillers and corresponding SBR composites. Patterns for two SBR composites are shifted upwards for clarity. The curves for CTA-MMT/SBR and CTA-MMT were multiplied by factors of 10 and 0.125, respectively. Panel (a) plots the scale

The difference in filler dispersion cannot be discerned from SEM images (Figure 4.6). Both CTA-MMT and CTA-MGD appear to be dispersed uniformly in SBR composites with few filler aggregates in the images. Table 4.3 shows that CTA-MMT and CTA-MGD have almost the same dispersion rating in rubber composites.

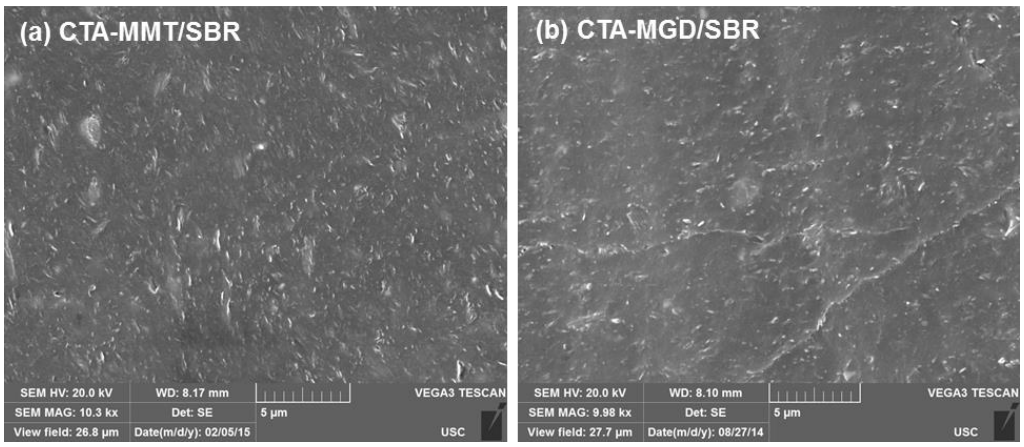

Figure 4.6 SEM images of (a) CTA-MMT/SBR and (b) CTA-MGD/SBR composites

Table 4.3 Crosslink densities, Mc values and dispersion ratings of CTA-MMT/SBR and CTA-MGD/SBR.

Sample	Sample ID	Dispersion Rating	Crosslink density (10^{-4} mol/cm^3)	M_c (10^4 g/mol)
CTA-MGD/SBR	YM2003	0.011	0.94±0.01	1.25±0.01
CTA-MMT/SBR	YM2001	0.012	1.55±0.02	0.76±0.01

The crosslink density values of CTA-MMT/SBR and CTA-MGD/SBR composites are very different. Compared to CTA-MGD/SBR, CTA-MMT/SBR has 65% greater crosslink density and 39% lower average molecular weight between crosslinks (M_c). One explanation for the higher crosslink density in CTA-MMT/SBR is the hypothesized partial exfoliation or disordered stacking of CTA-MMT in SBR. Each

exfoliated MMT platelet can effectively serve as a crosslink location to join many polymer chains, resulting in a considerable increase in crosslink density. More highly crosslinked polymer always leads to a decrease in average molecular weight between crosslinks (M_c).

In spite of the more numerous silanol sites on face surfaces and more CTAB surface area, the limited MGD interlayer expansion may not expose the interlayer surfaces to as many polymer chains available for crosslinking. The greater charge density on the MGD surfaces, thought to be an advantage of MGD, resulted in significant expansion of the interlayers by CTA^+. However, subsequent expansion by SI-69 and SBR prepolymer does not appear to have been sufficient to exfoliate the MGD.

Another explanation may be that CTA-MGD "sucks up" all of the SI-69 into the expanded interlayers, and so it may not be as effective for coupling the MGD to the polymer network. Free sulfur from SI-69 may be trapped in the interlayers, resulting in less SBR-SBR crosslinking. In contrast, SI-69 will mostly react with the edges of MMT. This may result in more of the SI-69 producing effective MMT-SBR crosslinks, plus allowing free sulfur to escape and help crosslink the SBR. This might be another reason that CTA-MMT/SBR has a higher crosslink density than that of CTA-MGD/SBR.

Stress-strain curves (Figure 4.7) and averaged data from multiple tests (Table 4.4) show that CTA-MMT/SBR has higher tensile strength and tensile moduli than CTA-MGD/SBR at all strains. The amount of filler is the same based on inorganic content. Even including CTA^+, the filler loadings are similar (Table 4.1). We speculate that the superior reinforcement observed in CTA-MMT/SBR can be explained by (1) the

presence of exfoliated or more disordered MMT in the composites, and (2) more effective filler-SBR crosslinking that occurs at the MMT platelet edges. Exfoliated MMT platelets dispersed homogeneously (Figure 4.6) provide highly effective, efficient locations to join many polymer chains. The exposed edge –OH groups provide accessible crosslinking sites for SI-69 and then SBR prepolymer. Together, these factors contribute to the 55% tensile strength improvement for CTA-MMT/SBR compared to CTA-MGD/SBR (Table 4.4). CTA-MGD/SBR shows an elongation at break of 424%, which is 67% more than CTA-MMT/SBR. The elongation at break commonly decreases as the tensile strength of polymer composites increases.[142]

Table 4.4 Tensile testing results for CTA-MGD/SBR, silica/SBR, and CTA-MMT/SBR composites.

Sample	ID	N	M10 (MPa)	M100 (MPa)	M250 (MPa)	Strain Energy Density (MJ/m^3)	Tensile Strength (MPa)	Strain at break (%)
CTA-MGD/SBR	YM2003	5	4.66±0.49	2.56±0.21	1.72±0.14	22.3±4.16	8.37±0.48	424±55.4
silica/SBR	YM2022	4	3.04±0.85	1.49±0.88	2.52±0.80	28.2±4.25	12.7±2.12	518±109
CTA-MMT/SBR	YM2001	5	8.98±0.88	5.26±0.82	3.45±0.40	19.9±3.26	13.0±1.56	255±25.7

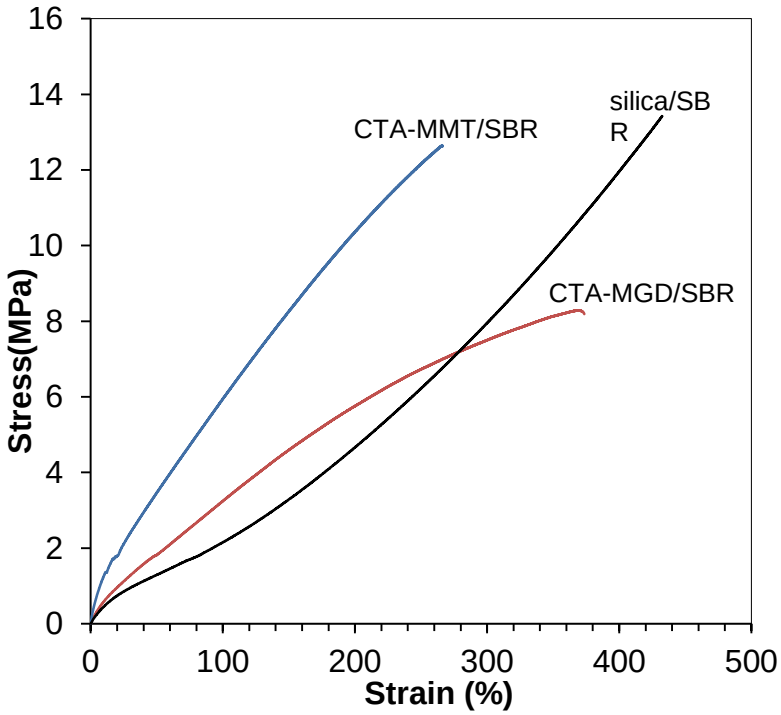

Figure 4.7 Stress-strain curves for CTA-MGD/SBR, silica/SBR, and CTA-MMT/SBR composites.

At low strain, compared to CTA-MGD/SBR, the higher M10 value for CTA-MMT/SBR is attributed to the possible exfoliation of MMT in CTA-MMT/SBR, resulting in a higher effective filler concentration. When the strain increases to 100% and 250%, the stronger reinforcement in CTA-MMT/SBR compared to CTA-MGD/SBR (M100, M250) is due to more MMT-SBR crosslinking at the edges of MMT platelets and thus higher crosslink density.

Strain energy absorbed per volume of material (toughness) is obtained from numerical integration of stress versus strain curves. CTA-MMT/SBR has a 55% larger tensile strength compared to CTA-MGD/SBR, but the latter has a 67% larger elongation

at break. These differences largely cancel each other out in the calculation of strain energy, which does not differ significantly between the two composites.

Silica is a widely used filler in formulation of tire treads.[9] Next, we compare the reinforcement of MMT in SBR composites with silica. CTA-MMT/SBR has much higher tensile moduli at all strains compared to those of silica/SBR. When the strain is low, the higher tensile modulus (M10) is attributed to higher effective concentration of CTA-MMT/SBR resulting from MMT's much higher CTAB surface area (335±14 m^2/g) compared to silica/SBR (150±4 m^2/g). As the strain increases, the higher M100 and M250 values are consistent with the higher crosslink density (Table 4.3) in CTA-MMT/SBR compared to silica/SBR (Table 3.9). The possible exfoliation of MMT in SBR allows the escape of free sulfur from SI-69 to SBR, similar to what occurs with silica. This results in a similar amount of SBR-SBR crosslinking in CTA-MMT/SBR and silica/SBR. However, partially exfoliated MMT in CTA-MMT/SBR contains more filler surface area per gram than that of silica/SBR (Section 3.3.1.1). The resulting amount of MMT-SBR crosslinking is more than the amount of silica-SBR crosslinking. After considering both SBR-SBR and filler-SBR crosslinking in SBR composites, CTA-MMT/SBR has higher crosslink density than that of silica/SBR, explaining the higher tensile moduli at all strains compared to silica/SBR.

Figures 4.8 and 4.9 show the dynamic mechanical properties (storage modulus and loss tangent) as functions of temperature for three SBR composites. CTA-MMT/SBR has higher storage moduli at all temperatures and a lower tan δ peak than CTA-MGD/SBR and silica/SBR. Table 4.5 shows averaged DMA data from multiple tests. When the temperature is below T_g, CTA-MMT/SBR has 77% higher E' than CTA-

MGD/SBR (Table 4.5). The reinforcement can be rationalized in terms of the partial exfoliation of MMT and the predominance of edge grafting, both resulting in more effective network structure. In CTA-MGD/SBR, SBR may be only partially grafted within the interlayer space, resulting in a less effective reinforcing effect. At temperatures above T_g (0 ºC and 60 ºC), the storage moduli of CTA-MMT/SBR are 3.6 and 2.7 times higher than those of CTA-MGD/SBR. The superior rubbery storage moduli of CTA-MMT/SBR may certainly be attributed to the higher crosslink density (Figure 4.3). Above T_g, SBR chains have sufficient energy to move relative to each other. More crosslink locations in CTA-MMT/SBR restrict the elastomer motion, resulting in higher storage moduli.

Table 4.5 Dynamic mechanical properties of CTA-MGD/SBR, silica/SBR, and CTA-MMT/SBR composites measured by DMA.

Sample	ID	N	E' at -60 ºC (GPa)	E' at 0 ºC (MPa)	E' at 60 ºC (MPa)	Avg. Tg (ºC)	Avg. value of tan δ peak	tan δ at 60 ºC
CTA-MGD/SBR	YM2003	2	2.38±0.12	21.8±0.28	8.40±0.31	-16.6±0.44	1.01±0.03	0.11±0.008
Silica/SBR	YM2022	3	1.95±0.34	8.75±1.50	4.32±0.49	-12.8±0.38	1.26±0.05	0.05±0.006
CTA-MMT/SBR	YM2001	2	4.22±0.26	77.8±1.91	23.0±2.66	-14.3±0.03	0.76±0.03	0.14±0.012

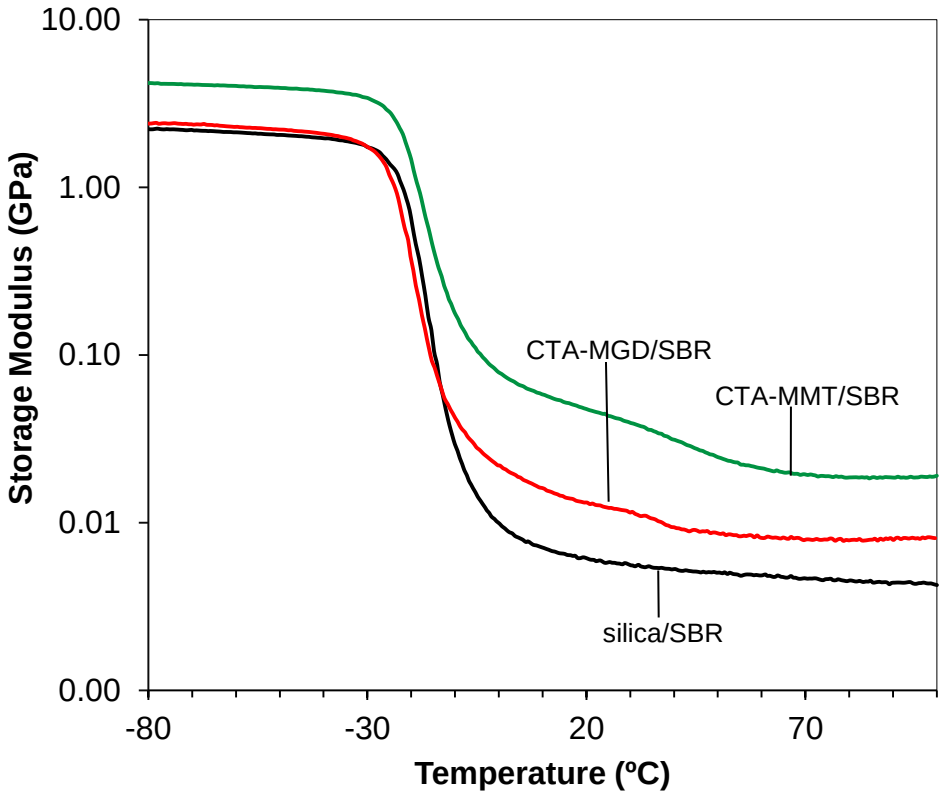

Figure 4.8 Storage modulus as a function of temperature for CTA-MGD/SBR, silica/SBR and CTA-MMT/SBR composites.

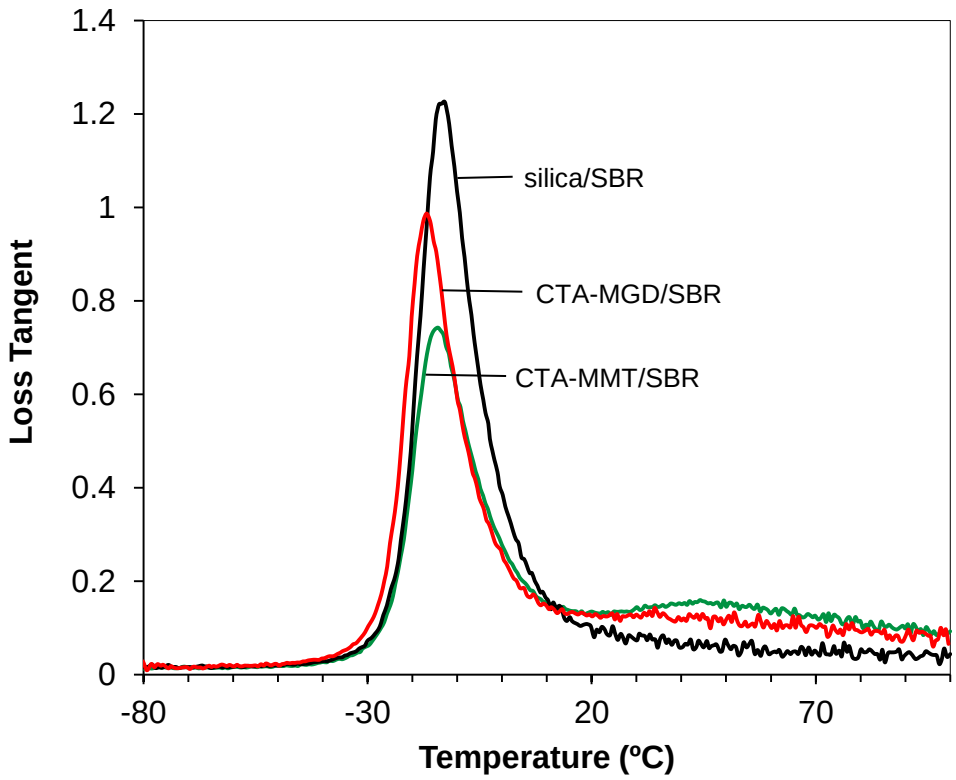

Figure 4.9 Loss tangent as a function of temperature for CTA-MGD/SBR, silica/SBR and CTA-MMT/SBR composites.

Table 4.5 shows that CTA-MMT/SBR has a larger loss tangent value (tan δ) at 60 ºC than CTA-MGD/SBR. However, due to the low number of replicates (N=2 for each composite), the confidence in this observation is only 79%. This observation goes against our expectations based on crosslink density (Table 4.3). Since CTA-MMT/SBR has a higher crosslink density, one might expect greater chain restriction and thus lower energy dissipation. On the other hand, if the MMT-SBR crosslinking occurs primarily at the edge of MMT platelets, the SBR chains might have more translational freedom and thus greater energy dissipation in the rubbery state. The tan δ peak of CTA-MGD/SBR is

higher than that of CTA-MMT/SBR (91% confidence), indicating a faster transition from the glassy to rubbery state for CTA-MGD/SBR compared to CTA-MMT/SBR.

4.4 Conclusion

In this chapter, we present a head-to-head comparison of the reinforcement behavior of MGD (layered silicate) and MMT (smectite clay) in SBR composites, which may help us to formulate rubber composites using other members of the two mineral families.

Based on XRD results, CTA-MMT might be partially exfoliated in the cured CTA-MMT/SBR composite. The loading of MMT (6.10 vol.%) is beyond the critical value for the onset of nematic ordering in composites. The broad peaks in XRD patterns may suggest partial MMT exfoliation or disordered platelet stacking in CTA-MMT/SBR. In contrast, the interlayers of CTA-MGD/SBR are expanded rather than exfoliated and restacked. The partial exfoliation of MMT in CTA-MMT/SBR contributes to superior crosslink density (Table 4.3), tensile properties (tensile moduli at all strains and tensile strength, Table 4.4) and dynamic mechanical properties (higher storage moduli, Table 4.5) compared to these of CTA-MGD/SBR.

Naturally-obtained MMT and MGD are usually impure. For MGD, it can also be synthesized, resulting in high purity MGD. At large production scale, the cost of synthetic MGD could be comparable to that of MMT, which must be mined and purified. In terms of properties, CTA-MGD/SBR has comparable strain energy density (toughness, Table 4.4) to CTA-MMT/SBR. In this respect, CTA-MGD/SBR may have an advantage

over CTA-MMT/SBR, even though the mechanical properties of the latter are generally superior.

REFERENCES

(1) *Rubber Technologist's Handbook.*; De, S. K., Ed.; Rapra Technology Ltd: Shrewsbury, Shropshire, 2001.

(2) *Rubber-Clay Nanocomposites: Science, Technology, and Applications*; Galimberti, M., Ed.; John Wiley & Sons: Hoboken, N.J, 2011.

(3) Usuki, A.; Kojima, Y.; Kawasumi, M.; Okada, A.; Fukushima, Y.; Kurauchi, T.; Kamigaito, O. Synthesis of Nylon 6-Clay Hybrid. *J. Mater. Res.* **1993**, *8*, 1179–1184.

(4) Lan, T.; Pinnavaia, T. J. Clay-Reinforced Epoxy Nanocomposites. *Chem. Mater.* **1994**, *6*, 2216–2219.

(5) *ISO/TS 80004-2:2015-Nanotechnologies -- Methodology for the Classification and Categorization of Nanomaterials*; ISO/TR 11360:2010.

(6) *ISO/TS 80004-2:2015-Nanotechnologies -- Vocabulary -- Part 1: Core Terms*; ISO/TS 80004-1:2010.

(7) *ISO/TS 80004-2:2015-Nanotechnologies -- Vocabulary -- Part 2: Nano-Objects*; ISO/TS 80004-2:2015.

(8) *Polymer Nanocomposites Based on Inorganic and Organic Nanomaterials*; Mohanty, S., Ed.; Polymer science and plastics engineering; Wiley Wiley & Sons Inc: Hoboken, New Jersey, 2015.

(9) *Rubber Nanocomposites: Preparation, Properties, and Applications*; Thomas, S.; Stephen, R., Eds.; John Wiley & Sons: Singapore ; Hoboken, NJ, 2010.

(10) Plueddemann, E. P. *Silane Coupling Agents*; Plenum Press: New York, 1982.

(11) Goerl, U.; Hunsche, A.; Mueller, A.; Koban, H. G. Investigations into the Silica/Silane Reaction System. *Rubber Chem. Technol.* **1997**, *70*, 608–623.

(12) Bokobza, L.; Ladouce, L.; Bomal, Y.; Amram, B. Infrared Dichroism and Birefringence Studies of Silica-Filled Styrene-Butadiene Rubbers. *J. Appl. Polym. Sci.* **2001**, *82*, 1006–1012.

(13) Ko, J. Y.; Prakashan, K.; Kim, J. K. New Silane Coupling Agents for Silica Tire Tread Compounds. *J. Elastomers Plast.* **2012**, *44*, 549–562.

(14) Tian, M.; Qu, C.; Feng, Y.; Zhang, L. Structure and Properties of Fibrillar silicate/SBR Composites by Direct Blend Process. *J. Mater. Sci.* **2003**, *38*, 4917–4924.

(15) Alkadasi, N. A. N.; Hundiwale, D. G.; Kapadi, U. R.; Mishra, S. Effect of Silane Coupling Agent on the Mechanical Properties of Clay Filled Styrene Butadiene Rubber. *Polym.-Plast. Technol. Eng.* **2005**, *44*, 1159–1171.

(16) Wang, L.-L.; Tong, Y.-P.; Zhang, L.-Q.; Tian, M. Comparison of Ethylene-Propylene Diene Terpolymer Composites Filled with Natural and Synthesized Micas. *J. Appl. Polym. Sci.* **2010**, 3184–3192.

(17) Ismail, H.; Kheong, O. W. The Effect of Bis-(3-Triethoxysilylpropyl)--Tetrasulfide, Si69 on Properties of Recycled Poly (Vinyl chloride)/Acrylonitrile--

Butadiene Rubber/Fly Ash (PVCr/NBR/FA) Composites. *J. Reinf. Plast. Compos.* **2008**, *27*, 1649–1661.
(18) Sun, D.; Li, X.; Zhang, Y.; Li, Y. Effect of Modified Nano-Silica on the Reinforcement of Styrene Butadiene Rubber Composites. *J. Macromol. Sci. Part B* **2011**, *50*, 1810–1821.
(19) Ward, A. A.; Yehia, A. A.; Bishai, A. Dynamic - Mechanical Properties of Solution Styrene Butadiene Rubber Loaded with Silica. *KGK Kautsch. Gummi Kunststoffe* **2008**, *61*, 569–575.
(20) Tabsan, N.; Wirasate, S.; Suchiva, K. Abrasion Behavior of Layered Silicate Reinforced Natural Rubber. *Wear* **2010**, *269*, 394–404.
(21) Yamsaengsung, W.; Sombatsompop, N. Interfacial Adhesion and Molecular Diffusion in Melt Lamination of Wood Sawdust/ebonite NR and EPDM. *Polym. Compos.* **2009**, *30*, 248–256.
(22) Thongsang, S.; Sombatsompop, N. Effect of NaOH and Si69 Treatments on the Properties of Fly Ash/natural Rubber Composites. *Polym. Compos.* **2006**, *27*, 30–40.
(23) Sombatsompop, N.; Wimolmala, E.; Markpin, T. Fly-Ash Particles and Precipitated Silica as Fillers in Rubbers. II. Effects of Silica Content and Si69-Treatment in Natural Rubber/styrene–butadiene Rubber Vulcanizates. *J. Appl. Polym. Sci.* **2007**, *104*, 3396–3405.
(24) De, D.; De, D.; Adhikari, B. The Effect of Grass Fiber Filler on Curing Characteristics and Mechanical Properties of Natural Rubber. *Polym. Adv. Technol.* **2004**, *15*, 708–715.
(25) Tredger, J. M.; Chhabra, R. S.; Fouts, J. R. Postnatal Development of Mixed-Function Oxidation as Measured in Microsomes from the Small Intestine and Liver of Rabbits. *Drug Metab. Dispos. Biol. Fate Chem.* **1976**, *4*, 17–24.
(26) Lopattananon, N.; Jitkalong, D.; Seadan, M. Hybridized Reinforcement of Natural Rubber with Silane-Modified Short Cellulose Fibers and Silica. *J. Appl. Polym. Sci.* **2011**, *120*, 3242–3254.
(27) Noriman, N. Z.; Ismail, H. Properties of Styrene Butadiene Rubber (SBR)/recycled Acrylonitrile Butadiene Rubber (NBRr) Blends: The Effects of Carbon Black/silica (CB/Sil) Hybrid Filler and Silane Coupling Agent, Si69. *J. Appl. Polym. Sci.* **2012**, *124*, 19–27.
(28) Yue, D.; Liu, Y.; Shen, Z.; Zhang, L. Study on Preparation and Properties of Carbon Nanotubes/rubber Composites. *J. Mater. Sci.* **2006**, *41*, 2541–2544.
(29) Jiang, M.-J.; Dang, Z.-M.; Xu, H.-P. Giant Dielectric Constant and Resistance-Pressure Sensitivity in Carbon Nanotubes/rubber Nanocomposites with Low Percolation Threshold. *Appl. Phys. Lett.* **2007**, *90*, 042914.
(30) Kim, Y. A.; Hayashi, T.; Endo, M.; Gotoh, Y.; Wada, N.; Seiyama, J. Fabrication of Aligned Carbon Nanotube-Filled Rubber Composite. *Scr. Mater.* **2006**, *54*, 31–35.
(31) Jiang, M.-J.; Dang, Z.-M.; Yao, S.-H.; Bai, J. Effects of Surface Modification of Carbon Nanotubes on the Microstructure and Electrical Properties of Carbon Nanotubes/rubber Nanocomposites. *Chem. Phys. Lett.* **2008**, *457*, 352–356.
(32) Zhan, Y.; Lavorgna, M.; Buonocore, G.; Xia, H. Enhancing Electrical Conductivity of Rubber Composites by Constructing Interconnected Network of

Self-Assembled Graphene with Latex Mixing. *J. Mater. Chem.* **2012**, *22*, 10464–10468.
(33) Abraham, E.; Elbi, P. A.; Deepa, B.; Jyotishkumar, P.; Pothen, L. A.; Narine, S. S.; Thomas, S. X-Ray Diffraction and Biodegradation Analysis of Green Composites of Natural Rubber/nanocellulose. *Polym. Degrad. Stab.* **2012**, *97*, 2378–2387.
(34) H, B. D.; Co, C. P. Ceramic-Rubber Composites, May 16, 1967.
(35) Peponi, L.; Puglia, D.; Torre, L.; Valentini, L.; Kenny, J. M. Processing of Nanostructured Polymers and Advanced Polymeric Based Nanocomposites. *Mater. Sci. Eng. R Rep.* **2014**, *85*, 1–46.
(36) Yue, D.; Liu, Y.; Shen, Z.; Zhang, L. Study on Preparation and Properties of Carbon Nanotubes/rubber Composites. *J. Mater. Sci.* **2006**, *41*, 2541–2544.
(37) Barlow. *Rubber Compounding: Principles: Materials, and Techniques, Second Edition*; CRC Press, 1993.
(38) *Basic Rubber Testing: Selecting Methods for a Rubber Test Program*; Dick, J. S., Ed.; ASTM: West Conshohocken, PA, 2003.
(39) Heideman, G. Reduced Zinc Oxide Levels in Sulphur Vulcanisation of Rubber Compounds : Mechanistic Aspects of the Role of Activators and Multifunctional Additives. info:eu-repo/semantics/doctoralThesis, University of Twente: Enschede, 2004.
(40) Kumar, C. S.; Nijasure, A. Vulcanization of Rubber - Indian Academy of Sciences - Index Ebooks Library and Manual Online - Avang.com. *Resonance* **1997**, *2*, 55.
(41) Okada, A.; Usuki, A. The Chemistry of Polymer-Clay Hybrids. *Mater. Sci. Eng. C* **1995**, *3*, 109–115.
(42) *Handbook of Clay Science*; Bergaya, F.; Lagaly, G., Eds.; Developments in clay science; Elsevier: Amsterdam, 2013.
(43) Auerbach, S. M.; Carrado, K. A.; Dutta, P. K. *Handbook of Layered Materials*; M. Dekker: New York, 2004.
(44) Utracki, L. A. *Clay-Containing Polymeric Nanocomposites*; Rapra Technology Ltd: Shrewsbury, 2004.
(45) Ploehn, H. J.; Liu, C. Quantitative Analysis of Montmorillonite Platelet Size by Atomic Force Microscopy. *Ind. Eng. Chem. Res.* **2006**, *45*, 7025–7034.
(46) Park, S.-J.; Seo, D.-I.; Lee, J.-R. Surface Modification of Montmorillonite on Surface Acid–Base Characteristics of Clay and Thermal Stability of Epoxy/Clay Nanocomposites. *J. Colloid Interface Sci.* **2002**, *251*, 160–165.
(47) Usha Devi, K. S.; Ponnamma, D.; Causin, V.; Maria, H. J.; Thomas, S. Enhanced Morphology and Mechanical Characteristics of Clay/styrene Butadiene Rubber Nanocomposites. *Appl. Clay Sci.* **2015**, *114*, 568–576.
(48) Zhang, B.; Xi, M.; Zhang, D.; Zhang, H.; Zhang, B. The Effect of Styrene–butadiene–rubber/montmorillonite Modification on the Characteristics and Properties of Asphalt. *Constr. Build. Mater.* **2009**, *23*, 3112–3117.
(49) Mousa, A.; Karger-Kocsis, J. Rheological and Thermodynamical Behavior of Styrene/Butadiene Rubber-Organoclay Nanocomposites. *Macromol. Mater. Eng.* **2001**, *286*, 260–266.
(50) Zhang, L.; Wang, Y.; Wang, Y.; Sui, Y.; Yu, D. Morphology and Mechanical Properties of Clay/styrene-Butadiene Rubber Nanocomposites. *J. Appl. Polym. Sci.* **2000**, *78*, 1873–1878.

(51) Ganter, M.; Gronski, W.; Reichert, P.; Mülhaupt, R. Rubber Nanocomposites: Morphology and Mechanical Properties of BR and SBR Vulcanizates Reinforced by Organophilic Layered Silicates. *Rubber Chem. Technol.* **2001**, *74*, 221–235.
(52) Schön, F.; Thomann, R.; Gronski, W. Shear Controlled Morphology of Rubber/organoclay Nanocomposites and Dynamic Mechanical Analysis. *Macromol. Symp.* **2002**, *189*, 105–110.
(53) Sookyung, U.; Nakason, C.; Thaijaroen, W.; Vennemann, N. Influence of Modifying Agents of Organoclay on Properties of Nanocomposites Based on Natural Rubber. *Polym. Test.* **2014**, *33*, 48–56.
(54) Boonchoo, P.; Rempel, G. L.; Prasassarakich, P. Synthesis of Polyisoprene–montmorillonite Nanocomposites via Differential Microemulsion Polymerization and Application of PIP–Mt in Natural Rubber. *Appl. Clay Sci.* **2014**, *88-89*, 186–193.
(55) Rooj, S.; Das, A.; Stöckelhuber, K. W.; Mukhopadhyay, N.; Bhattacharyya, A. R.; Jehnichen, D.; Heinrich, G. Pre-Intercalation of Long Chain Fatty Acid in the Interlayer Space of Layered Silicates and Preparation of Montmorillonite/natural Rubber Nanocomposites. *Appl. Clay Sci.* **2012**, *67-68*, 50–56.
(56) Yehia, A. A.; Akelah, A. M.; Rehab, A.; El-Sabbagh, S. H.; Nashar, D. E. El; Koriem, A. A. Evaluation of Clay Hybrid Nanocomposites of Different Chain Length as Reinforcing Agent for Natural and Synthetic Rubbers. *Mater. Des.* **2012**, *33*, 11–19.
(57) Ramorino, G.; Bignotti, F.; Pandini, S.; Riccò, T. Mechanical Reinforcement in Natural Rubber/organoclay Nanocomposites. *Compos. Sci. Technol.* **2009**, *69*, 1206–1211.
(58) Varghese, S.; Karger-Kocsis, J.; Gatos, K. G. Melt Compounded Epoxidized Natural Rubber/layered Silicate Nanocomposites: Structure-Properties Relationships. *Polymer* **2003**, *44*, 3977–3983.
(59) Carretero-González, J.; Valentín, J. L.; Arroyo, M.; Saalwächter, K.; Lopez-Manchado, M. A. Natural Rubber/clay Nanocomposites: Influence of Poly(ethylene Glycol) on the Silicate Dispersion and Local Chain Order of Rubber Network. *Eur. Polym. J.* **2008**, *44*, 3493–3500.
(60) Arroyo, M.; López-Manchado, M. .; Herrero, B. Organo-Montmorillonite as Substitute of Carbon Black in Natural Rubber Compounds. *Polymer* **2003**, *44*, 2447–2453.
(61) Das, A.; Stöckelhuber, K. W.; Jurk, R.; Jehnichen, D.; Heinrich, G. A General Approach to Rubber–montmorillonite Nanocomposites: Intercalation of Stearic Acid. *Appl. Clay Sci.* **2011**, *51*, 117–125.
(62) Fontana, J. P.; Camilo, F. F.; Bizeto, M. A.; Faez, R. Evaluation of the Role of an Ionic Liquid as Organophilization Agent into Montmorillonite for NBR Rubber Nanocomposite Production. *Appl. Clay Sci.* **2013**, *83-84*, 203–209.
(63) Mohamed, R. M. Radiation Induced Modification of NBR and SBR Montmorillonite Nanocomposites. *J. Ind. Eng. Chem.* **2013**, *19*, 80–86.
(64) de Sousa, F. D. B.; Mantovani, G. L.; Scuracchio, C. H. Mechanical Properties and Morphology of NBR with Different Clays. *Polym. Test.* **2011**, *30*, 819–825.

(65) Kim, J.; Oh, T.; Lee, D. Preparation and Characteristics of Nitrile Rubber (NBR) Nanocomposites Based on Organophilic Layered Clay. *Polym. Int.* **2003**, *52*, 1058–1063.
(66) Ahmadi, S. J.; G'Sell, C.; Huang, Y.; Ren, N.; Mohaddespour, A.; Hiver, J.-M. Mechanical Properties of NBR/clay Nanocomposites by Using a Novel Testing System. *Compos. Sci. Technol.* **2009**, *69*, 2566–2572.
(67) Zheng, H.; Zhang, Y.; Peng, Z.; Zhang, Y. Influence of the Clay Modification and Compatibilizer on the Structure and Mechanical Properties of Ethylene-Propylene-Diene Rubber/montmorillonite Composites. *J. Appl. Polym. Sci.* **2004**, *92*, 638–646.
(68) Ahmadi, S. J. Morphology and Characterization of Clay-Reinforced EPDM Nanocomposites. *J. Compos. Mater.* **2005**, *39*, 745–754.
(69) Ahmadi, S. J.; Huang, Y.-D.; Ren, N.; Mohaddespour, A.; Ahmadi-Brooghani, S. Y. The Comparison of EPDM/clay Nanocomposites and Conventional Composites in Exposure of Gamma Irradiation. *Compos. Sci. Technol.* **2009**, *69*, 997–1003.
(70) Takahashi, N.; Kuroda, K. Materials Design of Layered Silicates through Covalent Modification of Interlayer Surfaces. *J. Mater. Chem.* **2011**, *21*, 14336.
(71) Iler, R. . Ion Exchange Properties of a Crystalline Hydrated Silica. *J. Colloid Sci.* **1964**, *19*, 648–657.
(72) Ide, Y.; Ochi, N.; Ogawa, M. Effective and Selective Adsorption of Zn2+ from Seawater on a Layered Silicate. *Angew. Chem.* **2011**, *123*, 680–682.
(73) Guerra, D. L.; Ferrreira, J. N.; Pereira, M. J.; Viana, R. R.; Airoldi, C. Use of Natural and Modified Magadiite as Adsorbents to Remove Th(IV), U(VI), and Eu(III) from Aqueous Media – Thermodynamic and Equilibrium Study. *Clays Clay Miner.* **2010**, *58*, 327–339.
(74) Ogawa, M.; Takahashi, Y. Preparation and Thermal Decomposition of Co (ii)-Magadiite Intercalation Compounds. *Clay Sci.* **2007**, *13*, 133–138.
(75) Li, S. Reinforcement and Energy Dissipation in Platelet-Filled Elastomers. Ph.D. Dissertation, University of South Carolina, 2012.
(76) Lagaly, G.; Beneke, K.; Weiss, A. Magadiite and H-Magadiite: I. Sodium Magadiite and Some of ITs Derivatives. *Am. Mineral.* **1975**, *60*, 642–649.
(77) Kooli, F.; Mianhui, L.; Alshahateet, S. F.; Chen, F.; Yinghuai, Z. Characterization and Thermal Stability Properties of Intercalated Na-Magadiite with Cetyltrimethylammonium (C16TMA) Surfactants. *J. Phys. Chem. Solids* **2006**, *67*, 926–931.
(78) Wang, Z.; Lan, T.; Pinnavaia, T. J. Hybrid Organic−Inorganic Nanocomposites Formed from an Epoxy Polymer and a Layered Silicic Acid (Magadiite). *Chem. Mater.* **1996**, *8*, 2200–2204.
(79) Wang, Z.; Pinnavaia, T. J. Hybrid Organic−Inorganic Nanocomposites: Exfoliation of Magadiite Nanolayers in an Elastomeric Epoxy Polymer. *Chem. Mater.* **1998**, *10*, 1820–1826.
(80) Okutomo, S. Preparation and Characterization of Silylated-Magadiites. *Appl. Clay Sci.* **1999**, *15*, 253–264.
(81) Isoda, K.; Kuroda, K.; Ogawa, M. Interlamellar Grafting of γ-Methacryloxypropylsilyl Groups on Magadiite and Copolymerization with Methyl Methacrylate. *Chem. Mater.* **2000**, *12*, 1702–1707.

(82) Fujita, I.; Kuroda, K.; Ogawa, M. Synthesis of Interlamellar Silylated Derivatives of Magadiite and the Adsorption Behavior for Aliphatic Alcohols. *Chem. Mater.* **2003**, *15*, 3134–3141.
(83) Hansen, T. J. *Synthesis and Characterization of Oxide Materials: Polymer-Layered Oxide Nanocomposites and Crystal Growth of Lanthanide Containing Platinates*; ProQuest, 2007.
(84) Wang, D.; Jiang, D. D.; Pabst, J.; Han, Z.; Wang, J.; Wilkie, C. A. Polystyrene Magadiite Nanocomposites. *Polym. Eng. Sci.* **2004**, *44*, 1122–1131.
(85) Zhu, J.; Morgan, A. B.; Lamelas, F. J.; Wilkie, C. A. Fire Properties of Polystyrene−Clay Nanocomposites. *Chem. Mater.* **2001**, *13*, 3774–3780.
(86) Wang, D.; Zhu, J.; Yao, Q.; Wikie, C. A Comparison of Various Methods for the Preparation of Polystyrene and Poly(methyl Methacrylate) Clay Nanocomposites - Chemistry of Materials (ACS Publications). *Chem. Mater. 14*, 3837–3843.
(87) Utracki, L. A.; Sepehr, M.; Boccaleri, E. Synthetic, Layered Nanoparticles for Polymeric Nanocomposites (PNCs). *Polym. Adv. Technol.* **2007**, *18*, 1–37.
(88) Morgan, A. B.; Whaley, P. D.; Lin, T. S.; Cogen, J. M. The Effects of Inorganic-Organic Cations on EVA-Magadiite Nanocomposite Flammability. In *Fire and Polymers IV*; Wilkie, C. A.; Nelson, G. L., Eds.; American Chemical Society: Washington, DC, 2005; Vol. 922, pp. 48–60.
(89) *Food Oxidants and Antioxidants: Chemical, Biological, and Functional Properties*; Bartosz, G., Ed.; Chemical and functional properties of food components series; CRC Press: Boca Raton, Fla., 2013.
(90) Bloomfield, G. F. Modern Views on the Chemistry of Vulcanization Changes. III. Reaction of Sulfur with Squalene and with Rubber. *J. Polym. Sci.* **1946**, *1*, 312–317.
(91) Bloomfield, G. F. The Reaction of Sulphur and Sulphur Compounds with Olefinic Substances. Part III. The Reaction of Sulphur with Squalene. *J. Chem. Soc. Resumed* **1947**, 1546.
(92) Wachter, R. F.; Briggs, G. P.; Pedersen, C. E. Precipitation of Phase I Antigen of Coxiella Burnetii by Sodium Sulfite. *Acta Virol.* **1975**, *19*, 500.
(93) Rodriguez, S.; Masalles, C.; Agullo, N.; Borros, S.; Comellas, L.; Broto, F. Identification of the Intermediates Sulfur Vulcanization of Natural Rubber. *Kautsch. Gummi Kunststoffe* **1999**, *52*, 438–445.
(94) Boretti, L. G.; Woolard, C. D. An Appropriate Model Compound for the Accelerated Sulfur Vulcanization of Polyisoprene: I. The Mechanism of Bisbenzothiazole-2,2′-Disulfide Accelerated Vulcanization of Squalene in the Absence of ZnO. *Rubber Chem. Technol.* **2006**, *79*, 135–151.
(95) Vega, B.; Agulló, N.; Borrós, S. Study of the Influence of Microwaves in the Mechanism of Sulfenamide Accelerated Vulcanization of Natural Rubber Using Squalene as a Model Compound. *Rubber Chem. Technol.* **2007**, *80*, 739–750.
(96) Tricás, N.; Vidal-Escales, E.; Borrós, S.; Gerspacher, M. Influence of Carbon Black Amorphous Phase Content on Rubber Filled Compounds. *Compos. Sci. Technol.* **2003**, *63*, 1155–1159.
(97) Heideman, G.; Datta, R. N.; Noordermeer, J. W. M.; van Baarle, B. Influence of Zinc Oxide during Different Stages of Sulfur Vulcanization. Elucidated by Model Compound Studies. *J. Appl. Polym. Sci.* **2005**, *95*, 1388–1404.

(98) Garreta, E.; Agullo, N.; Borros, S. The Role of the Activator during the Vulcanization of Natural Rubber Using Sulfenamide Accelerator Type. *KGK Kautsch. Gummi Kunststoffe* **2002**, *55*, 82–85.
(99) Guzmán, M.; Reyes, G.; Agulló, N.; Borrós, S. Synthesis of Zn/Mg Oxide Nanoparticles and Its Influence on Sulfur Vulcanization. *J. Appl. Polym. Sci.* **2011**, *119*, 2048–2057.
(100) Chun, H. J.; Weiss, T. L.; Devarenne, T. P.; Laane, J. Vibrational Spectra and DFT Calculations of Squalene. *J. Mol. Struct.* **2013**, *1032*, 203–206.
(101) Boerio, F. J.; Tsai, Y. M.; Kim, D. K. Adhesion of Natural Rubber to Steel Substrates: The Use of Plasma Polymerized Primers. *Rubber Chem. Technol.* **1999**, *72*, 199–211.
(102) Karger-Kocsis, J.; Wu, C.-M. Thermoset Rubber/layered Silicate Nanocomposites. Status and Future Trends. *Polym. Eng. Sci.* **2004**, *44*, 1083–1093.
(103) Giannelis, E. P. Polymer Layered Silicate Nanocomposites. *Adv. Mater.* **1996**, *8*, 29–35.
(104) Alexandre, M.; Dubois, P. Polymer-Layered Silicate Nanocomposites: Preparation, Properties and Uses of a New Class of Materials. *Mater. Sci. Eng. R Rep.* **2000**, *28*, 1–63.
(105) Sadhu, S.; Bhowmick, A. K. Effect of Chain Length of Amine and Nature and Loading of Clay on Styrene-Butadiene Rubber-Clay Nanocomposites. *Rubber Chem. Technol.* **2003**, *76*, 860–875.
(106) Wan, C.; Dong, W.; Zhang, Y.; Zhang, Y. Intercalation Process and Rubber–filler Interactions of Polybutadiene Rubber/organoclay Nanocomposites. *J. Appl. Polym. Sci.* **2008**, *107*, 650–657.
(107) Meng, X.; Wang, Z.; Zhao, Z.; Du, X.; Bi, W.; Tang, T. Morphology Evolutions of Organically Modified Montmorillonite/polyamide 12 Nanocomposites. *Polymer* **2007**, *48*, 2508–2519.
(108) Meng, X.; Du, X.; Wang, Z.; Bi, W.; Tang, T. The Investigation of Exfoliation Process of Organic Modified Montmorillonite in Thermoplastic Polyurethane with Different Molecular Weights. *Compos. Sci. Technol.* **2008**, *68*, 1815–1821.
(109) Lertwimolnun, W.; Vergnes, B. Influence of Compatibilizer and Processing Conditions on the Dispersion of Nanoclay in a Polypropylene Matrix. *Polymer* **2005**, *46*, 3462–3471.
(110) Tunç, S.; Duman, O. Preparation and Characterization of Biodegradable Methyl Cellulose/montmorillonite Nanocomposite Films. *Appl. Clay Sci.* **2010**, *48*, 414–424.
(111) Song, M.; Wong, C.; Jin, J.; Ansarifar, A.; Zhang, Z.; Richardson, M. Preparation and Characterization of Poly(styrene-Co-Butadiene) and Polybutadiene Rubber/clay Nanocomposites. *Polym. Int.* **2005**, *54*, 560–568.
(112) López-Manchado, M. A.; Arroyo, M.; Herrero, B.; Biagiotti, J. Vulcanization Kinetics of Natural Rubber-Organoclay Nanocomposites. *J. Appl. Polym. Sci.* **2003**, *89*, 1–15.
(113) López-Manchado, M.; Herrero, B.; Arroyo, M. Organoclay–natural Rubber Nanocomposites Synthesized by Mechanical and Solution Mixing Methods. *Polym. Int.* **2004**, *53*, 1766–1772.

(114) Mousa, A. Cure Characteristics and Thermal Properties of Sulfur-Cured EPDM-Based Composites by Compounding with Layered Nano-Organoclays. *Polym.-Plast. Technol. Eng.* **2006**, *45*, 911–915.
(115) Dirksen, A.; Nieuwenhuizen, P. J.; Hoogenraad, M.; Haasnoot, J. G.; Reedijk, J. New Mechanism for the Reaction of Amines with Zinc Dithiocarbamates. *J. Appl. Polym. Sci.* **2001**, *79*, 1074–1083.
(116) Reyneke-Barnard, C. P.; Gradwell, M. H. S.; Mcgill, W. J. N,N'-Pentamethylenethiuram Disulfide- andN,N'-Pentamethylenethiuram Hexasulfide-Accelerated Sulfur Vulcanization. II. Relative Stability ofN,N'-Pentamethylenethiuram Disulfide and Tetramethylthiuram Disulfide with Respect to Amine Formation. *J. Appl. Polym. Sci.* **2000**, *77*, 2732–2739.
(117) Ghasemi, I. Evaluating the Effect of Processing Conditions and Organoclay Content on the Properties of Styrene-Butadiene Rubber/organoclay Nanocomposites by Response Surface Methodology. *EXPRESS Polym. Lett.* **2010**, *4*, 62–70.
(118) Sadhu, S.; Bhowmick, A. K. Unique Rheological Behavior of Rubber Based Nanocomposites. *J. Polym. Sci. Part B Polym. Phys.* **2005**, *43*, 1854–1864.
(119) Sadhu, S.; Bhowmick, A. K. Preparation and Properties of Nanocomposites Based on Acrylonitrile-Butadiene Rubber, Styrene-Butadiene Rubber, and Polybutadiene Rubber. *J. Polym. Sci. Part B Polym. Phys.* **2004**, *42*, 1573–1585.
(120) Marzocca, A. J. Evaluation of the Polymer–solvent Interaction Parameter χ for the System Cured Styrene Butadiene Rubber and Toluene. *Eur. Polym. J.* **2007**, *43*, 2682–2689.
(121) Flory, P. J.; Rehner, J. Statistical Mechanics of Cross-Linked Polymer Networks II. Swelling. *J. Chem. Phys.* **1943**, *11*, 521.
(122) Sperling, L. H. *Introduction to Physical Polymer Science*; 4th ed.; Wiley: Hoboken, N.J, 2006.
(123) Bristow, G. M.; Watson, W. F. Cohesive Energy Densities of Polymers. Part 1.?Cohesive Energy Densities of Rubbers by Swelling Measurements. *Trans. Faraday Soc.* **1958**, *54*, 1731.
(124) Cho, K.; Jang, W. J.; Lee, D.; Chun, H.; Chang, Y.-W. Fatigue Crack Growth of Elastomers in the Swollen State. *Polymer* **2000**, *41*, 179–183.
(125) Witten, T. A.; Rubinstein, M.; Colby, R. H. Reinforcement of Rubber by Fractal Aggregates. *J. Phys. II* **1993**, *3*, 367–383.
(126) Vansant, E. F.; van der Voort, P.; Vrancken, K. C. *Characterization and Chemical Modification of the Silica Surface*; Elsevier: Amsterdam; New York, 1995.
(127) Xiao, Y.; Li, C. M. Nanocomposites: From Fabrications to Electrochemical Bioapplications. *Electroanalysis* **2008**, *20*, 648–662.
(128) Wiebeck, H.; Borrelly, D. F.; Xavier, C.; Santos, P. S.; Asciutti, S. A.; Corrêa, M. P. The Effect of Silane Coupling Agents on a Composite Polyamide-6/Talc. *Braz. J. Chem. Eng.* **1998**, *15*.
(129) Rashmi, M. Kinetic Studies of Some Esters and Amides in Presence of Micelles. *Pt Ravishankar Shukla Univ.* **2012**.
(130) Vasudevan, D.; Arey, T. A.; Dickstein, D. R.; Newman, M. H.; Zhang, T. Y.; Kinnear, H. M.; Bader, M. M. Nonlinearity of Cationic Aromatic Amine Sorption

to Aluminosilicates and Soils: Role of Intermolecular Cation−π Interactions. *Environ. Sci. Technol.* **2013**, *47*, 14119–14127.
(131) Gillespie, L. K. *Troubleshooting Manufacturing Processes: Adapted from the Tool and Manufacturing Engineers Handbook : A Reference Book for Manufacturing Engineers, Managers, and Technicians*; Society of Manufacturing Engineers, 1988.
(132) Kojima, Y.; Usuki, A.; Kawasumi, M.; Okada, A.; Fukushima, Y.; Kurauchi, T.; Kamigaito, O. Mechanical Properties of Nylon 6-Clay Hybrid. *J. Mater. Res.* **1993**, *8*, 1185–1189.
(133) Karthikeyan, C. S.; Nunes, S. P.; Schulte, K. Ionomer-Silicates Composite Membranes: Permeability and Conductivity Studies. *Eur. Polym. J.* **2005**, *41*, 1350–1356.
(134) Venkataraman, N. V.; Vasudevan, S. Conformation of Methylene Chains in an Intercalated Surfactant Bilayer. *J. Phys. Chem. B* **2001**, *105*, 1805–1812.
(135) *Handbook of Soil Science*; Sumner, M. E., Ed.; CRC Press: Boca Raton, Fla, 2000.
(136) Shori, S. Surface Modification of Nanoplatelets in Polymer Nanocomposites. *Theses Diss.* **2014**.
(137) Kim, C. S. The Layered Sodium Silicate Magadiite: An Analog to Smectite for Benzene Sorption from Water. *Clays Clay Miner.* **1997**, *45*, 881–885.
(138) Li, B.; Zhenxing. Synthesis and Characterization of Ordered Mesoporous Silica Pillared Clay with HPW Heteropoly Acid Encapsulated into the Framework and Its Catalytic Performance for Deep Oxidative Desulfurization of Fuels. In *Metal, Ceramic and Polymeric Composites for Various Uses*; Cuppoletti, J., Ed.; InTech, 2011.
(139) Manias, E.; Touny, A.; Wu, L.; Strawhecker, K.; Lu, B.; Chung, T. C. Polypropylene/Montmorillonite Nanocomposites. Review of the Synthetic Routes and Materials Properties. *Chem. Mater.* **2001**, *13*, 3516–3523.
(140) Khatua, B. B.; Lee, D. J.; Kim, H. Y.; Kim, J. K. Effect of Organoclay Platelets on Morphology of Nylon-6 and Poly(ethylene- *r an* -Propylene) Rubber Blends. *Macromolecules* **2004**, *37*, 2454–2459.
(141) Chen, X.; Gao, H.; Ploehn, H. J. Montmorillonite–levan Nanocomposites with Improved Thermal and Mechanical Properties. *Carbohydr. Polym.* **2014**, *101*, 565–573.
(142) Morton, M.; American Chemical Society; Rubber Division. *Rubber Technology*; Chapman & Hall: London; New York, 1995.

APPENDIX A- Calculations for m-SI-69-MGD/SQ

m-SI-69-MGD/SQ is taken as an example to explain the calculations of the composition based on TGA and EA results.

Calculate the Composition of m-SI-69-MGD

The formula of m-SI-69-MGD is expressed on a molar basis as $(CTA)_x(OS)_yNa_{0.75}Si_{14}O_{29}\cdot nH_2O$. TGA and EA results for m-SI-69-MGD are shown in Table A1. Each SiO_2 is a "unit cell". The amount of unit cells is calculated based on the TGA results. The total loss of m-SI-69-MGD sample is 20.73% up to 800°C, and the residue (SiO_2) percent is 79.27%. The total weight is 14.30 mg, thus the weight of residue is 11.34 mg (0.1863 mmols). Both silane and MGD are sources of Si in the residue. The residue has 0.1863/(14+2y) mmols of unit cells.

Table A.1 TGA and EA results for m-SI-69-MGD.

sample ID	total weight (mg)	total loss (%)	water loss (%)	dehydroxylation loss (%)	organic loss (%)	C%	H%	N%	S%
m-SI-69-MGD (SL2235)	14.30	20.73	2.77	1.98	5.98	8.94	1.74	0.14	6.47

SI-69 is the only source of sulfur, so the amount of SI-69 is calculated based on S%. m-SI-69-MGD has 6.47% S. Each mole of m-SI-69-MGD provides four moles of S. Thus, there is 7.215×10^{-3}mmols of SI-69 in sample. According to the assumed composition, the number of SI-69 per unit cell is y, which is equal to ratio of 7.215×10^{-3}

mmols of SI-69 to 0.1863/(14+2y) mmols of unit cells. By solving this equation, 0.588 mole of SI-69 (y=0.588) is calculated in each mole of m-SI-69-MGD. There is 0.0123mmols of unit cells in m-SI-69-MGD sample.

N is the only source of CTAB, so the amount of CTAB is calculated based on N%. M-SI-69-MGD has 0.14% N. Considering the total weight 14.30 mg, there is 1.429×10^{-3}mmol of CTA^+ in sample. The number of CTAB per unit cell is x, which is equal to the ratio of 1.429×10^{-3}mmol of CTAB to 0.0123mmols of unit cells. It is calculated that there is 0.116 mol of CTAB in each unit cell (x=0.116). The formula of m-SI-69-MGD is expressed on a molar basis as $(CTA)_{x=0.116}(OS)_{y=0.588}Na_{0.75}Si_{14}O_{29}\cdot nH_2O$.

Calculate the Composition of m-SI-69-MGD/SQ

There are three assumptions for the calculations of the amount of grafting squalene (SQ). First, we assume that after reacting with SQ, the amount of CTA^+ does not change. Because there are not CTAB characteristic peaks in IR spectra for m-SI-69-MGD. The small interlayer spacing of m-SI-69-MGD also indicates limited CTA^+ remained in the interlayers. Therefore, it is reasonable to assume that the amount of CTA^+ keeps the same after reacting with SQ. We also noticed from EA results that wt% N of m-SI-69-MGD and m-SI-69-MGD/SQ are 0.14% and 0.31%, respectively. The increase of wt% of N is not realistic considering the addition of SQ. It might be experiment error.

Each SI-69 has four sulfur atoms. During SQ reaction, two S are still bound to SI-69, while the other two are released to the matrix (called free sulfur). The second

assumption is that the amount of fixed S does not change, but the amount of free sulfur changes.

Third assumption is that wt% of Na stays the same after reacting with SQ, because the wt% of Na is not significant.

The formula of m-SI-69-MGD/SQ expressed on a molar basis is $(CTA)_{0.116}(OS')_{0.588}S_{y'}Na_{0.75}Si_{14}O_{29}\cdot nH_2O$. (OS') represents the silane molecular with two bounded S atoms. The mole number of (OS') is the same as that of (OS) in m-SI-69-MGD based on the second assumption. Free S is denoted as $S_{y'}$ in formula. TGA and EA results for m-SI-69-MGD/SQ are shown in Table A2.

Table A.2 TGA and EA results for m-SI-69-MGD/SQ.

sample ID	total weight(mg)	total loss (%)	water loss (%)	dehydroxylation loss (%)	organic loss (%)	C%	H%	N%	S%
m-SI-69-MGD/SQ (SL2269YM)	8.96	32.66	0.89	1.68	30.09	21.21	3.37	0.31	4.26

The total weight of m-SI-69-MGD/SQ is 8.96 mg. The total weight loss is 32.66%, and the residue is 67.34%. Based on the assumed composition, there is 6.618×10^{-3} mmol of unit cells in m-SI-69-MGD/SQ sample.

The amount of free S is calculated by subtracting the amount of fixed S from the total sulfur amount. Considering 4.26% of S and 8.96 mg of total weight, there is 0.012 mmol of S in m-SI-69-MGD/SQ sample. The amount of S in each unit cell is the ratio of 0.012 mmol to 6.618×10^{-3} mmol of unit cells, which is equal to $(2\times0.588+y')$. So, there is 0.637 mmol of free S in SQ-l-m-SI-69-MGD.

The amount of CTAB is calculated based on N% in m-SI-69-MGD/SQ, which is similar to that for m-SI-69-MGD. It is calculated that there is 0.300 mol of CTAB in each unit cell (x=0.116). The formula of m-SI-69-MGD/SQ expressed on a molar basis is $(CTA)_{0.116}(OS')_{0.588}S_{y'}Na_{0.75}Si_{14}O_{29}\cdot nH_2O$.

The weight of SQ in m-SI-69-MGD/SQ is calculated by the organic loss from TGA. The organic loss for m-SI-69-MGD consists of the loss of CTA^+, OS, and sodium (the amount of Si in OS is negligible). For m-SI-69-MGD/SQ, the organic loss consists of those mentioned above plus the amount of SQ and free sulfur. The amount of SQ is calculated by comparing the organic loss for both samples. It is calculated that m-SI-69-MGD/SQ contains 0.58 moles of grafting SQ per unit cells. Since each SI-69 molecule yields two S-sites, the ratio of grafted SQ to S-sites is 0.49.